DOUBLE DIFFERENTIAL CROSS SECTION OF THE SECONDARY PARTICLES (n, p, α) AFTER SPALLATION FOR $_{90}Th^{232}$, $_{5}B^{10}$ ELEMENTS

MASTER THESIS

MAJD HAMAD SMAIL

Department Institute: PHYSICS

THESIS SUPERVISOR
Prof. Dr. İskender DEMIRKOL

BINGOL-2018

DOUBLE DIFFERENTIAL CROSS SECTION OF THE SECONDARY PARTICLES (n, p, α) AFTER SPALLATION FOR $_{90}Th^{232}$ AND $_5B^{10}$ ELEMENTS

MASTER'S THESIS

Majd Hamad SMAIL

Department Institute   :   PHYSICS

This thesis was unanimously approved by the following jury on 07.05.2018

Associate Prof. Dr.	**Prof. Dr.**	**Assistant Prof.Dr.**
Bayram GÜNDÜZ	**İskender DEMİRKOL**	**Kamuran DİLSİZ**
Member	**President of the Jury**	**Member**

I confirm the results above

Associate Professor Dr. ZaferŞİAR
Director of the Institute

ACKNOWLEDGEMENTS

COTENTS

LIST OF ABBREVIATIONS AND SYMBOLS

CERN   : European Council for Nuclear Research

PHITS   : Particle and Heavy Ion Transport Code System

ADS   : Accelerator Driven System

INC   : Intra Nuclear Cascade

CEM   : Cascade Exciton Model

ADS-R   : Accelerator-Driven Subcritical Reactors

SINQ   : Swiss Spallation Neutron Source

SNS   : Spallation Nutron Source

ESS   : European Spallation Source

NSP   : Northern States Power Company

INPRO   : International Project on Innovative Nuclear Reactors and Fuel Cycles

GDHM   : Geometry Dependent Hybrid Models

HMB   : Harp-Miller-Berne

MTA   : Materials Testing Accelerator

JAERI   : Japan Atomic Energy Research Institute

OMEGA   : Option Making Extra Gains from Actinides and Fission Products

ATW   : Accelerator Transmutation of Waste

LANL   : Los Alamos National Laboratory

ADEP   : Accelerator Driven Energy Production

JQMD   : Jaeri Quantum Molecular Dynamics

CCC   : Close-Coupling Computations

HLW   : High-Level Waste

NEA   : Nuclear Energy Agency

Bq   : Becquerel (is the SI derived unit of radioactivity)

FRS   : Fragment Separator

OECD   : Organisation for Economic Co-Operation and Development

G	: Gigaelectron Volt
MeV	: Megaelectron Volt
KeV	: Kiloelectron Volt
mb	: Milibarn
sr	: Steradian
θ	: Angle
α	: Alpha
p	: Proton
e	: Electron
n	: Neutron
A	: Atomic Number
Z	: Mass Number
σ	: Cross Section
^{0}	: Degree
He	: Helium
B	: Boron
Th	: Thorium
ρ	: Density
N_A	: Numbers of Avogadro
V	: Velocity
fm	: Femtometer
σ_{tot}	: Total Cross-Section
$d\sigma/dE$	: DifferentialCross Section
$d^2\sigma/dE.d\theta$	: Double Differential Cross Section

LIST OF FIGURES

LIST OF TABLES

xiv

$_{90}$TH^{232} VE $_5$B^{10} ELEMANTLERI İÇİN SPALLASYON SONRASI OLUŞAN İKİNCİL PARÇACIKLARIN (n, p, α) ÇİFT DİFERANSİYEL TESİR KESİTİ

ÖZET

Bu çalışmada p + $_{90}$Th^{232} ve p + $_5$B^{10} spallasyon reaksiyonu sonrası oluşan ikincil parçacıkların (n.p.α) çift diferansiyel tesir kesiti hesaplamaları elde edilmiştir. Hesaplamalar kaskat eksiton modeli kullanan CEM03 bilgisayar programı kullanılarak yapılmıştır. Protan ışını spallasyonu oluşturan mermi olarak kullanıldı ve enerjisi 20 ile 660 Mev aralığında seçilmiştir. Hesaplamalarda spallasyon sonrası oluşan toplam, kaskad, bileşiköncesi ve buharlaşma safhaları için n,p ve α'nın çift difereransiyel tesir kesitleri de ayrıca elde edilmiştir. Elde edilen sonuçlar Nükleer Enerji Ajansı (NEA) dan elde edilen deneysel datalar ile karşılaştırılmıştır.

Anahtar Kelimeler: Çift diferansiyel, spallasyon, enerji, nükleer reaksiyon, hızlandırıcı, tesir kesiti ve CEM03 kodu.

DOUBLE DIFFERENTIAL CROSS SECTION OF THE SECONDARY PARTICLES (n, p, α) OCCURED AFTER SPALLATION FOR $_{90}TH^{232}$ AND $_5B^{10}$ ELEMENTS

ABSTRACT

In this study, double differential cross section of the secondary particles (n, p, α) occurring after spallation in the reactions p + $_{90}Th^{232}$ and p + $_5B^{10}$ were obtained. Calculations were made by Cascade Exciton Model (CEM03) computer program. The protan beam was used as the projectile forming, the spallation and the energy was selected in the range of 20 to 660 MeV. In the calculations, double differential cross sections of n, p and α were also obtained for the total, cascade, pre-compound and evaporation phases after spallation. The results are compared with the experimental data obtained from the Nuclear Energy Agency (NEA).

Keywords: Doubledifferential, spallation, energy, nuclear reaction, accelerator, cross section and CEM03 code.

1. INTRODUCTION

The spallation reactions are one branch of the nuclear reactions. In general, they are de-
fined as the collision or interaction of two particles, more often than the collision of a
nucleon with nucleus. The first particle is a projectile which is a fast bombarding particle
and the second particle is a stationary called the target (Meyerhof 1967). The bombard-
ment energy is more or less between (100 – 3000) MeV. Through this interaction many
nucleons are emitted such as (n, α, p) emitted and the remaining nucleus be able to be
very various for the target nucleus also near the beginning studies of spallation reactions
took place in 1947 at the University of California in the Berkeley cyclotron (Brobeck et
al. 1947).

Recently, spallation reactions have attracted significant attention due to their significance
in technical applications. For instance, they can be utilized for the production of neutrons
in a spallation neutron source, and they can perform as an intense neutron source in ac-
celerator-driven subcritical reactors (ADS-R), capable of incendiary nuclear waste and of
producing energy. It is suggested that in the following production radioactive beam facili-
ties, projectile disintegration at relativistic energies will be one of the main producing
modes. The production of remaining output nuclei in proton collisions with an intense
target nucleus is due to the intranuclear process of spallation, fragmentation, fission, and
the total evaporation of light nuclei and nucleons (Demirkol 2006).

A large quantity of spallation neutrons or alpha is emitted from a target nucleus by proton
bombarding together with incident intermediate energy around (MeV or GeV). Recently,
the studies on the spallation reaction have been made for this application as spallation
neutron sources and accelerator driven transmutation systems. Nuclear data are very es-
sential for these objectives in the energy region nearly up to a few GeV. Several spalla-
tion sources for solid state and material physics are under structure or study many coun-
tries, for instance spallation nutron source.

Spallation neutron sources also be utilized in Accelerator Driven Systems to drive sub-critical reactors, in which long lived nuclear waste could be burned (Bowman et al. 1992), (Takizuka 1994) and (Rubbia et al. 1995). All of that systems have in mutual a spallation target made of a heavy element, either solid (Th) or liquid (Hg) (Armstrong and Chandler 1977). Nuclear power is a type of capable and cleanly energy.

The Accelerator Driven Nuclear Energy System (ADS) is a credible option to dissolve the efficient utilize of the resources and the eventual processing of long-lived nuclear waste, and will become the transmission between current commercial nuclear power system and fusion energy system. The capability and fuel of nuclear waste transmutation deepened using of accelerator driven system broadly depend on the energy and number distribution of outer neutron sources maintain the subcritical reactor of accelerator driven system and are produced from the height energy proton bombardment of heavy nuclei. For the whole ADS system in the high energy proton nuclear reactions depended on the basis of micro data. Therefore studying theory and micro data is very importance for high energy protons and heavy metals reactions (Kirkby and Link 1966). As in traditional reactor physics, the basic of nuclear reaction information is preliminary point of any gross-scale modeling of an accelerator driven system (ADS). Practically computations of such systems, such as energy balance and neutron with radiotoxicity of spallation products, damage and activation calculations depend on nuclear data, and the provision of this information to the engineering community in a form that produces macroscopically transfer and an activation account is a task for assessing nuclear data. Nucleon induced reaction experiments have been implemented because of in the second half of this century has resources of high energy bigger than 20 MeV and are as yet implemented.

This experiment has been conducted; the main purpose of these experiments is to promote basic knowledge of direct reactions, nuclear physics in general and nucleon-nucleon interactions. The various accelerator based nuclear energy applications that have come out in the past decade provide a new application justification of these measurements. The dissimilar accelerator based nuclear energy applications that have emerged in the past decade provide a modern application best reason of these measurements (Patrick 2017). Transmutations of long lived actinides and fission produces from nuclear waste or thorium as an energy source are being inspected with rising interest in the latest two decades.

Different notion of transmutation involve and the Accelerator Driven Systems based on a subcritical nuclear reaction (Rubbia et al. 2004), (Nifenecker et al. 1999). The Accelerator Driven Subcritical Systems have given a modern look at the employ of thorium fuel cycle in a lead–bismuth coolant climate. In parallel to the accelerator driven subcritical systems (Sinha and Kakodkar 2006), (Saha and Sinha 2005) and (Dulera, Basak, Kelkar and Sinha 2005) to advancement reactors require enhanced nuclear data (Ganesan 2004; 2005) that overlap with the on-going international efforts to improve innovative, inherently safe, reproduction resistant and long-lived cores, with features utilizing thorium like in International Project on Innovative Nuclear Reactors and Fuel Cycles (INPRO) and after that generation nuclear energy systems famous as "Generation IV".

The function of the spallation target is to transform (1 GeV) protons produced by the proton accelerator to low energy (less than 20 MeV) neutrons and distinguish them to the energy amplifier area. The effective transformation of fertile to fissionable nuclei or the transmutation of radioactive nuclei to stable ones takes place in the Accelerator Driven Subcritical System blanket favorably in the resonance power area (less than 50 keV) and thermal regions where the capture cross section is the greater. In executing this designing function, the spallation target must be cooled adequately. Nuclear data to [forecast nuclear collision, isotope produce, formation of gases and heat reproduction] are requirement at that first step. Nuclear data are too needed to decrease the hazard related to radiological releasing or other harmful outcome like, for example, that are resulting from off-normal status [loss of coolant in the target, Non-modified proton beam with respect to time and spatial distribution]. Maximizing neutron and alpha particle production are one of the tasks for a target designing. The chosen of high atomic number Z material is preferred, as the target should have a large number of nucleons per proton (Nucleon/proton) to reason intra-nuclear reactions. For such energy types, the proton expels bound neutrons directly. Accordingly, the emitted neutrons tend to be forward pointed and have rise energy up to the proton energy.

On the other hand, Accelerator Driven System is a newest nuclear reactor which study to creation energy and transformed radioactive waste also is important for starting to breed the necessary U-233 in a Thorium (Th) based type of fuel cycle. (Barros et al. 2010). The concept of Accelerator Driven Systems integrated a particle accelerator with a subcritical

core. Most offers suppose proton (p) accelerators, delivering continuous-wave beams with energy nearly around 1 GeV.

The accelerator has two dimensions; either a linear accelerator or a circular accelerator (cyclotron). High potential accelerator has been under continuous evolution, and the construction of machines with the required specifications. The protons are injected onto a spallation target to product source neutrons for driving the sub-critical core. The target is made of heavy metal in solid state or liquid state. In every proton incident; the spallation reactions in the target are not emitted by many neutrons, which are inserted into the sub-critical nucleus to induce further nuclear reactions. However, the core is very similar to the critical reactor in the subcritical state. It can be designed to operate either with a thermal or fast neutron spectrum. An Accelerator driven subcritical reactor ability meant a nuclear squander handling or energy production, is constituted of this assemblage (a spallation target, a high power proton driver, a sub critical reactor and nuclear data), (Meot et al. 2015).

2. LITERATURE REVIEW

(Boudard et al. 2002) reported that a modern version of the intranuclear cascade model is proposed for the explanations of spallation reactions. Spallation reaction are one branch of nuclear reaction. Compared to the preceding, version, it combine new features; (1) it can conform a spread nuclear surface; (2) the treating of the Pauli blocking effect gets better; (3) impacts or collisions between dynamic spectator nucleons are clearly suppressed; (4) improved the pionsdynamic, essentially related the delta lifetime. Furthermore, another important advantage is the self-proportionate determination of the stopping time. Utilized the evaporation code with forecasts of the model are tested against a large body of experimental data in a range at 200 MeV to 2 GeV for incident energy per nucleon then including total reaction cross sections are composite double differential cross sections, neutron, proton and particle multiplicities.

Double differential cross sections for light particles (proton, deuteron, triton and alpha) also neutrons were produced by bombardment incident proton beam at 62.9 MeV which was calculated at the CYCLONE facility in Louvain-la-Neuve in Belgium (Guertin and Arnaud et al. 2005). These calculation have been executed using two independent experimental set-ups including; (1) neutron (Demon counters); (2) light charged particles (Si-Si-CsI telescopes) detection. The light charged particle data was calculated at nearly eleven various angular positions from 25° -140° allowing the determination of angle differential cross section, energy differential and total production cross sections.

(Kenji Ishibashi et al. 1997) reported that the calculated double differential cross section $d2\sigma/dE.d\theta$ of neutron production were calculated for the spallation reaction induced by (0.8, 1.5, 3.0) GeV protons on the targets (Al, Fe, C, Pb). The experiments were completed by time-of-flight technique with an exemplary flight path length of one meter (1m), and the cross sections were acquired with energy decision better than (8) percent at

neutron energies below 100 MeV. The experimental data was compared with the outcomes of computation codes based on an intranuclear-cascade evaporation model.

(Tashenov and Stanislav et al. 2011) reported that atomic field bremsstrahlung has been calculated with a longitudinally polarized electron beam. The interconnection between the initial orientation of the electron spin and the angle of photon polarization has been calculated at the photon high energy tip area. In the reflection time this agree to a so-far unobserved phenomenon of output of longwise polarized electrons by photoionization of unpolarized atoms with linearly polarized photons. The consequences emphasize the completely relativistic computations for radioactive re combination and propose a modern method for electron beam polarimetry.

(Niita et al. 2006) were presented three applications of the codes; are spallation neutron source, heavy ion therapy, space radiation. New evolution of the multi-purpose Monte Carlo Particle and Heavy Ion Transfer code System, PHITS was also presented in this study. In particular, they discussed in detail the expansion of two new models, JAM and JQMD, for high energy particle interactions, incorporated in PHITS which compare model computations and experiments for the validations of these models.

(Röder et al. 2013) presented that a convergent experimental and theoretical research of ionization by 40 eV incident energetic electron of the ground state. Absolute (in and out) of-plane measurements are provided for slow electron energy at 4 eV. These are set up to be in best agreement with the convergent close-coupling (CCC) computations.

The report (Gibson and Reid 1986) presented the cross section calculations for the ejection of electrons and angles from 5 to 100 eV and 0 to 100 degrees, respectively. Helium atoms bombardment by protons energies range from 20 to 100 keV with differential in the angle of electron ejection and energy. The measurements were instilled by comparing the assessments of the total cross section, derived from double integration of the measured distributions with published absolute values of the ionization cross section. Although the energy distribution agrees with the available data, there was a substantial divergence in the angular attitude.

The research that was reported by (Fernández-Menchero and Otranto 2014) is about a theoretical study of completely differential cross sections for the single ionisation of O-H-O by collisions with H^+ and He^{2+} at an effect energy of (2, 6) MeV/amu. In that research double differential cross sections in terms of the electron emission angle are also offered for this molecular orbital (1B1, 1B2, 2A1 and 3A1), which indicate almost isotropic distribution for the electron energies under discernment.

(Sarpün et al. 2014) investigated that the double differential cross section for these elements are (O^{16}, Al^{27}, Ni^{80} , Sn^{120}, $Fe^{54,56}$, Au^{197}, $Bi^{209,}$ Pb^{208} and Y^{80}) by TALYS code program at 62 MeV proton energy. The computation involved the Hauser- Feshbch and the pre-equilibrium exciton model was also measured by TALYS code. The calculated outcomes were compared with the experimental data. Likewise, the results were in good agreement.

(Demirkol and Eyyup 2011) multiplicities of neutron and different particles per incident proton in collision of ($15x10^2$) MeV energetic proton beam for such thin targets (Au, Pb, W, Bi, Th, U, Fe and Cu) have been approximated with the models ; Cascade-Exciton Model, intranuclear cascade and Evaporation model. The computation have been made utilizing simulation codes based on specific models which charecterize elementary output of particles in nuclear reactions. The acquired results have been compared with the available data.

(Junghans 2014) reported that studying nuclear reactions in the ranges of several keV kinetic energy, the neutrons produced by the reactions that below requirement were slowed down by elastic collisions with light nuclei. Spallation reactions and photonuclear could product a beamy spectrum of neutrons with height density, while from the fusion of this isotopes "Hydrogen" for instance D(t, xn) Helium-4 or transformation reactions such as 7Li(p, xn)7Be quasi-monoenergetic neutrons ability to be produced. Utilize of a pulsed beam allows to determined the neutron energy through measuring the time-of-flight of the neutrons with a known flight path. Photo-neutron sources utilize typically an electron linear accelerator to make intensive pulses of "electromagnetic radiation produced by the acceleration " in an intense metal target that also acts as the neutron radiator

in which neutrons were produced by (p, xn), (n, xn), ... and (α, xn) reactions with the heavy nuclei.

(Demirkol 2006) were measured the production cross sections of intense remaining nuclides in the p + Pb^{208} for (1GeV/nucleon) reaction. The computations were equipped with the Cascade Exciton Model computations the pre-equilibrium effect, the Intranuclear Cascade Model, the empirical, and the semi-empirical parameterization. The outcome of the cross sections acquired were compared with the available experimental data, and the relevance between them was calculated.

(Drosg and Hoop 2016) calculated cross section and double differential cross section from triton bombardment of Au-197 that were concluded from measurements of triton interactions with gas targets that utilized Au-197 as a triton beam stop material. That process used for produced neutron. For calculated differential cross section the energies (5.97, 7.47, 10.45, 16.41, and 19.14) MeV tritons on 197Au for production neutron were used.

(Getahun 2011) reported that a calculations of the excitement function of [Nb^{93}(α, n)T^{96}c, Nb^{93} (α, 2n)T^{95}c, Nb^{93}(α, 3n)T^{94} c] reactions have been executed in the incident alpha energy range from 10 to 42 MeV. The computations were utilizing ALICE-91 computer code program. In these calculations used pre-equilibrium nuclear models. The nuclear models includes: (1) Intra-Nuclear Cascade (INC); (2) Harp-Miller-Berne(HMB); (3) Exciton model; (4) Geometery Dependent Hybrid (GDH).

(Kerveno et al. 2002) studied that the calculations double differential cross sections for hydrogen isotope production have been ejected in 62.7 MeV neutron induced reactions on a lead target. The angular distribution from 20 to 160 for eight angles allowing the taking out of (total production cross sections, angle differential and energy differential) has been calculated. A first set of comparisons with several theoretical computations is also offered.

(Abdelbagi 2017) calculated the neutron total cross section experimentally based on Transference and assimilation of intensive neutron beams. This study present the funda-

mental atomic nucleusradius experimentally utilizing plutonium-beryllium source by comparing the Ramsauer model computation for the elements C, Al, S, Fe, Cu, Hg and Pb and neutron wavelength. In this investigation, the experimental methods were compared to the Ramsauer model.

(Patrick 2017) provided that a Measurement of the Antineutrino Double-Differential Charged-Current Quasi-Elastic Scattering Cross Section at Minerva. This thesis characterizes a measurement of a charged-current double-differential antineutrino scattering cross section on carbon scintillation at the Minerva detector at Fermilab.

(Wachter et al. 2015) reported that a measurement of the experimental production cross-section of the reaction $Zn^{nat}(p, x) Ga^{67}$ has been calculated in the energy range from 1.678 to 2.444 MeV. In this investigation X-ray emitted after radiation by the daughter nucleus that decays through electron capture. In this study used the ALICE/ASH and Talys-1.6 computer code then compared with experimental data.

(Sümmerer and Blank 2000) reported that a modern experimental data acquired fundamentally at the GSI/FRS facility allow to modify the experimental parameterization of spallation cross sections. It will be shown that minor modifications of the parameters lead to a so best reproduction of calculated cross sections.

(Taieb et al. 2003) investigated that spallation evaporation reaction by heavy nuclide production such as U-238 induced by 1 GeV energetic protons was calculated in inverse kinematics. The evaporation remains from tungsten to uranium were specified in-flight in mass and atomic number. It was also determined production cross-sections and the momentum distributions were also determined. During the study, the data was compared with experimental data. A comparison with previous results from the spallation of 208Pb and 197Au reveals the strong influence of fission in the spallation of 238U.

3. MATERIALS AND METHODS

3.1. Nuclear Reaction

When two nuclei, overcome their Coulomb repulsion, come within the variety of the nuclear force, a reorganization of nucleus maybe happen. This may product in a nuclear reaction, similar to the reorganization of atoms in reacting molecules through a chemical reaction. Nuclear reactions were generally produced by bombarding a target nucleus with a nuclear projectile in most cases a nucleon (proton or neutron) or a light nucleus for instance, a deuteron or α- particle.

A nuclear reaction was characteristically represented as; X(a, b)Y. In which an incident particle a, and interacts with the target nucleus X emits an resulting particle b, then leaving behind the remaining nucleus Y, this is usually written in one of two ways:

$$X + a \rightarrow Y + b \qquad \text{or by this way} \qquad X(a, b)Y.$$
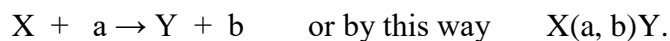
Where:
a = a projectile
b = an emitted particle
X = target nucleus and
Y = the residual nucleus.

Two quantities are very important for energetic considerations in evaluating a nuclear reaction:

(1) The threshold energy is the minimum projectile energy essential to satisfy mass energy and momentum protection in a nuclear reaction to form products in their ground state.
(2) The excitation energy is the surplus energy over the ground state for the production of a nuclear reaction.

Generally, should be known the system before and after the reaction however what punctually occurs during the reaction process is not known. It also is impossible to look into the reaction process immediately, models for reaction mechanism is suggested to demonstrated the product and angular and energy distributions of the reaction productions. The initial tried for model a reaction was made by Niels Bohr (Bohr 1936).

Nuclear reaction occurs in two steps:

1. The projectile was absorbed by the target nucleus and a compound nucleus was formed and a thermodynamic equilibrium was established.
2. The compound nucleus decays by emitting particles or by radiations. It was supposed that the decay of the compound nucleus depends only on the excitement energy and other perfect quantum numbers of the compound nucleus and which was completely freelance of its mode of forming. Also, it was described "independent hypothesis".

In the compound nucleus mechanism, the calculations are well the isotropic distributions of emitted particles in the center of mass framework at bring down excitement energies. Nevertheless, at relatively higher excitement energies, the forward peaked angular distribution of particles show the existence of direct reaction mechanism (Lane and Lynn 1959), (Fesbach 1992). The system is completely in the complex nucleus mechanism, however only a few nucleons participate in the direct reaction mechanism in the development of interactions. The consequences of modern measurements were explained the presence of reaction process which was intermediate between these two extreme reaction mechanisms. The continuous particle spectra illustrates the existence of that more than one step process which was indicates in reaction process started by a few tens of MeV. Preequilibrium or precompound particles were the particles which were emitted during the equilibrium; this process is called preequilibrium nuclear reaction (Fesbach 1992), (Kabach 1995). A drawn representation of the advances of a typical nuclear reaction produced by a medium energy proton is shown in (Figure 3.1).
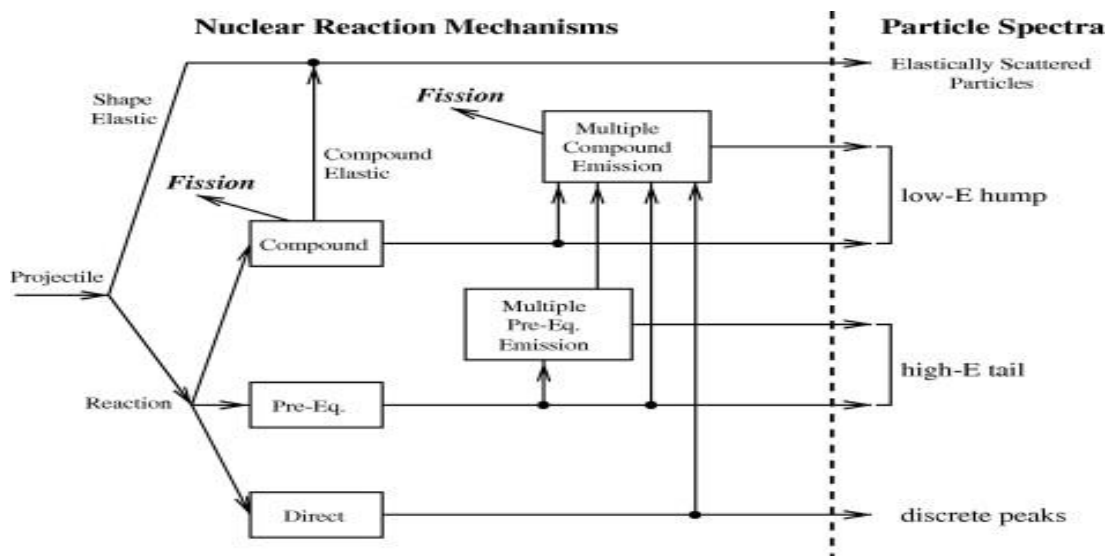
Figure 3.1. Advances of typical nuclear reaction produced by a medium energy protons (Gadioli and Hodgson 1992)

3.1.1. Direct Reaction

(Getachew 2011). When a projectile and a target nucleus were in the range of nuclear forces for the extremely short time, then allowing for an interaction of a single nucleon only. This type of reactions are called "direct nuclear reactions". The remaining nucleus is only the coupled produce of the cluster with the ground state of the object nucleus. This form is normally hard to meet for transmit reaction involving large numbers of nucleons.

There are many properties of direct reactions are ;

1- The emission of much larger number of high energy particles than are expected from evaporation model.

2- All of particles emission in forward direction (approximately $\theta=0^0$ or 10^0) then the angular distributions of emission particles illustrate a forward option ($\theta=0^0$).

3- Energy increases with a monotonic of cross section.

4- Generally high energy of projectiles is caused to occur direct reactions.

3.1.2. Compound Nucleus

Calculation of reaction cross sections theoretically developed by Weisskopf and Ewing (Weisskopf and Ewing 1940) is consistent with the Bohr's model (Bohr 1936) utilize partial wave analysis. In the compound model the conservation of angular momentum and evenness for each partial wave is not acceptable. Nevertheless, it gives a better estimate for the magnitude of the cross section. Otherwise, Hauser-Feshbach theory (Hauser and Feshbach 1952) treated the problem in a more exhaustive method and has clearly in use interested the conservation of angular momentum and parity. The compound nucleus might exist to describe by statistical mechanics because of a state of statistical equilibrium. The compound nucleus has life- time nearly gets to ($\sim 10^{-16}$) second as well as it will decay into various channels; however, it will depend only on the angular momentum, energy of excitation, and parity.

3.2. Stopping Power

An accelerator beam pass through a target will lose energy. This energy loss is due to scattering at electrons and nuclei with the electronic stopping most outstanding almost every energy regions. The energy loss at a given energy is commonly expressed in terms of the stopping power which can be defined as the energy loss per given amount of material. The energy loss itself depends on the energy or more precise the velocity of the beam. The average at which a particle loses energy per unit path length is known as the stopping power of the medium. Aquantum mechanical derivation including relativistic effects is known as the Bethe - Bloch formula (Cottingham and Greenwood 2001).

$$-dE/dx = ze^4/8\pi^2 (\varepsilon_0)^2 (4\pi Z\rho N_A/ Amv^2 [\ln(2mv^2/ I) - \ln(1-\beta^2) - \beta^2] \qquad (3.1)$$

Where:

ze = Charge of the charged particle or ion charge

Z = atomic number

A = mass number

ρ = density of the stopping material

N_A = Numbers of Avogadro

m = electron mass, and

v = Velocity of the charged particle or ion velocity.

For electron account by Bethe-Bloch formula should known these information (Ershaidat 2006):

1- The heavy particles have a higher mass than the electron.

2-The electron is very similar to the particles with which it is interacting, therefore giving the option of the exchange of identity.

3.3. Charged Particle Range

The range of a charged particle can be derived from the stopping power formula, as defined in the following expression.

$$R = \int dx = \oint_E^0 \frac{dE}{dE/dX} \qquad (3.2)$$

The range R defined in equation (3.2) is inversely dependent on ρ (the density of the stopping medium), since the stopping power (dE/dx) depends immediately on ρ as it is showed in equation (3.1). The range R is differently dependent on ρ in these two equations (3.1) and (3.2) since, the scattering process is statistical, and ions will be spread out over a certain range width, if stopping in matter. Near the end of the path, when most of its energy has been comes to down, - dE/dx get to maximum, corresponding to the peak in energy loss at low energy, after which kinetic energy goes from down to zero as the particle comes to rest (Lee 1963). An example of this behavior showed in Figure (3.2) its form was known as the Bragg curve for an α-particle of more than a few MeV of initial energy.

Bragg Curve

$$-\frac{dT}{dx}$$

Distance of Penetration →
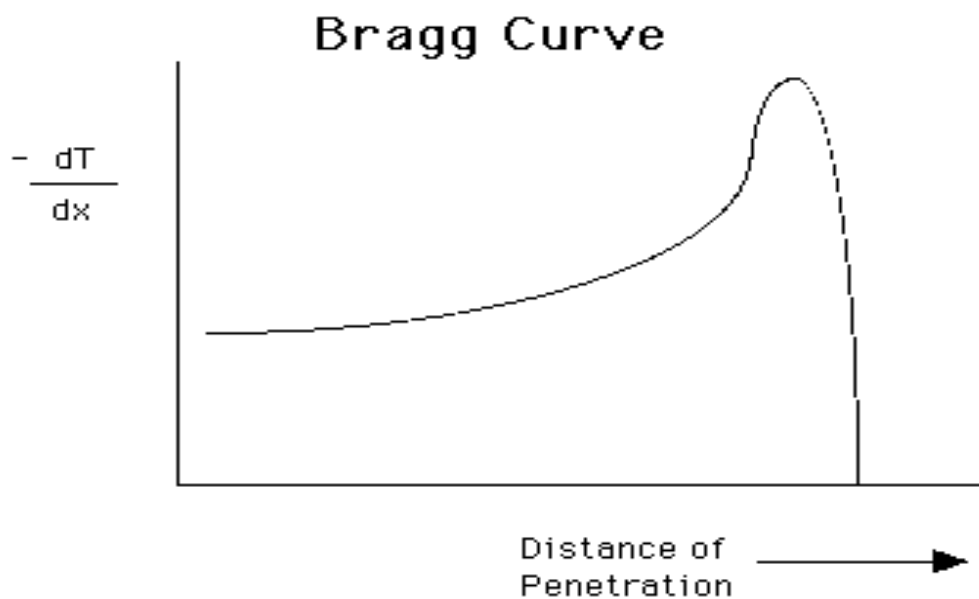
Figure 3.2. Bragg Curve is characteristic for intense charged particles and schemes the energy loss throughout its travel through matter (Wagenaar 1995)

The most important factors affecting Range (R) are:

1- Energy: the range is approximately linear with energy since the Bethe Bloch formula for stopping power is inversely proportionate to kinetic energy E.

2- Mass: the electron is alot faster than the alpha because of it has smaller mass, and also the electron has less time to spend nearby orbital electrons. This decrease by the effect of Coulomb interactions, and increases range. All of these truly for the same kinetic energy.

3- Charge: the more stopping power, the lower range and the more charge then Range is inversely proportionate to the square of the charged particle. For instance, a radioactive isotope of hydrogen a tritium particle with atomic number ($z = 1$) will have (1/4) the stopping power of a He-3 particle with atomic number ($z = 2$).

4- Density: the stopping power directly proportional with density, it means that, the stopping power increases with increasing density. However, the range is inversely proportional with density of the absorbing medium (Ziegler 1988).

3.4. Nuclear Level Density

Nuclear level densities play an important role in estimating nuclear reaction cross sections in general. The nuclear level density is the number of levels per unit energy interval. The nuclear power state perhaps is dividing into two regions. When the number of levels is limited then the state up to certain excitement energy (usually between 1 and 2 MeV), it is comparatively well separated. In this energy region the levels densities are comparatively modest in structure, while can be understood on the foundation of nuclear models. Number of levels increases with increases excitement energy and the spacing between them decreases while the nature of excitation becomes much complex. Consequently at high excitement energy the only way to explain them is utilizing a statistical procedure. The concepts of level density were introduced by Bethe (Bethe 1937) for function ρ in this form

$$\rho\ (E) = \frac{dN(E)}{dE} \qquad (3.3)$$

Where N(E) is the accumulative number of levels bring to the excitement energy .

3.5. Cross Section of Nuclear Reaction

The cross sections in nuclear reaction utilize to describe the probability that a reaction will occur of nucleus (Lane and Thomas 1958). Furthermore, the area of the target nucleus able to be seen by the incident particle is proportionate to the rate of reaction; as well the term of the cross section is utilized to denote a constant related to the rate of a reaction. The unit of the cross section more often is used the (barn) (Basdevant, Rich, and Spiro 2005);

$$1\ b = 100\ fm^2 = 10^{-28}\ m^2 = 10^{-24}\ cm^2$$

On the other hand, the probability for a nuclear reaction is characterized in terms of a cross section, indicated by σ, in fact the proportional cross sectional area given by the target to the arriving projectile.

As a nuclear reaction includes a collision between two nuclei, these correspond to a second order rate law. The cross section is defined by (Vértes et al. 2010):

$$\sigma = R/I \tag{3.4}$$

Where:

σ = the cross section,

I = the number of incident particles per unit area, and

R = the number of reaction per unit time per nucleus.

Generally, the probability of a reaction is extremely dependent on the energy of the projectile, in addition to what the projectile is.

A different amount of interest is the microscopic cross section, defined as the produce of n; it is number of atoms per volume and cross section. A beam of a given form of particle can induce a lot of various types of nuclear reaction in a particular target (Kox et al. 1987), so that it is means if the material contains various kinds of objects (i) then the probability to interact is only the summing ($\sum$) of the probability on each type. Summing is related to the microscopic cross section (σ) by the relationship shown below (Handbook 1993).

$$\sigma_{tot} = \Sigma_i \ \sigma_i \tag{3.5}$$

In addition, there are different types of cross section (Nuclear Reactions Some Basics; (https://facultystaff.richmond.edu/~ggilfoyl/research/nuclearCrossSections.pdf):

1- Total cross section (σ): detect reaction products in 4π.

2- Differential cross section or angular distribution ($d\sigma/d\theta$): detect only reaction products emitted at θ in a solid angle $d\theta$. The unit of it is (mb/sr).

3- Double differential cross section ($d^2\sigma/dE.d\theta$): is proportional to the number of incident probe particles scattered within an energy range $\mathbf{\Delta}E$ and momentum variation into a solid angle $\mathbf{\Delta}\theta$. The unit of the double differential cross section is (mb/MeV.sr).

4- Triply differential cross section: The formula for (3He (e,eʻ,p) 2H) is [d5σ/dθeʻ. dθp.dEʻ]. The unit of this type is (mb/MeV.sr^2).

3.6. Spallation

3.6.1. The Historical Note About Spallation Reaction

At the beginning in 1930's the particle cascades in cosmic ray interactions was observed. At the earth's surface (Rossi 1933), the thermal neutron flux density outputted by cosmic ray-protons is nearly amount 10^{-4} to 10^{-3} neutrons cm^{-2}/s (Masarik , Kim and Reedy 2007). BB. Cunningham at Berkeley in 1947 discovered the first accelerator driven spallation reactions (Cunningham et al. 1974). Then theoretical characterization was given quickly after by Serber (Serber 1947). In the same year Sullivan WH and Seaborg GT invented the term "spallation" (Harvey 1959).

Spallation reactions have been studied for a lot of years, but it has not been exactly explained yet. They are being studied with the rising utility in the last two decades, as the spallation applications require additional exact knowledge.

Spallation neutron sources are of utility for; (1) transmutation of long lived actinides, (2) fission production from nuclear waste (Bowman et al. 1992), (3) plutonium from nuclear weapons (Krása 2010), (4) thorium as an energy source (Carminati et al. 1993), (5) material research and industry (Mason et al. 2005), or medicine for radiotherapy (Angelone Atzeni and Rollet 2002).

3.6.2. Spallation Reaction

The spallation reactions are one sector of the nuclear reactions. It is a practicability in which a light projectile like, proton, neutron and or light nucleus with the kinetic energy from a number of hundreds of MeV to several GeV interacts with a intensive or heavy nucleus for instance, pb while causes the emission of a big number of hadrons (especially neutrons) or fragments. Spallation reactions play a significant role in a broad field of applications for instance, simulation of detector set-ups in nuclear also particle physics experimentation, neutron sources for basic science, radioactive ion beam and material radiation otherwise ADS (David et al. 2011).

In 1974 at the University of California occurs early study of spallation reaction (Brobeck et al. 1947). Furthermore, a spallation reaction has three stages (Cugnon 1993): (1) intra nuclear cascade, (2) pre-equilibrium stage, and (3) evaporation or fission, (2) and (3) called Deexitation, as shown in schematic view in Figure 3.3 of spallation reaction.
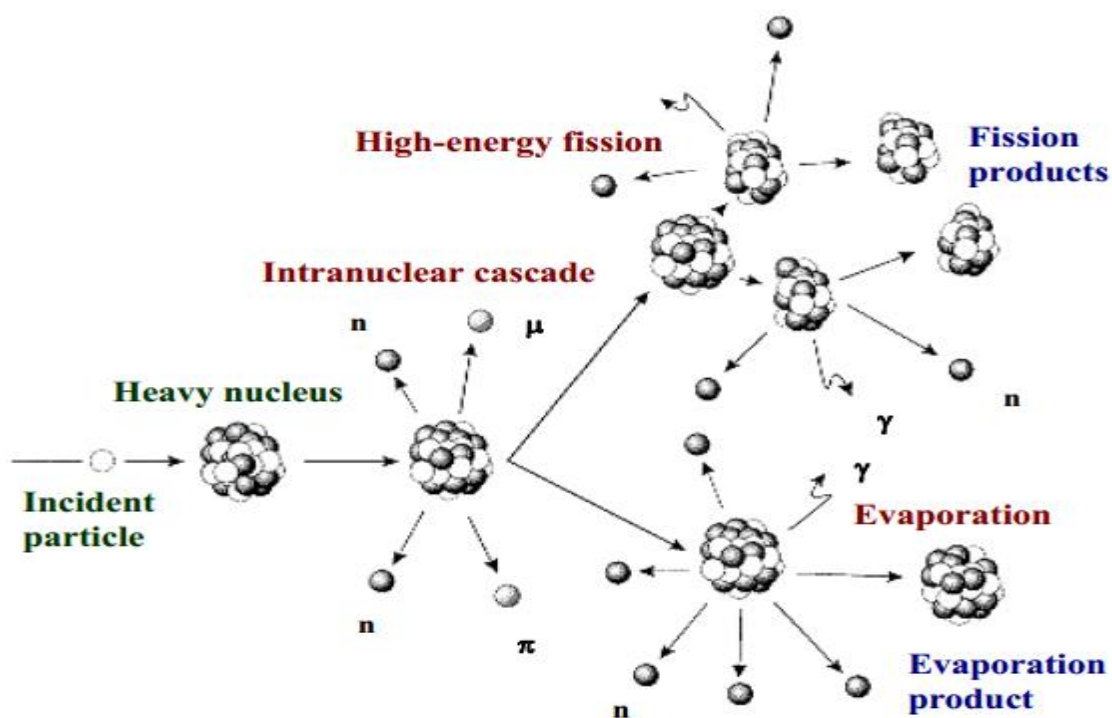
Figure 3.3. The scheme of a spallation reaction (Krása and Rez 2010)

3.6.2.1. Intra Nuclear Cascade (INC)

The Intra Nuclear Cascade process is foundation on the ideas of Heisenberg and Serber, who viewed intranuclear cascades as a sequence of consecutive quasi-free collisions of the quick main particle with the individual nucleons of the nucleus. It is a speedy direct step (nearly amount 10^{-21} s), illustrated in Figure 3.4. As the reduced de Broglie wavelength nearly amount ($\sim 10^{-1}$ fm), if the energy of proton is nearly amount (~ 1 GeV). All interactions take place only between nucleons if the process at low projectile energies, for example nearly amount (~ 100 MeV), then the process is called nucleon cascade. When incident particle energy rising in a gradual way, then the threshold energies for particle produce in nucleon-nucleon impact are being exceeded.

At beginning, pion is coming at energies of about hundreds of MeV, subsequently at larger energies nearly amount 2 to 10 GeV, heavier hadrons are being produced. It can ability also contribute in the intra nuclear cascade and interact between every other, which was called hadron cascade. Particles that acquired energy height sufficient to fleeing from the nucleus are being emitted fundamentally in the direction of the incident particle. The rest of the energy is equally distributed between nucleons in the nucleus which is left in an extremely excited status. The intra nuclear cascade (INC) is not stridently separating from the equilibrium decay.

In a pre-compound step (lower than 10^{-18} s), also the pre-equilibrium emission can happen. During this stage, speedy particles or fragments perhaps emitted after all interaction among the incident or other cascade particle and a nucleon inside the nucleus. The energies of particles emitted during the equilibrium decay are lower than the energies of pre-equilibrium particles.
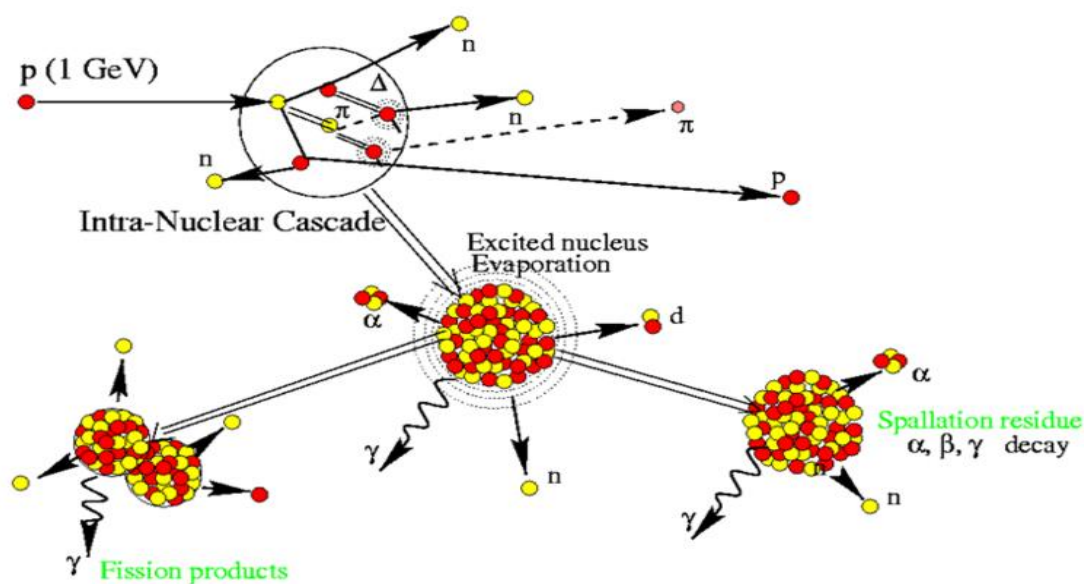
Figure 3.4. schema of Intra Nuclear Cascade (Krása 2010)

3.6.2.2. Deexcitation

After the intra nuclear cascade, the equilibrium stage comes up. Energy is evenly distributed over the nucleus that is in an extremely excited state with small angular momentum. Evaporation of neutrons or light charged fragments are caused for loses nucleus energy (Adair 1954).

Competitive process to evaporation is fission (into two fragments identical in proton number). Fission production as well undergoes evaporation (depending on their excitation energy). When the nucleus does not have to energy sufficient to emit neutrons (its binding energy becomes bigger than the excitation energy), it deexcites by β-and γ-transformations.

Finally, two sections of main important in spallation reactions are: residual nuclei or (spallation products) and emitted neutrons or (spallation neutrons) (Krása 2008).

3.6.3. Spallation Products in Nuclear Reaction

For the duration of the spallation process without neutrons also protons and other light nuclei are emitted from the excited nuclei (Bauer 2001). On the other hand, spallation products spread out in two regions of the table of the nuclides: (1) the heavy proton remains produced from evaporation; it is called spallation evaporation products. (2) The medium mass remains produced from fission, it is called spallation fission products.

The spallation products enable measured utilizing two procedures: direct kinematics (Titarenko et al. 1998), (Michel et al. 1997), or inverse kinematics (Enqvist et al. 2001).

3.6.3.1. Direct Kinematics

In direct kinematics process, a relativistic light projectile hits a heavy target. Using Mass spectrometry and γ- spectroscopy for detected the spallation products which stop in the target. This process has the prospect to measure the productions of the meta-stable states of remaining nuclei, which is able to utilize radioactive targets, and it wasted minimal beam time. However, it is impossible to measure the yields of (extremely long-lived, stable, and very short-lived nuclei, and the off-line outputs) measurements are more time consumption (Krása 2008).

3.6.3.2. Inverse Kinematics

In the process of inverse kinematics, a relativistic heavy nucleus hit a light target. The spallation products desertion the target in forward direction and can be recognized instantly in flight utilizing the suitable technique. [Example, the magnetic spectrometer FRS "Fragment Separator" (Geissel et al. 1992) equipped with an energy degrader, multiple-sampling ionization chambers, multi-wire proportional counters, two position scintillator detectors] can be specified directly in flight.

3.6.4. Pre-equilibrium in Nuclear Reactions

Pre equilibrium reaction is not direct reaction or compound nuclear reaction however in some cases it is likely for particles to be emitted after the first stage of a nuclear interactions but before the realization of statistical equilibrium or compound nucleus forming. Statistical decay of the compound nucleus and the instant emission after collision is neither by emission of particles from the excited target nucleus in pre-equilibrium reactions. Also, the emission of a particle by the target nucleus occurs is not instantly after the collision or by the statistical decay of the compound nucleus.

The projectile splits its energy between a small numbers of nucleons in the target. The hitter nucleons start a cascade of reactions in the target, at the course of which a particle can be emitted (before the compound nucleus has arrived at a case of statistical equilibrium). The pre-equilibrium effects beginning evidencing themselves at energies approximately 20 MeV, and at excitation energies over 50 MeV their contribution starts becoming important. It is supposed that every probable methods of distribution of the excitation energy among every various particle-hole arrangements with the equal exciton number have equal possibility to happen. Also, the pre-equilibrium models are very essential instrument to analyze and understand nuclear reactions at excitation energies ranging from several tens of MeV above to the GeV regions (Getachew G. 2011). On the other hand, nuclear reaction models based on semiclassical, also totally quantum mechanical theories are suggested for pre - equilibrium emission mechanism (Bethe 1937).

Several of the significant semiclassical models are (Bethe 1937):

1- Intranuclear Cascade Model (INCM)

2- Exciton model

3- Hybrid and Geometry Dependent Hybrid model (GDH)

4- Index Model

3.6.4.1. Intranuclear Cascade Model (INCM)

In 1947 Serber was proposed the first intra-nuclear cascade model (INCM) (Serber 1948) also it is the initial nuclear reaction model that included pre - equilibrium emission. The first computation of pre-equilibrium angular distributions was completed by this model utilizing the quasi-free scattering inside the nucleus. Figure. 3.3, shown the graphic explain the (INCM).

Intranuclear Cascade Models (Gudima, Mashnik, and Toneev 1983), (Bertini 1963), (Yariv and Fraenkel 1981), (Boudard et al. 2002) characterizing interactions among an impinging particle and target nucleons throughout intranuclear cascade as a series of binary collisions separated in space and time. This is proper if a mean free path of the incident particle in the target nucleus is greater than the inter-nucleon lengths then the incident particle wavelength is smaller than a mean distance among nucleons of the target nucleus. The path among collisions is given to be linear.

The collisions progress until an appointed degree of equilibrium is arrived. The standard utilized in the Intra-Nuclear Cascade Model (INCM) of Cugnon (INCL4) is an empirical time of equilibrium (so is called cutoff time, is nearly equal to $T_{cut} \approx 30$ fm/c that permits five consecutive nucleon-nucleon interactions on the average), which was deduced from a clear change of the studied quantities (Pienkowski et al. 1994). The Intra-nuclear Cascade Model in CEM03 is founded on the standers version of the Dubana cascade model (Barashenkov and Toneev 1972). The CEM03.1 code utilizes a standard for the escape of a primary particle from the cascade stage by the effective native optical potential $W_{opt.mod}(r)$ determined from the native interaction cross sections, including the blocking effects because of the Pauli Exclusion Principle. The Intra-Nuclear Cascade model (INCM) is a factual model but in general; the model forecasts are not satisfying at backward angles and in several forward angles also. To determine the secondaries produced in the interaction and calculate the momenta of the particles utilizes process classes and model classes. (Getachew 2011). The momenta of the two nucleons contributing in the absorption are chosen at random from the Fermi distribution and the pion energy is distributed evenly among these nucleons in the center of mass system of the three particles contributing in the absorption (Mashni 2005).

To sum up, the fundamental steps of the INC model are abbreviated are (Getachew 2011):

1- The space point at which the incident particle enters the nucleus is chosen uniformly above the projected region of the nucleus.

2- Total cross sections particle-particle and region-dependent nucleon densities are utilized to select a trajectory length for the projectile.

3- The kind of reaction, the momentum of the struck nucleon and the four momentums of the reaction outputs are determined.

4- If the Pauli Exclusion Principle permits and $E_{cut\ off} < E_{particle} = 2$ MeV, step (2) is performed to transmit the products. Then the exciton model updated as the cascade proceeds.

3.6.4.2. Exciton Model

The Exciton model is offered and first introduced by Griffin in 1996 and later modulate by many researchers. The number of excited particles and holes (the excitons) at any phase of the nucleon-nucleon cascade, in the Exciton model it is called the compound nucleus states. In that model the equilibration among target and projectile is accomplished by the series of nucleon-nucleon interactions (Nigussie 2012). The initial configuration is unchanging by the nature of the projectile. For example in case of a nucleon induced reaction, it is a two particle (2p) one hole (h) configuration because of the interaction of the incident nucleon with a nucleon of the target which is excited from a state below to a state on top of the Fermi energy. Where p is the number of particles and h is the number of holes, then the exciton number (n) is describe by n = p+h.

An excited nucleus is considered as a gas of quasi particles i.e., particle-hole degree of freedom is incorporated. In this the nuclear potential is shown with evenly spaced singular particle levels, i.e., levels whose occupancy is each 0 or 1. At first the target nucleus is in ground state. The projectile nucleon enters the target nucleons with a given energy and form a one particle (p=1) without hole (h=0) state, i.e., a state with exciton number n = 1. At this phase, the projectile has entered the nuclear force field but has not been absorbed by the target.

It is still in the entry channel and the field of nuclear force can be left with out of interaction with any individual target neuelion. As every the levels under the Fermi energy are filled, the first interaction among the projectile and target nucleon will raise the later on top of the Fermi energy and go away a hole below. The absorption of the projectile nucleon by the target leads to the configuration of n = 3 exciton state, it is means a 2p-1h state is formed (Koning, Hilaire and Goriely 2013). After configuration of the n = 3 exciton state any of the excited particles perhaps emitted if it has due energy to escape. If but, particle emission does not occur; consequently there will be a extra two body interaction either between one of the two excited particles and a particle under the Fermi surface or between the two excited particles themselves. For this reason a two body interaction will lead to transitions in which the modification in the exciton number $\Delta n = \pm 2, 0$ (Getachew 2011).

3.6.4.3. Hybrid and Geometry Dependent Hybrid (GDH) Model

The intra-nuclear cascade (INC) computation outcomes indicated that the exciton model shortage resulted from a failure to satisfactorily reproduce enhanced emission from the nuclear surface. So as to provide a first order correction for this deficiency the hybrid model was reformulated. This model was redrafted and it was proposed by Blann and vonach (Blann and Vonach 1983).

The Hybrid Model preserves the physical transparency and ease of the exciton model while permitting the calculation absolute spectral produce as in the Harp-Miller-Bern (HMB) model. The continuum decay rates are calculated from the partial state densities while the intra-nuclear transmission rates are calculated from the mean free path of the nucleons in the nuclear matter. The mean free path, in turn, perhapes estimated either from free nucleon - nucleon scattering cross sections or from the imaginary part of the optical potential (Gadioli and Hodgson 1992). Furthermore, this model multi pre-equilibrium particle emission beside with equilibrium decay is considered while the spectra of emitted particles are computed for all steps in the energy dissipation process induced by the interaction among projectile and target nucleons.

On the other hand, the ability of the hybrid model of pre-equilibrium nuclear reaction to predict unidentified excitation functions and to perform alpha priori computations of nuclear reactions cross sections for a wide diversity of reaction sorts is an outstanding feature of this model. Other than, there are distinct dissimilarities in the quality of such computations depending on the type of bombarding particle and on the excitation energies of the reacting systems (Michel et al. 1985). The geometry dependent hybrid model is a variant of the hybrid model in which the nuclear geometry effects are considered.

In hybrid model computations the nuclear matter intensity is taken as consistent throughout the nucleus while the geometry dependent hybrid (GDH) model takes into calculation the reduced matter density and hence also the surface potential at the nuclear surface.

3.6.4.4. Index Model

Index model was developed by Ernst (Ernst et al. 1987), of independently interacting excitons, for pre equilibrium emission which unifies the exciton and hybrid models. The basic supposition of the index model is that every excited particle which survives emission experiences two - body collisions and generate further particle (p), hole (h) pairs independently from each other. Thus the energy of all exciton is shared by the three excitons of the subsequent phase.

The average nucleon - nucleon collisions rates and the interior energy in this model are possessed from the interaction rate of nucleons inside the nuclear matter. This model is not generally utilized as compared to exciton and Geometry Dependent Hybrid model (GDH) (Ernst et al. 1987).

3.7. Accelerator Driven System (ADS)

3.7.1. The Historical Notes About ADS and Transmutation

That the bombarding of uranium target by high-energy protons would generate major yields of neutrons studied by researchers in the 1940s. The neutrons output by these reaction could be utilized to produce fissionable material through nuclear reactions. Glenn Seaborg produced the first man-made plutonium in 1941, using an accelerator. In the period 1950-54, the Materials Testing Accelerator (MTA) program at Lawrence Livermore National Laboratory in California in 1950 (Heilbron et al. 1996) examined in detail the utilize of accelerators to generate fissionable material. Nearly at the same time as in Canada, Lewis realized the assessment of accelerator breeding in the power programmed and initiated spallation neutron yield measurements with the McGill cyclotron. The project ended in 1954 and the documents were declassified in 1957.

Lawrence et al, suggested to radiate different thick targets such as (U, Be and Li) by protons and deuterons to measure the cross-sections, neutron yields, and the feasibility of changing the fertile (depleted uranium or thorium) to produced or fissile material Pu^{239}, U^{233} respectively (Rubbia, Aleixandre and Andriamonje 2001). This was the first incentive, because the United States of America (USA) were dependent on overseas uranium sources. A few years later, the MTA project was stopped up when rich domestic uranium ores were found in the Colorado plateau. Over the coming decades, important investigations have been estimation to assess deficiencies in different transmutation modes. For instance, neutron yields and spectra in uranium targets radiated by relativistic protons (Tolstov 1989), (Vasil'kov et al. 1978) and nuclei (Voronko et al. 1991) and neutron cross-sections for a number of isotopes have been measured in JINR Dubna. At the end of 1980's at Japan Atomic Energy Research Institute (JAERI) has started the first fully conceptual and complex research of the radioactive waste transmutation.

Later studies from 1975 to 1988 on the Fertile-to-Fissile transformation (FERFICON) Program - a cooperating attempt with different laboratories - researched the energy dependence, able to 800 MeV, of the fertile-to-fissile transformation capacity utilizing incorporated target materials and geometries (Rubbia, Aleixandre and Andriamonje 2001).

Option Making Extra Gains from Actinides and Fission Products (OMEGA) it is A long-term program for examine and development on nuclide partition and transmutation technology (Mukaiyama 2003). From the beginning of 1990's the OMEGA program which initiated the global interest in transmutation topic. A detailed concept of the Accelerator Transmutation of Waste (ATW), utilizing thermal neutrons have been created by Bowman C, from Los Alamos National Laboratory (LANL), also he proposed the utilize of a linear accelerator with a high-intense proton current nearly amount to ($\sim$ 250 mA) of 1.6 GeV energy (Bowman et al. 1992). From European Council for Nuclear Research (CERN), C.Rubbia suggested a basic concept of the Energy Amplifier, also called Accelerator Driven Energy Production (ADEP) (Carminati et al. 1993) illustrated in Figure 3.5. The stimulus for ADEP is comparable as for the MTA project. This conception is based on the utilize of Th^{232} as a fuel for the produce of fissile U^{233} (Krása 2010), it seen by this equation

$$n + ^{232}Th \xrightarrow{\gamma} {}^{233}Th \xrightarrow[22\,m]{\beta^-} {}^{233}Pa \xrightarrow[27\,d]{\beta^-} {}^{233}U$$
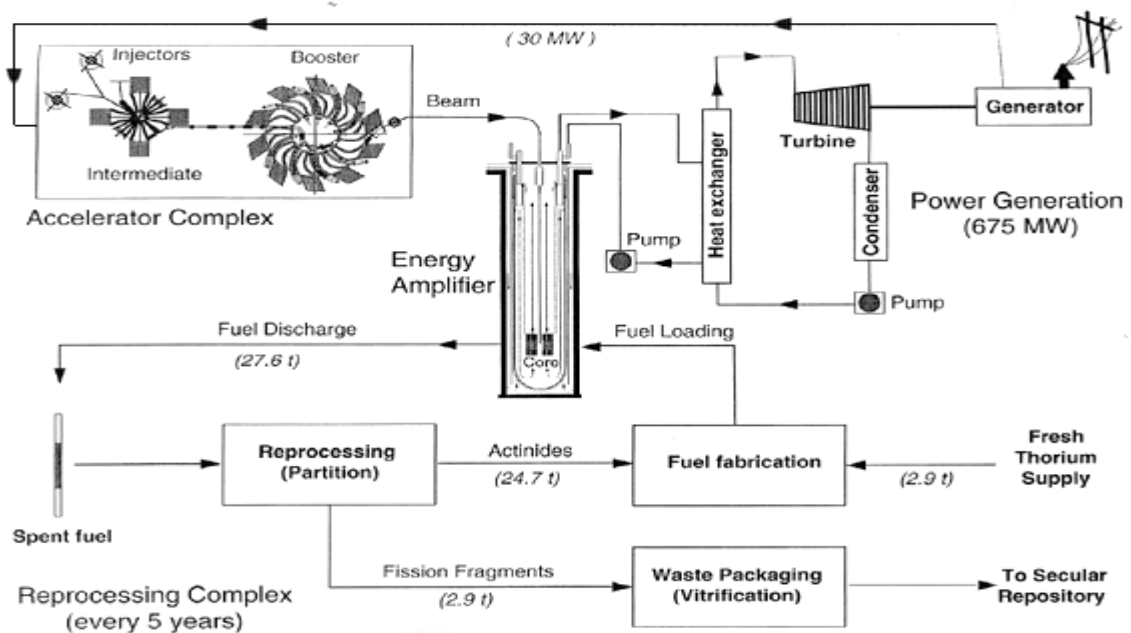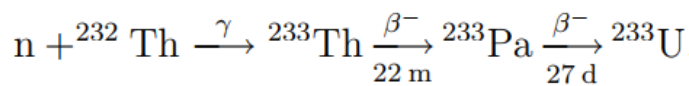
Figure 3.5. Fast energy amplifier (General lay out of the Energy Amplifier complex) (Rubbia et al. 1995)

3.7.2. Nuclear Transmutation

In 1919 Ernest Rutherford, demonstrated transmutation, as the first, on instance of 14N + α →17O (Rutherford 1919). Afterward demonstrate the first accelerator-driven transmutation in 1932 by J. D. Cockroft and E. T. S. Walton . They bombarded (Li) target with (125 to 500) keV protons (from linear accelerator) and "transmuted" Li-nucleus into two α-particles (Cockcroft and Walton 1932).

Nuclear transmutation is a process where in the structure of an atomic nucleus changes. The nucleus physics properties are change when changing the number of neutrons such as, activity, half-life and radiation energy. However, when changing the number of protons, the nucleus obtains also different chemical properties for instance, chemical coupling and reaction rate (Krása 2008).

The main advantage of transmutation is a reduction in the minor actinide and long lived fission product content of the High-level waste (HLW). The first and most efficient stage to decrease the total mass of the High-level waste is the transmission from an Light water reactor (either pressurised or boiling) once-through strategy with immediate elimination of the fuel elements to a plutonium burning strategy with High-level waste (HLW) vitrification. Compared with the latest, transmutation strategies have only an unassuming mass reduction potential. While the radiotoxic nuclides in the High-level waste (HLW) are able to only partly be eliminated, transmutation does not make geologic elimination concepts extra, however must be careful as a complementary waste management method which might ease the design and licensing requirements for geologic depository because the geosphere barrier would no longer have a significant safety function.

Transmutation aims at decreasing the radiological impact of actinides and fission products in the High-level waste by nuclear transmutation of trouble some long-lived nuclides in strong radiation fields. (NEA Nuclear Science Committee 2002).

It seems that, suitably induced transmutations could be utilized to reduce the half-lives of long-lived a radioactive isotopes (Table 3.1) included in the high level waste that is being generated during the nuclear fuel burn up in nuclear reactors.

Produced the radioactive nuclei during the operation of nuclear reactors in two ways: Fission products and higher actinides (Krása 2008).

Table 3.1. Fission products and higher actinides consist of in nuclear burnt up fuel, which are predictable for transmutation. The quantities are yearly waste production (after 10 years of decay) from a typical commercial reactor (3 GW power, with fuel burnt to 33 GW days per ton with the yearly removal of 33 metric tons uranium equivalent of spent fuel per year) (Bowman 1992)

Fission product	Half-life [years]	quantity [10^{23} atoms]	Activity [Bq]
Se^{79}	1×10^6	13	3×10^{10}
Sr^{90}	30	900	7×10^{16}
Zr^{93}	2×10^6	1500	2×10^{12}
Te^{99}	2×10^5	1500	2×10^{13}
Sn^{126}	1×10^5	46	1×10^{12}
I^{129}	2×10^7	270	4×10^{10}
Cs^{137}	30	1400	1×10^{17}
Higher actinide	Half-life [years]	quantity [10^{23} atoms]	Activity [Bq]
Np^{237}	2×10^6	366	4×10^{11}
Am^{241}	400	413	2×10^{15}
Am^{243}	7×10^3	73	2×10^{13}
Cm^{244}	20	13	2×10^{15}
Pu^{238}	90	113	3×10^{15}
Pu^{239}	2×10^4	4160	4×10^{14}
Pu^{240}	7×10^3	1920	6×10^{14}
Pu^{241}	10	640	1×10^{17}
Pu^{242}	4×10^5	390	2×10^{12}

3.7.2.1. Fission Products

Fission products are being produced by the fission of U^{235} or Pu^{239} in classical or quick nuclear reactors so are mostly slightly over the line of β-stability. To transform them to stable nuclides, they should capture one or more neutrons and then go through β-decay (Krása 2010).

3.7.2.2. Higher Actinides

To transmute higher actinides to stable nuclides, they must undergo neutron capture and in order fission, which is a process that generates energy and makes the transmutation attractive from the point of view of energetic. On the other hand, higher actinides, representing about one per cent of spent fuel, are being generated by the neutron capture within nuclei of U^{235}, U^{238}, or Pu^{239} and their resulting β-decays (Krása 2010).

3.7.3. Accelerator Driven System (ADS)

The Accelerator Driven System is a modern form of nuclear reactor which produces energy even though it residue sub-critical during its life. Every operating reactor in the world is "critical" reactors, which denote that the number of neutrons generated by fission is precisely balanced by the number absent by leakage and absorption by different materials in the reactor. This balance is accountable for maintaining a constant reactor power at any required level. Sub-critical reactors output a small number of neutrons via fission than are lost by absorption and leakage, and require an external supply of neutrons to preserve a constant reactor power. Interaction of a high energy proton beam with a heavy atom nucleus like lead, it is caused of comes the external neutron supply, and this process in nuclear physics is called spallation. The power level in an Accelerator Driven System (ADS) is bigger for stronger external sources and for reactors which are nearer to "critical". (Nifenecker, Meplan and David 2003).

Cyclotrons, high-energy accelerators or high-current are able generate neutrons from heavy elements by spallation. A number of investigate facilities exist which explore this phenomenon, and there are plans for much bigger ones. In this process, a beam of high-energy protons usually bigger than to 500 MeV is directed at a high-atomic number target such as, depleted uranium, tungsten, tantalum, thorium, lead and mercury and up to one neutron can be outputted per 25 MeV of the incident proton beam. (These numbers contrast with 200 to 210 MeV out by the fission of one uranium-235 or plutonium-239 atom). A 1000 MeV beam will make 20 to 30 spallation neutrons per proton (World Nuclear Association 2014).

Additionally, can be described neutrons produced in spallation reactions by heir energy and spatial distributions and multiplicity. The neutron multiplicity ought to decide the current and beam energy of the proton driver accelerator as their energy and spatial distribution forms the geometry of the spallation target and the protecting to high-energy neutrons (Armbruster and Benlliure 2001). Also, the spallation neutrons have only an extremely very small probability of causing extra fission proceedings in the target (Rhodes 2013). Produced residual nuclei and neutrons also by spallation reactions that are means the Spallation reactions do not only produce neutrons. Mainly of these nuclei are

radioactive. Furthermore, the residual nuclei will contribute to the rust and the corrosion and to the radiation damages in the target, accelerator window and structural materials (Armbruster and Benlliure 2001).

The produce neutrons in the spallation reactions have huge potential in research such as, in energy production, in medical industry, in earth and in space. However, the risk of radioactive waste emerging from nuclear energy production is a subject of continuous discussion and public concern in a lot of countries (Hossain, Taher and Das 2015).

Transmutation of extremely radioactive nuclear waste can be carry out utilizing an accelerator driven system (ADS), when the spallation target impact by high energy protons then produce neutrons. These neutrons are multiplied in a sub-critical core, whereas together fissioning the minor actinides at stable nuclides or short-lived nuclides (Shetty 2013).

The accelerator driven system has recently getting raised interest because of its potential to get better the flexibility and safety Properties of transmutation systems (Hossain, Taher and Das 2015). A subcritical reactor is a nuclear fission reactor that generates fission without realizing criticality. Instead sustaining a series reaction, a sub-critical reactor utilizes extra neutrons from an outside source. Like a reactor coupled to a particle accelerator to output neutrons by spallation is called an Accelerator Driven System (Hossain, Taher and Das 2015).

Consequently, a sub-critical reactor is driven by an Accelerator Driven System (ADS) to recompense for the loss of neutron economy which or else would have been self-sustaining in a critical reactor (Shetty 2013).

Transuranics (higher atomic number than uranium-92, such as "Berkelium" is a transuranic element, atomic number is 97) and mostly minor actinides have such adverse special that they drastically decrease the substantial features capable of moderating and stabilizing the series reaction. Great rewarding exists subsequently, to burn such fuels in dedicated innovative systems with "compact" safety features such in a sub-critical reactor.

There exist different strategies with respect to nuclear power in the member states of the EU. Whereas there are countries that consider nuclear power as a role to a sustained energy stipulation, there are others countries which have today a position aiming to phase out of nuclear energy. Moreover, in several countries plutonium will be recycled either in fast reactors or in thermal while in different countries plutonium is considered as a waste. Partitioning and Transmutation utilizing ADS can play an important role.

The following are essential fundamentals for the development of ADS for the task expects (Kadi and Revol 2001).

1- A greatest beam power in this range of (12 to 40) MW (characteristically a current of 12 to 40 mA of protons at 1GeV) also a spallation target accepting up to 40 MW of thermal power is necessary for an industrial model to be built and operated approximately around 2030. This will agree to use of ADS with a power of (500-1500) MWth starting around 2040.

2- A dedicated fertile free fuel and regarding fuel cycle will be advanced by 2025. ADS prepared with that fuel will have the ability to burn about 12×10^4 g TRUs per TWh$_e$ which is equal to 10^6 g TRUs per GW$_e$ a (nearly around one years).

3.7.4. The Concept of Accelerator Driven System (ADS)

The concept of accelerator-driven systems (often called hybrid systems) comes together a particle accelerator with a sub-critical core. Most suggestions suppose proton accelerators, bringing continuous-wave beams with an energy around 1 GeV. The accelerator is both a linear accelerator (linac) and a circular accelerator (cyclotron). High-power accelerators have been under continuous development, and the building of machines with the necessary specifications (OECD Nuclear Energy Agency 2002).

The protons are inserted upon a spallation target to produce source neutrons for driving the sub-critical core. The target is made of heavy metal in liquid or solid state. Spallation reactions in the target produce a few tens of neutrons per incident proton, which are put in at the sub-critical core to stimulate more nuclear reactions. Excepting for the subcritical state and the core is quite comparable to that of a critical reactor. It can be designed to operate with a fast or thermal neutron spectrum (Shetty 2013).

The energy transformation portion of an accelerator driven nuclear power system is comparable to that of a normal power plant. However, the electrical energy which is recycled to the accelerator reduces the net electrical efficiency of the system in the accelerator driven system. For an Accelerator Driven System with a neutron multiplication factor of 0.95, the decrease amounts to around 12%. This means that the accelerator driven system produces about 14% more high-level waste and refuses about 20% more heat to the atmosphere than a normal power plant with the same net electrical produce (NEA Nuclear Science Committee 2002). Subcritical reactor uses for generated the electric energy as shown in (Figure 3.6).
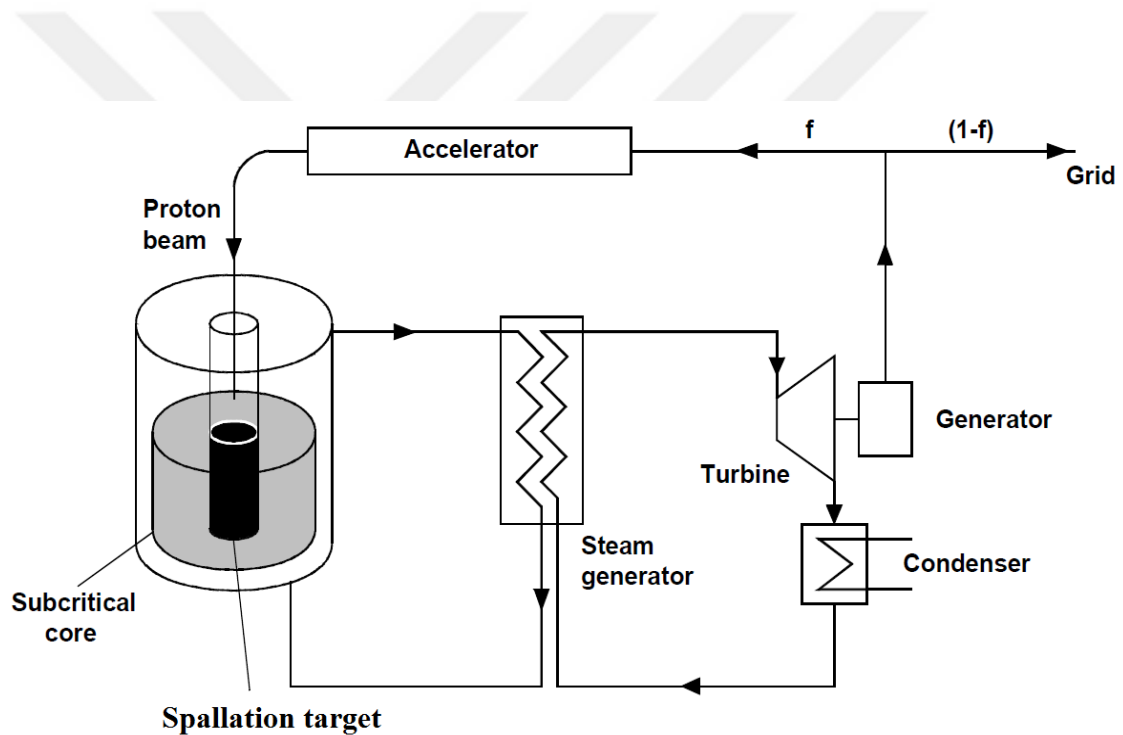
Figure 3.6. ADS based electric energy generation (NEA Nuclear Science Committee 2002)

4. RESULT AND DISCUSSION

4.1. Calculation Method

In the present study, the reaction double differential cross section $d^2\sigma/dE.d\theta$ of intensive elements were calculated by using nuclear reaction models such us; (equilibrium, pre-equilibrium). Excitement functions of double differential cross section $d^2\sigma/dE.d\theta$ for elements Thorium and Boron was calculated using CEM03.01 program. Theoretical calculations of double differential cross section $d^2\sigma/dE.d\theta$ prophesy that most probable energy proton were fundamentally emitted from compound nucleus mechanism while higher energy protons were mainly emitted due to pre-equilibrium and direct reaction mechanism.

The present study describes calculation of the double differential cross section of the secondary particles (n, p, α) occurring after spallation in the reactions p + $_{90}$Th^{232} and p + $_{5}$B^{10}. Nuclear model calculations are a major attention in nuclear reaction programmes, especially with regard to their predictive power in event of unknown double differential cross sections $d^2\sigma/dE.d\theta$.

In this study, $_{90}$Th^{232} and $_{5}$B^{10} bombardment by the accelerated proton at different energies is utilized by several energy range randomly. For instance, p + $_{90}$Th^{232}, (p, α) was used in the ranges (20-500) MeV and for that reaction p + $_{5}$B^{10}, (p, α) was used only at 660 MeV. On the other hand, for p + $_{5}$B^{10}, (p, n) reactions passed out in the (30, 50 and 186) MeV proton incident energy range. In this study, also all reactions were used at many angles for the calculations such as; CEM03.01 codes.

In addition, compared d2σ/dE.dθ for $_{90}$Th^{232} and $_{5}$B^{10} in the p + $_{90}$Th^{232} and p + $_{5}$Th^{10} reactions for (p, n), (p, α), (p, ṕ) forms at 360 MeV with various angles (0^0, 20^0, 40^0, 60^0) respectively.

4.2. CEM03 Computer Program

CEM03.01 is the most modern computer program in a sequence of codes include CEM97, CEM2k+GEM2, and CEM95. It is an prolonged and gets better version of the previously codes, which perform versions of the Cascade-Exciton Model of nuclear reactions. This program considers Intra Nuclear Cascade, preequilibrium, fission, evaporation and Fermi Break-up mechanisms of nuclear reactions as well as coalescence of complicated particles up to Alpha(α) from speedy INC nucleons.

This computer program measures total reaction and fission cross-sections, nuclear facilities, excitation functions, nuclide distributions (yields) of all generated isotopes separately. Furthermore, to their (A) and (Z) distributions, energy and double-differential cross-sections, angular spectra, mean multiplicities, i.e. the numeral of ejectiles per inelastic interaction of the projectile together with the target, ejectile yields and their mean energies for p, n, d, t, 3He, α, $\pi+$, π-, and π^0. By modifying an input changing, evaporation of as many as sixty isotopes heavier than α (up to ^{28}Mg) perhaps also modeled. Beside that, CEM03.01 provides in its output separately the yields of Backward and Forward created isotopes, their denote kinetic energies, Z and A distributions of the mean emission angle, their parallel velocities, and the Forward/Backward ratio of commonalty products in the laboratory system, distributions of the indicate angle between two fission spall of momentum and angular momentum , of neutron multiplicity, of the excitation energy, and of mass and charge numbers of residual nuclei after the Intranuclear Cascade and preequilibrium stages of reactions, as well as for fissioning nuclei before and after fission.

CEM03.01 calculates reactions produced by nucleons, pions, bremsstrahlung and monochromatic photons on not too light targets at incident energies nearly from ~10 MeV (~30 MeV, in the case of γ + A) up to various GeVs. (Mashnik et al. 2005). The Cascade-Exciton Model of nuclear reactions was suggested firstly at the Laboratory of Theoretical Physics (Ganesan 2007) to describe average-energy spallation reactions yield by nucleons and pions. It was determined on the Dubna IntraNuclear Cascade and the Modified Exciton Model (Kadi 2001) and (Barros 2010).

4.3. Reactions

4.3.1. p + $_{90}$Th^{232} Reaction

Thorium is a chemical and radioactive element by indication (Th) and atomic number 90. That occurs naturally in low condensation about ten parts per million in the earth's crust. Thorium in also unmixed appearance is a silvery heavy metal which is about intense lead (pb). In nature, approximately all thorium is $_{90}$Th^{232}, as the same time as several additional isotopes could be present in small quantities. The half-live of thorium-232, the isotope of most concern, is very long. Thorium-232 is present in soil and ore in temporal equilibrium with radium.

The main use of thorium has been in the preparation of the Welsbach cloak for portable gas lanterns. It was an important mix up element in magnesium which used to mantle tungsten wire for components of electronic tools, while it was used for more ways. Thorium can also be used as a fuel in nuclear reactors.

However, Th itself was not fissile, it convert into the fissile isotope U-233 onto absorption of a neutron. Thorium is mostly a health hazard only if it uses into the body. External gamma disclosure was not a great concern because thorium emits only a small quantity of gamma radiation (http://hpschapters.org/northcarolina/NSDS/thorium.pdf). In this study, the thoriuom element using for p + $_{90}$Th^{232} Reaction formation by CEM03 program.

In that reactions, at different energies the double differential cross section with the all forms cross section with the same mass number were calculated also thoughtful that result by CEM03 program and compared so as to result with experimentally measured values.

4.3.1.1. Alpha Double Differential Cross Section for p + $_{90}$Th^{232} Reaction at E$_p$=20 MeV; θ= 60^0

The double differential cross sections d^{2}σ/dE.dθ of emission (alpha, neutron and proton) particle for p + $_{90}$Th^{232} reactions are calculated by CEM03 code program.

The calculate double differential cross section d^{2}σ/dE.dθ of alpha emission for p + $_{90}$Th^{232} at 20 MeV incident energetic protons are illustrative in the Figure and Table 4.1., respectively. The shape of calculate results curve of double differential cross section (d^{2}σ/dE.dθ) for alpha emission at this energy for four steps (Total, Cascade, Precompound and Evaporation) are different at angle 60^0. The form of calculate results curve are nearly similar to total and precompound.

On the other hand, the evaporation increases together with increases alpha energies emission. However, the cascade in this case not shown because, all results are zero, the incident proton energy is smaller to target element, has large mass number.

Additionally, number of elastic interactions and number of inelastic interactions are (341590 and 1000000), respectively. While, reaction cross section and elastic cross section are about (1477.87 and 504.82 mb), respectively.

Table 4.1. Alpha scattered double differential cross section (mb/MeV.sr) for p + $_{90}$Th^{232} reaction

^{232}Th(p, α); E$_p$=20 MeV; θ= 60^0 CEM03 - Code			
E$_α$(MeV)	Total	Precompound	Evaporation
	Double differential cross section (mb/MeV.sr)	Double differential cross section (mb/MeV.sr)	Double differential cross section (mb/MeV.sr)
22	0.001	0.001	0.000
24	0.008	0.008	0.000
26	0.005	0.005	0.000
28	0.003	0.001	0.002

Figure 4.1. Double differential cross section (mb/MeV.sr) of the alpha generated as a result of bombardment of element $_{90}Th^{232}$ with 20 MeV energetic protons and $\theta= 60^0$ degree

4.3.1.2. Alpha Double Differential Cross Section for p + $_{90}Th^{232}$ Reaction at $E_p=20$ MeV; $\theta= 60^0$, Compare between CEM03 and Experimental Data

Figure 4.2. Shows that the comparison of calculated double differential cross section of alpha emission with experimental data at the incident proton energy 20 MeV with angle 60^0 degree. For $^{232}Th(p, x\alpha)$ reaction the pre-equilibrium calculations (cascade- exciton CEM03 and hybrid models) are in good agreement with the measurements. However, the experimental data and CEM03 have an inconsistency at energies 20 MeV Figure 4.2.

Also, the higest value in CEM03 code program is 0.008 at 24 MeV but in experimental data the highest value is 0.089 at 25.511 MeV. However, the lowest value in CEM03 code program is recording as 0.001 at 22 MeV but in experimental data the lowest value is about 0.001 at 29.953 MeV.

Table 4.2. Alpha scattered double differential cross section (mb/MeV.sr) for p + $_{90}$Th^{232} reaction

^{232}Th(p, α); E_p=20 MeV; θ= 60^0, Total Double Differential Cross Section (mb/MeV.sr)		
$E_α$(MeV)	CEM03 – Code	Experimental E_p=20 MeV; θ= 60.25^0, (Milazzo-Colli, Braga-Marcazzan and Milazzo 1975)
21.28	...	0.019
21.54	...	0.023
21.93	...	0.021
22.00	0.001	...
22.00	...	0.025
22.51	...	0.039
22.94	...	0.047
23.02	...	0.029
23.54	...	0.038
23.97	...	0.051
24.00	0.008	...
24.04	...	0.044
24.55	...	0.064
24.98	...	0.040
25.05	...	0.076
25.51	...	0.089
25.94	...	0.061
26.00	0.005	...
26.02	...	0.084
26.51	...	0.067
26.99	...	0.051
27.04	...	0.055
27.10	...	0.036
27.50	...	0.061
27.93	...	0.044
28.00	0.003	…
28.01	...	0.044
28.52	...	0.027
28.57	...	0.023
29.05	...	0.006
29.55	...	0.015
29.62	...	0.005
29.68	...	0.005
29.82	...	0.002
29.95	...	0.001

Figure 4.2. Double differential cross section (mb/MeV.sr) of the alphas generated as a result of bombardment of element $_{90}Th^{232}$ with 20 MeV energetic protons and θ= 60^0 degree

4.3.1.3. Alpha Double Differential Cross Section for p + $_{90}Th^{232}$ Reaction at E_p=360 MeV; θ= 22^0

The double differential cross sections $d^2σ/dE.dθ$ of emission (alpha, neutron and proton) particle for p + $_{90}Th^{232}$ reactions are calculated by CEM03 code program. The calculate double differential cross section $d^2σ/dE.dθ$ of alpha emission for p + $_{90}Th^{232}$ at 360 MeV incident energetic protonsare illustrative in Figure 4.3 and Table 4.3. The results are showing different shapes of curve of the double differential cross section ($d^2σ/dE.dθ$) for alpha emission at this energy for four steps (Total , Cascade , Precompound and Evaporation) at angle 22^0. As can be seen in Figure 4.3 total double differential cross section with evaporation is increasing when alpha energies are increasing until the peack, after that each others are decreasing slightly when alpha energies are increasing. On the other hand, the cascade at the beginning of a graphic form is increasing with increasing of the alpha energy to reach the highest point. After it increases and decreases alternately with increasing alpha energy emitted.

Similarly, precompound is increasing by increasing of the alpha energy to reach the highest point after it, increases and decreases alternately with increasing alpha energy emitted. In addition, number of elastic interactions is 578028, number of inelastic interactions is 1000000, Reaction cross section is 1728.55 mb and elastic cross section is 999.15 mb.

Table 4.3. Alpha Scattered Double Differential Cross Section (mb/MeV.sr) for p + $_{90}$Th^{232} reaction

^{232}Th(p, α); E$_p$=360 MeV; θ= 22^0 CEM03 - Code				
E$_α$(MeV)	Total	Cascade	Precompound	Evaporation
	Double differential cross section (mb/MeV.sr)	Double differential cross section (mb/MeV.sr)	Double differential cross section (mb/MeV.sr)	Double differential cross section (mb/MeV.sr)
2	0.007	0.003	…	0.003
3	0.022	0.018	…	0.003
4	0.056	0.022	…	0.033
5	0.074	0.041	…	0.033
9	0.141	0.044	…	0.097
10	0.160	0.056	…	0.104
15	0.171	0.067	…	0.104
16	0.209	0.056	…	0.153
17	0.201	0.070	…	0.130
21	0.384	0.037	…	0.347
22	1.311	0.082	…	1.22
24	1.968	0.054	0.014	1.899
26	1.649	0.044	0.022	1.582
28	0.995	0.057	0.020	0.916
30	0.675	0.041	0.050	0.584
32	0.347	0.041	0.035	0.270
34	0.239	0.035	0.035	0.168
36	0.153	0.031	0.042	0.078
38	0.115	0.026	0.041	0.048
46	0.069	0.035	0.028	0.005
48	0.037	0.018	0.018	…
50	0.063	0.037	0.026	…
56	0.041	0.016	0.024	…
58	0.039	0.020	0.018	…
60	0.028	0.014	0.013	…
66	0.016	0.005	0.011	…
72	0.014	0.007	0.007	…
80	0.014	0.013	0.001	…
82	0.007	0.005	0.001	…
84	0.016	0.007	0.009	…
86	0.005	0.001	0.003	…
88	0.007	0.005	0.001	…

Figure 4.3. Double differential cross section (mb/MeV.sr) of the alpha generated as a result of bombardment of element $_{90}Th^{232}$ with 360 MeV energetic protons and $\theta= 22^0$ degree

4.3.1.4. Alpha Double Differential Cross Section for p + $_{90}Th^{232}$ Reaction at $E_p=360$ MeV; $\theta= 22^0$, Compare between CEM03 and Experimental Data

The comparison of calculate double differential cross section of alpha emission with experimental data at the incident proton energy 360 MeV with angle 22^0 degree are given in Figure 4.4 and Table 4.4. For $^{232}Th(p, x\alpha)$ reaction the pre-equilibrium calculations (cascade- exciton CEM03 and hybrid models) in good agreement with the measurements. However, the calculate results are also in good agreement with experimental data at energies 360 MeV Figure 4.4.

In addition, the higest value in CEM03 code program is 1.968 at 24 MeV but in experimental data the highest value is 1.39 at 110.9 MeV. However, the lowest value in CEM03 code program is 0.003 at 90MeV while in experimental data the lowest value is 0.81 at 239.1 MeV.

Table 4.4. Alphas Scattered Double Differential Cross Section (mb/MeV.sr) for p + $_{90}$Th^{232} Reaction

^{232}Th(p, α); E$_p$=360 MeV; θ= 22^0 , Total Double Differential Cross Section (mb/MeV.sr)		
E$_\alpha$ (MeV)	CEM03 – Code	Experimental E$_p$=360MeV; θ=22.5^0, (Iwamoto et al. 2009)
2.0	0.007	…
5.0	0.074	…
6.0	0.063	…
7.0	0.067	…
10.0	0.160	…
11.0	0.183	…
12.0	0.164	…
16.0	0.209	…
17.0	0.201	…
18.0	0.168	…
21.0	0.384	…
22.0	1.311	…
24.0	1.968	…
26.0	1.649	…
28.0	0.995	…
34.0	0.239	…
36.0	0.153	…
38.0	0.115	…
40.0	0.078	…
48.0	0.037	…
50.0	0.063	…
52.0	0.042	1.04
54.0	0.069	…
62.0	0.020	…
68.0	0.011	…
70.0	0.016	1.19
72.0	0.014	…
78.0	0.005	…
80.0	0.014	…
82.0	0.007	1.20
84.0	0.016	…
90.0	0.003	…
91.8	…	1.37
100.9	…	1.38
130.0	…	1.25
140.0	…	1.26
149.1	…	1.2
180.1	…	1.16
189.2	…	1.04
200.1	…	0.93
209.2	…	0.89
220.1	…	0.89
228.3	…	1.01
239.2	…	0.81

Figure 4.4. Double differential cross section (mb/MeV.sr) of the alphas generated as a result of bombardment of element $_{90}Th^{232}$ with 360 MeV energetic protons and $\theta = 22^0$ degree

.

4.3.1.5. Alpha Double Differential Cross Section for p + $_{90}Th^{232}$ Reaction at $E_p=500$ MeV; $\theta= 40^0$

The double differential cross sections $d^2\sigma/dE.d\theta$ of emission (alpha, neutron and proton) particle for p + $_{90}Th^{232}$ reactions arecalculated by CEM03 code program.

The calculate double differential cross section $d^2\sigma/dE.d\theta$ of alpha emission for p + $_{90}Th^{232}$ at 500 MeV incident energetic protons are showing in Figure 4.5 and Table 4.5. The shape of calculate results curve of double differential cross section $(d^2\sigma/dE.d\theta)$ for alpha emission at this energy for four steps (Total, Cascade, Precompound and Evaporation) are different at angle 40^0. As can be seen in Figure 4.5 total cross section and evaporation are increasing at beginning when alpha energy is increasing until the peak, after that, evaporation is decreasing slightly when alpha energy is increasing but total cross section is decreasing normally. On the other hand, when cascade and precompound at begin in a graphic form are increasing sharply with increaseing of the alpha energy to reach the highest point at the peck, while they are decreases slope form with increasing alpha energy emitted. In addition, number of elastic interactions is 529193, number of inelastic in-

teractions is 1000000, reaction cross section is 1746.35 mb and elastic cross section is 924.16 mb.

Table 4.5. Alpha Scattered Double Differential Cross Section (mb/MeV.sr) for p + $_{90}$Th^{232} Reaction

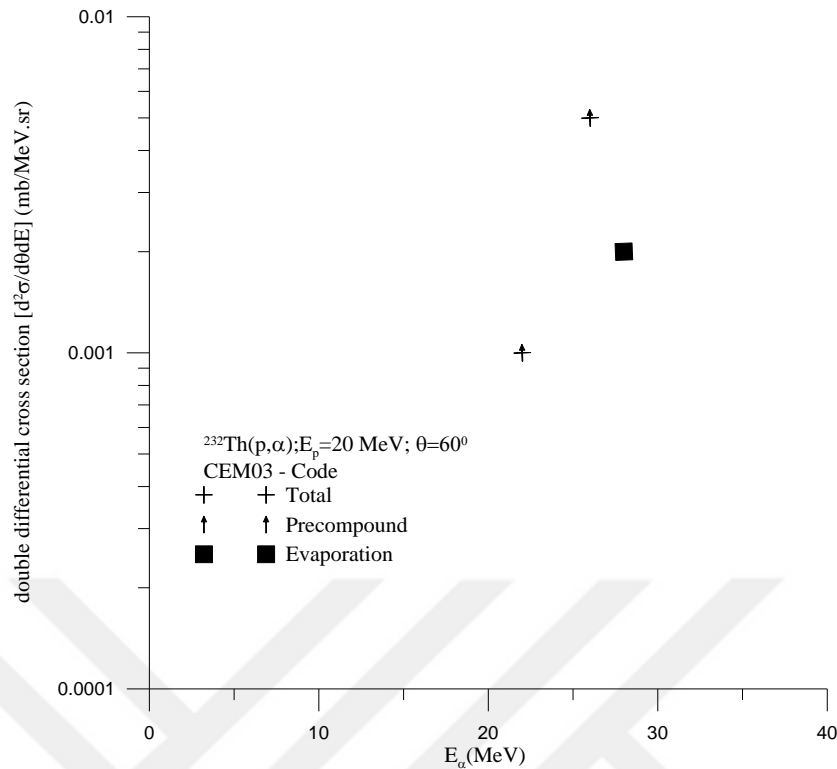| ^{232}Th(p, α); E_p=500 MeV; θ=40^0 degree CEM03 – Code				
$E_α$(MeV)	Total	Cascade	Precompound	Evaporation
	Double differen-tial cross section (mb/MeV.sr)	Double differen-tial cross section (mb/MeV.sr)	Double differen-tial cross section (mb/MeV.sr)	Double differen-tial cross section (mb/MeV.sr)
1	0.013	0.013	…	
2	0.022	0.011	…	0.011
3	0.040	0.022	…	0.018
6	0.115	0.031	…	0.083
7	0.180	0.038	…	0.142
8	0.225	0.049	…	0.175
9	0.212	0.056	…	0.155
12	0.225	0.060	…	0.164
13	0.257	0.069	…	0.187
14	0.248	0.087	…	0.160
20	0.365	0.083	…	0.281
21	1.060	0.049	0.002	1.008
22	2.591	0.067	0.004	2.519
24	3.698	0.068	0.011	3.618
26	2.866	0.056	0.016	2.793
28	2.000	0.060	0.029	1.91
30	1.203	0.050	0.047	1.105
32	0.758	0.054	0.049	0.655
34	0.482	0.052	0.043	0.385
36	0.351	0.052	0.051	0.246
48	0.068	0.030	0.030	0.007
50	0.072	0.032	0.032	0.006
52	0.059	0.014	0.041	0.003
54	0.078	0.032	0.043	0.002
56	0.064	0.024	0.037	0.002
68	0.042	0.021	0.021	
70	0.034	0.014	0.020	
72	0.031	0.009	0.022	
74	0.022	0.006	0.015	
84	0.016	0.007	0.009	
86	0.013	0.005	0.007	
90	0.015	0.011	0.004	

Figure 4.5. Double differential cross section (mb/MeV.sr) of the alpha generated as a result of bombardment of element $_{90}Th^{232}$ with 500 MeV energetic protons and $\theta = 40^0$ degree

4.3.1.6. Alpha Double Differential Cross Section for p + $_{90}Th^{232}$ Reaction at E_p=500 MeV; θ= 40^0, Compare between CEM03 and Experimental Data

The comparison of calculate double differential cross section of alpha emission with experimental data at the incident proton energy 500 MeV with angle 40^0 degree are showing in Figure 4.6 and the Table 4.6. For $^{232}Th(p, x\alpha)$ reaction the pre-equilibrium calculations (cascade- exciton CEM03 and hybrid models) are in good agreement with the measurements. From Figure 4.6, the calculate results are also in good agreement with experimental data at energies 500 MeV.

The higest value in CEM03 code program is 3.698 at 24 MeV but in experimental data the highest value is 0.83 at 118.2 ,128.5 and 137.5 MeV respectively. However, the lowest value in CEM03 code program is recording at 0.013 at 1MeV while in experimental data the lowest value is 0.0183 at 388.5 MeV.

Table 4.6. Alphas Scattered Double Differential Cross Section (mb/MeV.sr) for p + $_{90}$Th^{232} reaction

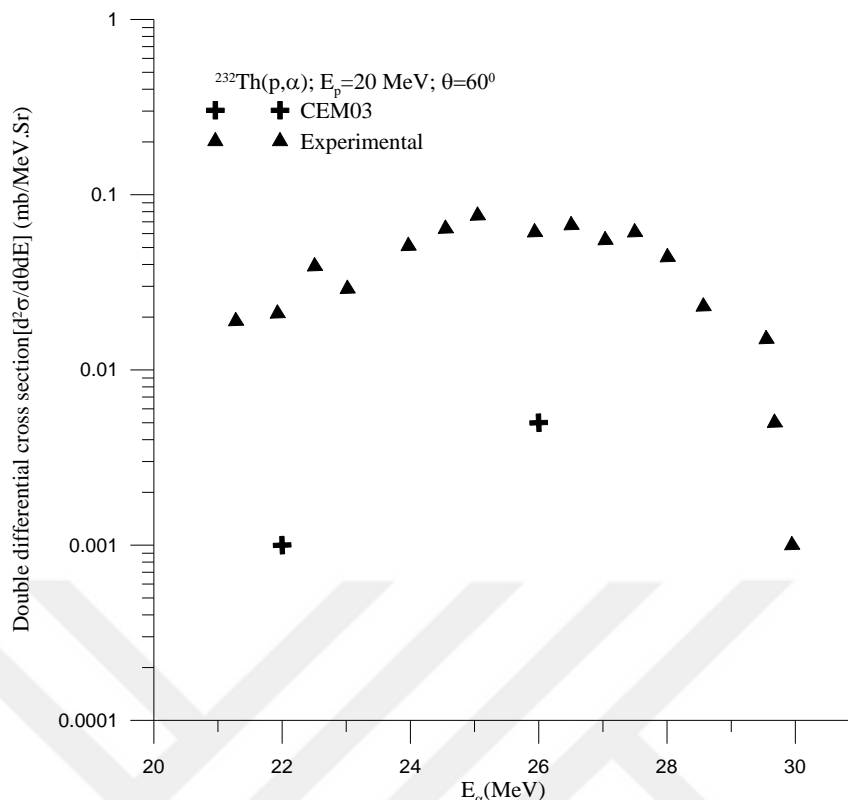| ^{232}Th(p, α); E$_p$=500 MeV ; θ= 40^0, Total Double Differential Cross Section (mb/MeV.sr)		
E$_\alpha$ (MeV)	CEM03 – Code	Experimental E$_p$=500MeV; θ= 40.5^0, (Iwamoto et al. 2009)
0.1	0.013	…
2.0	0.022	…
3.0	0.040	…
7.0	0.180	…
8.0	0.225	…
9.0	0.212	…
20.0	0.365	…
21.0	1.06	…
22.0	2.591	…
24.0	3.698	…
26.0	2.866	…
28.0	2.000	…
30.0	1.203	…
32.0	0.758	…
39.4	…	0.550
40.0	0.162	…
42.0	0.128	…
44.0	0.095	0.580
52.0	0.059	…
54.0	0.078	…
58.8	…	0.650
60.0	0.045	…
70.0	0.034	…
71.7	…	0.700
76.0	0.024	
79.5	…	0.740
80.0	0.030	…
82.0	0.016	…
91.1	…	0.740
101.4	…	0.780
104.0	…	0.620
110.4	…	0.780
118.2	…	0.830
128.5	…	0.830
137.5	…	0.830
180.1	…	0.700
187.8	…	0.620
198.1	…	0.580
260.0	…	0.430
270.3	…	0.340
289.6	…	0.280
299.9	…	0.234
310.2	…	0.183
359.0	…	0.055
370.6	…	0.038
388.5	…	0.0183

Figure 4.6. Double Differential Cross Section (mb/MeV.sr) of the alphas generated as a result of bombardment of element $_{90}Th^{232}$ with 500 MeV energetic protons and $\theta= 40^0$ degree

4.3.1.7. Alpha Double Differential Cross Section for p + $_{90}Th^{232}$ Reaction at E_p=500 MeV; $\theta= 70^0$

The double differential cross sections ($d^2\sigma/dE.d\theta$) of emission (alpha, neutron and proton) particle for p + $_{90}Th^{232}$ reactions are calculated by CEM03 code program. The calculate double differential cross section ($d^2\sigma/dE.d\theta$) of alpha emission for p + $_{90}Th^{232}$ at 500 MeV incident energetic protons are illustrative in Figure 4.7 and Table 4.7. The shape of calculate results curve of double differential cross section ($d^2\sigma/dE.d\theta$) for alpha emission at this energy for four steps (Total, Cascade, Precompound and Evaporation) are different at angle 70^0. The form of calculate results curve are nearly similar to total and evaporation because, both have one peak but evaporation decreases slightly when alpha energy increases. On the other hand, cascade and precompound double differential cross section are increasing with increasing alpha energies emission, it is to reach the highest value , then they both decreases in a slope form when increases alpha energy.

Moreover, number of elastic interactions and number of inelastic interactions are recoreded about (529193 and 1000000), separately. However, the reaction cross section is 1746.35 mb and elastic cross section is 924.16 mb.

Table 4.7. Alpha Scattered Double Differential Cross Section (mb/MeV.sr) for p + $_{90}$Th^{232} Reaction

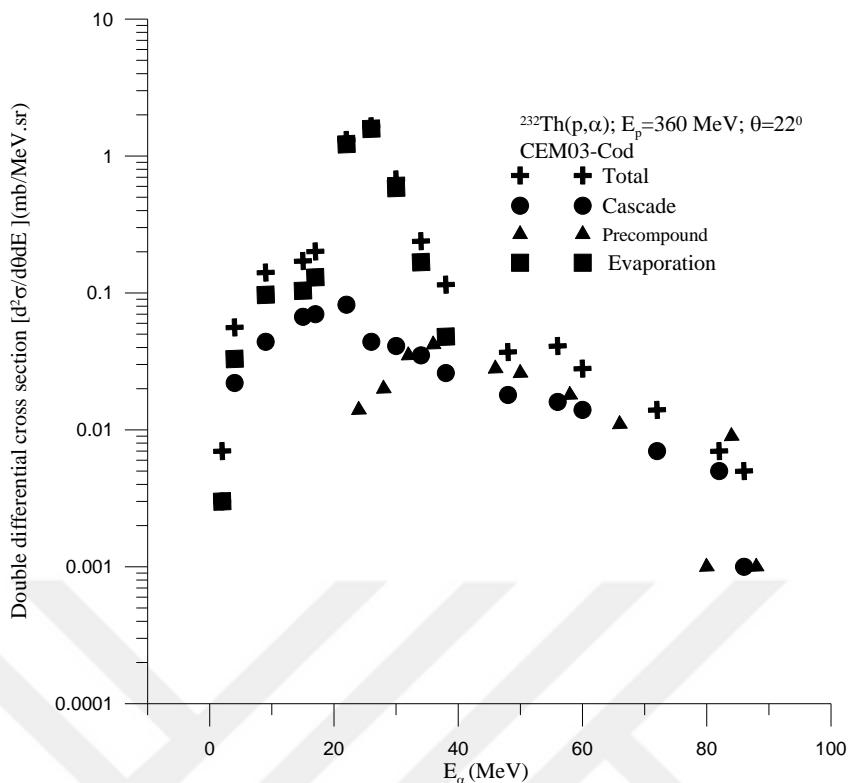| ^{232}Th(p, α); E$_p$=500 MeV; θ=70^0 degree CEM03 - Code				
E$_α$(MeV)	Total	Cascade	Precompound	Evaporation
	Double differential cross section (mb/MeV.sr)	Double differential cross section (mb/MeV.sr)	Double differential cross section (mb/MeV.sr)	Double differential cross section (mb/MeV.sr)
1	0.007	0.007	…	…
2	0.015	0.008	…	0.007
3	0.022	0.010	…	0.012
4	0.061	0.012	…	0.049
8	0.163	0.028	…	0.135
9	0.209	0.052	…	0.156
18	0.248	0.051	…	0.197
19	0.239	0.042	…	0.197
20	0.478	0.051	…	0.427
21	1.427	0.049	0.005	1.372
22	2.873	0.029	0.003	2.84
24	3.622	0.039	0.006	3.577
26	2.781	0.037	0.029	2.714
28	1.832	0.036	0.034	1.762
30	1.069	0.029	0.030	1.009
32	0.674	0.036	0.039	0.598
34	0.390	0.024	0.048	0.317
36	0.271	0.034	0.044	0.192
38	0.175	0.027	0.036	0.112
40	0.129	0.022	0.047	0.058
42	0.081	0.018	0.037	0.025
44	0.073	0.018	0.039	0.015
46	0.078	0.015	0.051	0.010
48	0.082	0.021	0.048	0.012
74	0.020	0.006	0.014	…
76	0.016	0.004	0.012	…
78	0.015	0.003	0.012	…
80	0.018	0.006	0.012	…
82	0.013	0.004	0.008	…
84	0.014	0.002	0.012	…
86	0.007	0.003	0.004	…
88	0.007	0.000	0.007	…
90	0.014	0.004	0.009	…

Figure 4.7. Double differential cross section (mb/MeV.sr) of the alpha generated as a result of bombardment of element $_{90}Th^{232}$ with 500 MeV energetic protons and $\theta = 70^0$ degree

4.3.1.8. Alpha Double Differential Cross Section for p + $_{90}Th^{232}$ Reaction at $E_p=500$ MeV; $\theta= 70^0$, Compare between CEM03 and Experimental Data

The comparison of calculate double differential cross section of alpha emission with experimental data at the incident proton energy 500 MeV with angle 70^0 degree. For $^{232}Th(p, x\alpha)$ reaction the pre-equilibrium calculations (cascade- exciton CEM03 and hybrid models) are in good agreement with the measurements. Results from Figure 4.8 are also shows that the calculate in good agreement with experimental data at energies 500 MeV. The higest value in CEM03 code program is 3.622 at 24 MeV but in experimental data the highest value is 0.66 at 52 MeV. However, the lowest value in CEM03 code program is 0.007 at 1 MeV but in experimental data the lowest value is 0.005 at 269 MeV.

Table 4.8. Alpha Scattered Double Differential Cross Section (mb/MeV.sr) for p + $_{90}$Th^{232} reaction

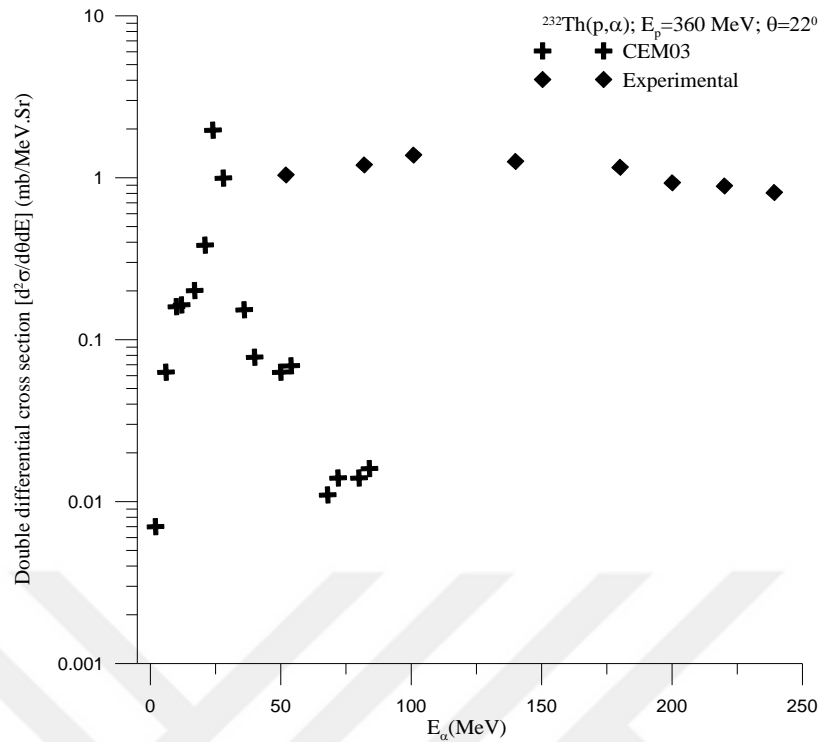| ^{232}Th(p, α); E$_p$=500 MeV; θ= 70^0, Total Double Differential Cross Section (mb/MeV.sr)		
E$_α$ (MeV)	CEM03 – Code	Experimental E$_p$=500 MeV; θ= 70.0^0, (Iwamoto et al. 2009)
1.0	0.007	…
2.0	0.015	…
3.0	0.022	…
4.0	0.061	…
7.0	0.156	…
9.0	0.209	…
10.0	0.223	…
13.0	0.276	…
17.0	0.255	…
20.0	0.478	…
21.0	1.427	…
22.0	2.873	…
24.0	3.622	…
26.0	2.781	…
30.0	1.069	…
0.40	0.129	…
43.9	…	0.500
44.0	0.073	…
50.0	0.051	…
51.6	…	0.590
52.0	0.056	0.660
60.0	0.033	…
64.0	0.024	…
70.0	0.028	…
72.0	0.020	…
0.80	0.018	…
81.0	…	0.500
81.3	…	0.590
90.0	0.014	…
100.9	…	0.620
119.1	…	0.540
140.0	…	0.400
150.8	…	0.360
160.1	…	0.297
170.1	…	0.234
189.2	…	0.195
189.4	…	0.163
200.1	…	0.129
220.1	…	0.090
228.3	…	0.071
230.5	…	0.053
249.2	…	0.047
267.4	…	0.023
269.0	…	0.005

Figure 4.8. Double differential cross section (mb/MeV.sr) of the alphas generated as a result of bombardment of element $_{90}Th^{232}$ with 500 MeV energetic protons and $\theta = 70^0$ degree

4.3.1.9. Alpha Double Differential Cross Section for p + $_{90}Th^{232}$ Reaction at E_p=360 MeV; θ= (0^0, 20^0, 40^0, 60^0)

The double differential cross sections ($d^2\sigma/dE.d\theta$) of emission (alpha, neutron and proton) particle for p + $_{90}Th^{232}$ reactions are calculated by CEM03 code program. The calculate consequences of the double differential cross sections ($d^2\sigma/dE.d\theta$) of alpha particle emission for p + $_{90}Th^{232}$ reaction are illustrative in Figure 4.9 and Table 4.9, at the proton incident energy 360 MeV. The calculation of total double differential cross section are various for angles (0^0, 20^0, 40^0 and 60^0). The form of calculated results curve are similar to each other. The peaks of the curves at high alpha emission energy are participates of the immediate reaction mechanism. From the line graph, total double differential cross section are decreasing in a different orientation, because of various angles. In addition, number of elastic interactions is 578028, number of inelastic interactions is 1000000, reaction cross section is 1728.55 mb and elastic cross section is 999.15 mb.

Table 4.9. Alpha scattered Double differential cross section (mb/MeV.Sr) for p + $_{90}$Th^{232} reaction , E$_P$=360 MeV energy with θ= (0^0, 20^0, 40^0, 60^0) degree Calculation have been made by CEM03 code program

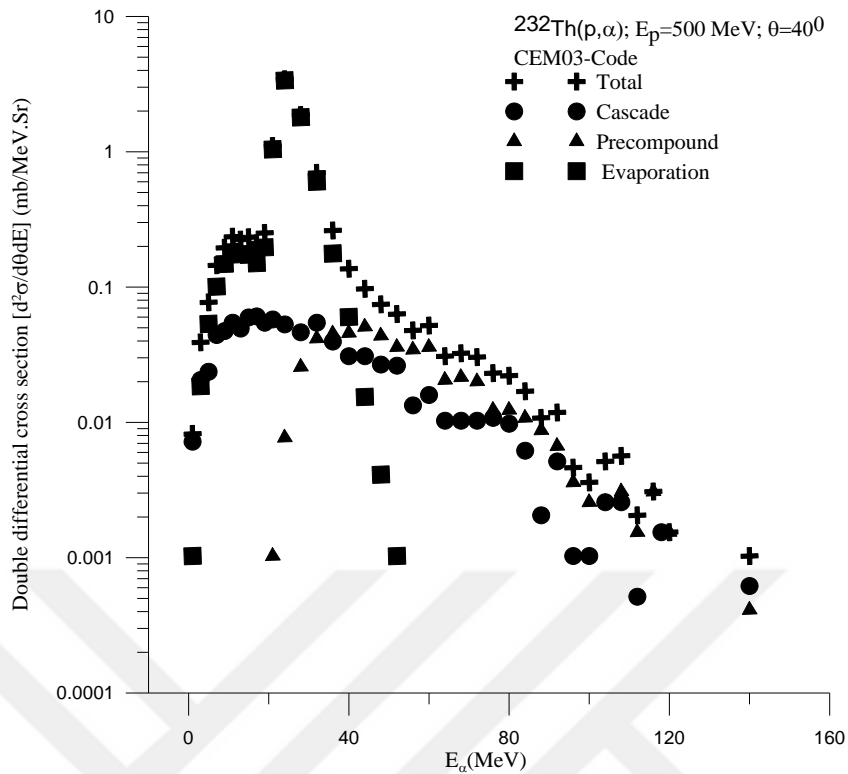| E$_α$(MeV)	^{232}Th(p, α); E$_p$=360 MeV; θ= (0^0, 20^0, 40^0, 60^0) respectively			
	Total Double Differential Cross Section (mb/MeV.sr) CEM03 - Code			
	Angle θ= 0^0	Angle θ= 20^0	Angle θ= 40^0	Angle θ= 60^0
1	0.018	0.003	0.004	0.010
3	0.036	0.014	0.022	0.019
4	0.072	0.037	0.058	0.060
5	0.018	0.074	0.053	0.055
6	0.090	0.070	0.100	0.073
7	0.072	0.100	0.104	0.090
10	0.144	0.134	0.140	0.121
11	0.163	0.145	0.125	0.109
12	0.144	0.168	0.138	0.125
13	0.036	0.119	0.147	0.120
17	0.235	0.130	0.174	0.172
18	0.181	0.186	0.147	0.142
19	0.126	0.153	0.151	0.127
20	0.072	0.171	0.178	0.200
26	1.539	1.61	1.567	1.397
28	1.177	1.048	0.920	0.831
30	0.651	0.601	0.585	0.496
32	0.362	0.382	0.335	0.257
34	0.217	0.205	0.203	0.157
40	0.081	0.097	0.075	0.067
42	0.072	0.080	0.065	0.052
44	0.063	0.095	0.044	0.042
46	0.036	0.070	0.054	0.035
48	0.108	0.054	0.041	0.028
58	0.054	0.050	0.023	0.016
60	0.027	0.022	0.022	0.027
62	0.009	0.029	0.017	0.017
64	0.045	0.035	0.024	0.013
66	0.027	0.018	0.014	0.016
68	0.036	0.016	0.012	0.008
74	0.009	0.016	0.010	0.013
76	0.0181	0.011	0.011	0.004
78	0.009	0.016	0.008	0.005
80	0.036	0.001	0.006	0.004
82	0.018	0.013	0.004	0.005
84	0.009	0.007	0.005	0.005
86	0.009	0.007	0.007	0.009
94	0.009	0.009	0.002	0.004
96	0.027	0.003	0.003	0.001
100	0.009	0.005	0.002	0.003

Figure 4.9. Double differential cross section (mb/MeV.sr) of the alphas generated as a result of bombard-
ment of element $_{90}Th^{232}$ with 360 MeV energetic protons and θ= (0^0, 20^0, 40^0, 60^0) degree respectively

4.3.1.10. Neutron Double Differential Cross Section for p + $_{90}Th^{232}$ Reaction at E_p=360 MeV; θ= (0^0, 20^0, 40^0, 60^0)

The double differential cross sections ($d^2\sigma/dE.d\theta$) of emission (alpha, neutron and proton)
particle for p + $_{90}Th^{232}$ reactions are calculated by CEM03 code program. The calculate
consequences of the double differential cross sections ($d^2\sigma/dE.d\theta$) of neutron particle
emission for p + $_{90}Th^{232}$ reaction are illustrative in Figure 4.10 and Table 4.10, at the
proton incident energy 360 MeV. The calculate results are at angles 0^0, 20^0, 40^0 and 60^0
that results for total double differential cross section are various for different angles. At
the beginning of the curves, total double differential cross section for different angles are
decreasing with increasing neutron energy emission. The form of calculated results curve
are similar to each other, until amount energy above 100 MeV after that values of total
double differential cross section are various. From the line graph, total double differential
cross section is not change, for 0^0 and 20^0 degree but on top of 300 MeV, total double
differential for 0^0 degree is increasing with increasing neutron energy emission. However,
for 20^0 degree was counteracted.

On the other hand, for 40^0 and 60^0 degree over 100 MeV the total differential are decreasing gradually when neutron energy emission are increasing. In addition, number of elastic interactions is 578028, number of inelastic interactions is 1000000, reaction cross section is 1728.55 mb and elastic cross section is 999.15 mb.

Table 4.10. Neutron Scattered Double Differential Cross Section (mb/MeV.sr) for p + $_{90}$Th^{232} Reaction

E_n(MeV)	^{232}Th(p, n); E_p=360 MeV; θ= (0^0,20^0, 40^0, 60^0) respectively			
	Total Double Differential Cross Section (mb/MeV.sr) CEM03 – Code			
	Angle θ= 0^0	Angle θ= 20^0	Angle θ= 40^0	Angle θ= 60^0
1	276	275.6	273.6	273.1
2	349.2	352.6	347	340.8
3	280.8	283.4	279.1	274.4
4	217.3	211.8	207.5	201.3
5	153.7	154.4	151.1	144.3
9	45.6	46.19	44.31	40.86
10	36.2	35.52	33.84	31.98
11	28.61	28.82	27.35	25.33
12	24.03	23.54	22.28	20.32
16	13.91	13.38	12.66	11.26
17	12.75	12.59	11.33	10.18
18	12.22	11.63	10.45	9.264
24	7.904	7.29	7.102	6.409
26	6.926	6.838	6.371	5.745
30	5.822	5.421	5.171	4.603
32	5.396	4.746	4.715	4.125
38	3.794	3.736	3.509	3.109
46	2.743	2.842	2.617	2.356
60	1.983	1.944	1.854	1.662
62	2.01	1.862	1.838	1.559
70	1.838	1.72	1.607	1.384
80	1.766	1.475	1.453	1.246
92	1.458	1.331	1.24	0.948
100	1.286	1.255	1.153	0.863
102	1.222	1.199	1.133	0.855
114	1.096	1.081	1.097	0.731
120	1.105	1.008	0.963	0.640
130	1.088	0.944	0.996	0.573
140	0.961	0.894	0.940	0.484
150	0.818	0.796	0.91	0.404
180	0.816	0.726	0.762	0.224
190	0.728	0.705	0.707	0.186
200	0.655	0.730	0.648	0.149
210	0.648	0.709	0.606	0.120
220	0.653	0.711	0.522	0.079
230	0.608	0.768	0.461	0.060
240	0.639	0.830	0.394	0.048
250	0.601	0.894	0.332	0.030
260	0.586	1.022	0.263	0.021

Contiue Table 4.19

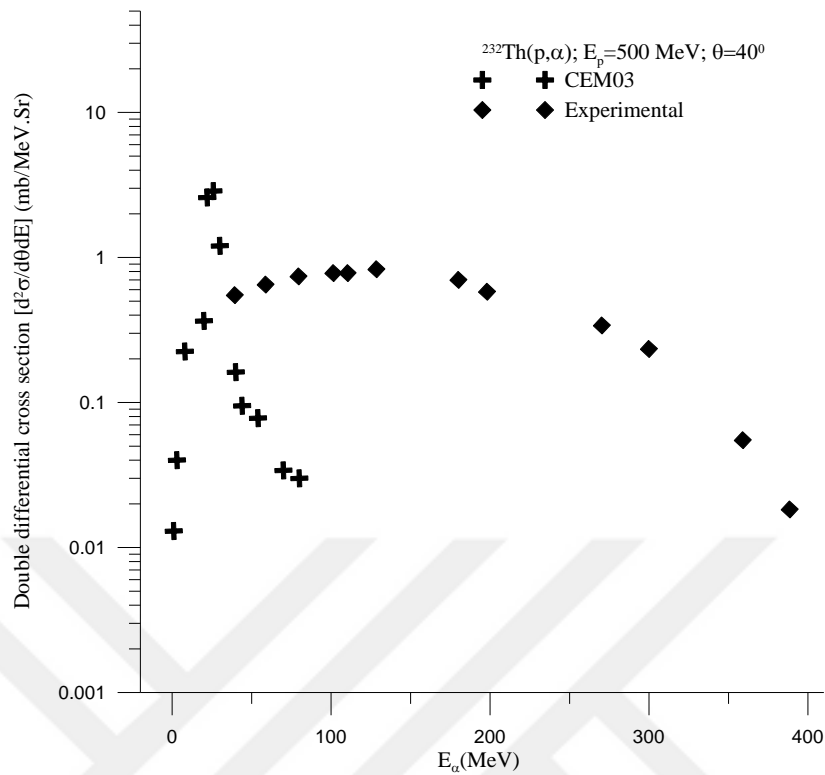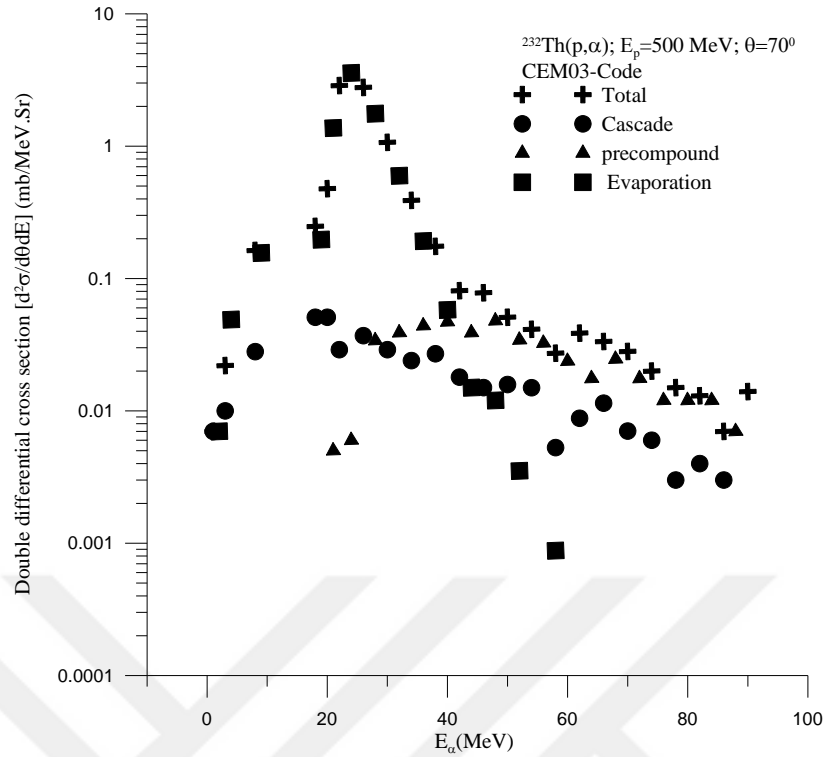| 270	0.581	1.114	0.211	0.012
280	0.507	1.227	0.155	0.007
290	0.557	1.253	0.113	0.005
300	0.537	1.31	0.088	0.003
310	0.523	1.275	0.058	0.001
320	0.517	1.111	0.032	000.0
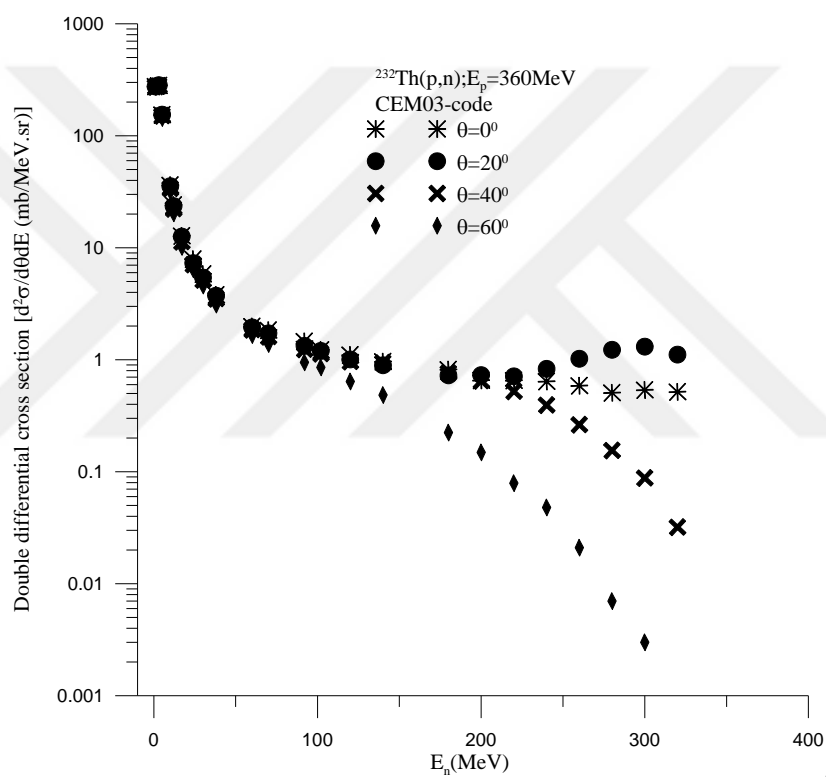
Figure 4.10. Double differential cross section (mb/MeV.sr) of the neutron generated as a result of bombardment of element $_{90}Th^{232}$ with 360 MeV energetic protons and $\theta = (0^0, 20^0, 40^0, 60^0)$ degree respectively

4.3.1.11. Proton Double Differential Cross Section for p + $_{90}$Th^{232} Reaction at E$_P$=360 MeV; θ= (0^0, 20^0, 40^0, 60^0)

CEM03 code program was applied to calculation the double differential cross sections (d^{2}σ/dE.dθ) of emission (alpha, neutron and proton) particle for p + $_{90}$Th^{232} reactions.

The calculate consequences of d^{2}σ/dE.dθ of proton particle emission for p + $_{90}$Th^{232} reaction are illustrative in Figure 4.11 and Table 4.11, at the proton incident energy 360 MeV.

The calculate results are at angles 0^0, 20^0, 40^0 and 60^0 that results for total double differential cross section are various for different angles. At the beginning of the curves, total double differential cross section for different angles are increasing sharply when proton energy emission is increasing. The peaks of the curves at high proton emission energy are participates of the immediate reaction mechanism.

The form of calculate results curve are similar to each other, they are decreasing while amount energy bring to above 100 MeV except 40^0 and 60^0 degree, after that accounts of total double differential cross section are various. From the graph, total double differential cross section on 100 MeV is not change until the quantity almost bring to 300 MeV for 0^0 degree, but after this value it is increasing.

However, subsequent to the peak, total differential cross section for 20^0 degree is decreasing until amount nearly bring to 200 MeV, after this amount increases and decreases alternately.

In addition, number of elastic interactions is 578028, number of inelastic interactions is 1000000, reaction cross section is 1728.55 mb and elastic cross section is 999.15 mb.

Table 4.11. Proton Scattered Double Differential Cross Section (mb/MeV.sr) for p + $_{90}$Th^{232} reaction

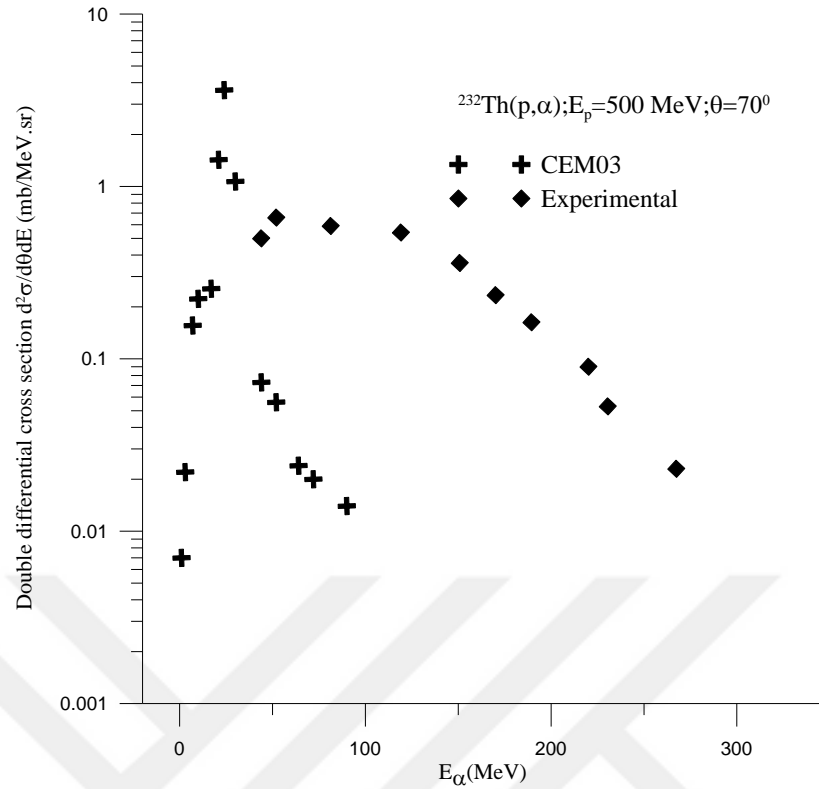| $E_{ṕ}$(MeV)	^{232}Th(p, ṕ); E_p=360 MeV; θ= (0^0, 20^0, 40^0, 60^0) respectively			
	Total Double Differential Cross Section (mb/MeV.sr) CEM03 - Code			
	Angle θ= 0^0	Angle θ= 20^0	Angle θ= 40^0	Angle θ= 60^0
2	…	0.003	0.006	0.006
3	0.036	0.067	0.055	0.062
4	0.181	0.171	0.125	0.149
5	0.199	0.268	0.225	0.238
6	0.289	0.317	0.316	0.303
7	0.380	0.354	0.348	0.330
9	0.851	1.001	1.174	1.322
10	3.296	3.335	3.527	3.880
11	4.418	4.395	4.451	4.636
12	5.070	4.578	4.551	4.439
13	4.600	4.313	4.243	4.247
15	3.694	3.675	3.658	3.471
19	2.843	2.644	2.618	2.589
28	1.919	1.798	1.822	1.781
38	1.168	1.303	1.248	1.411
46	0.986	0.918	1.049	1.242
54	1.014	0.782	0.962	1.100
56	0.977	0.786	0.959	1.100
58	0.688	0.763	0.922	1.093
60	0.769	0.784	0.881	1.044
76	0.823	0.778	0.947	0.983
86	0.715	0.732	1.035	0.907
94	0.887	0.745	1.037	0.810
100	0.977	0.722	1.081	0.766
102	0.905	0.746	1.139	0.760
114	0.860	0.728	1.220	0.567
150	0.702	0.612	1.312	0.309
160	0.713	0.595	1.312	0.243
170	0.612	0.652	1.253	0.188
180	0.608	0.670	1.172	0.141
190	0.583	0.706	1.027	0.113
200	0.574	0.791	0.900	0.084
210	0.550	0.907	0.735	0.055
260	0.496	1.946	0.202	0.011
270	0.487	2.200	0.128	0.004
280	0.461	2.393	0.094	0.002
290	0.403	2.320	0.059	
300	0.425	2.166	0.036	
310	0.418	1.896	0.018	
320	0.608	1.467	0.008	
330	1.307	1.018	0.003	
340	3.238	0.616	0.002	
350	6.706	0.332	0.006	
360	6.979	0.107	0.055	

Figure 4.11. Double differential cross section (mb/MeV.sr) of the proton generated as a result of bombardment of element $_{90}Th^{232}$ with 360 MeV energetic protons and $\theta = (0^0, 20^0, 40^0, 60^0)$ degree respectively

4.3.2. p + $_5B^{10}$ Reaction

4.3.2.1. Neutron Double Differential Cross Section for p + $_5B^{10}$ Reaction at $E_p = 30$ MeV; $\theta = 2^0$

The double differential cross sections ($d^2\sigma/dE.d\theta$) of emission (alpha, neutron and proton) particle for p + $_5B^{10}$ reactions are calculated by CEM03 code program. The calculate double differential cross section ($d^2\sigma/dE.d\theta$) of neutron emission for p + $_5B^{10}$ at 30 MeV incident energetic proton are illustrative in Figure 4.12 and Table 4.12.

The form of calculate results curve of double differential cross section ($d^2\sigma/dE.d\theta$) for neutron emission at this energy for four steps (Total, Cascade, Precompound and Evaporation) are different at angle 2^0 degree. At the begin total double differential cross section decreasing with increasing neutron energy emission until above 5 MeV.

After that this value is increasing gradually with increasing neutron energy emission as can be seen in Figure 4.12. For cascades, increases steadily when increases neutron energy emission until bring to the higest point, although increases with increases energy emission. On the other hand, evaporation is decreasing when neutron energies are increasing. However, the precompound in this case not shown in this line graph because all results are zero, the incident proton energy is bigger than target element, has small mass number.

In addition, number of elastic interactions is 1398484, number of inelastic interactions is 1000000, reaction cross section is 445.68 mb, elastic cross section is 623.28 mb.

Table 4.12. Neutron Scattered Double Differential Cross Section (mb/MeV.sr) for $p + {}_5B^{10}$ Reaction

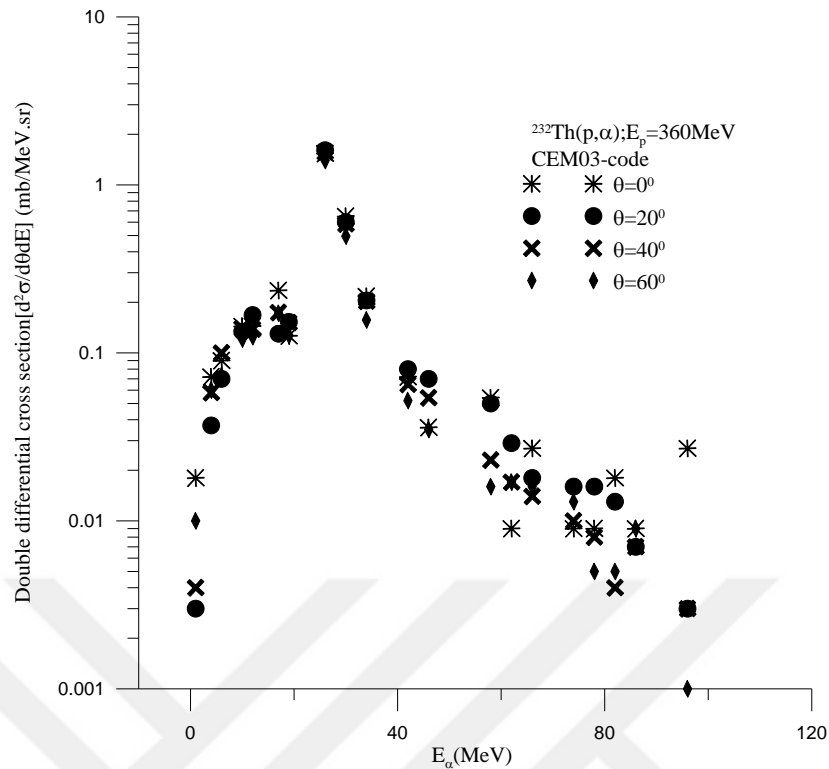| ^{10}B(p, n); E_p=30 MeV; θ= 2^0 CEM03 – Code			
E_n(MeV)	Total	Cascade	Total Evaporation
	Double differential cross section (mb/MeV.sr)	Double differential cross section (mb/MeV.sr)	Double differential cross section (mb/MeV.sr)
1	1.895	000.0	1.895
2	2.466	0.281	2.185
3	1.861	0.301	1.560
4	1.215	0.287	0.928
5	0.879	0.331	0.548
6	0.768	0.370	0.397
7	0.663	0.359	0.303
8	0.731	0.421	0.310
9	0.725	0.450	0.275
10	0.651	0.478	0.172
11	0.704	0.566	0.137
12	0.786	0.665	0.121
13	0.891	0.771	0.120
14	0.978	0.877	0.101
15	1.197	1.092	0.105
16	1.363	1.273	0.090
17	1.515	1.431	0.083
18	1.637	1.557	0.079
19	1.817	1.749	0.068
20	1.882	1.842	0.039
21	2.097	2.077	0.020
22	2.156	2.156	0.000
24	2.325	2.325	0.000
26	1.464	1.395	0.068

Figure 4.12. Double differential cross section (mb/MeV.sr) of the Neutron generated as a result of bombardment of element $_5B^{10}$ with 30 MeV energetic protons and θ= 20 degree

4.3.2.2. Neutron Double Differential Cross Section for p + $_5B^{10}$ Reaction at E_p= 30 MeV; θ= 2^0, Compare between CEM03 and Experimental Data

The comparison of calculate double differential cross section of neutron emission with experimental data at the incident proton energy 30 MeV with angle 2^0 degree are showing in Figure 4.13 and Table 4.13. For $^{10}B(p, xn)$ reaction the pre-equilibrium calculations (cascade- exciton CEM03 and hybrid models) are in good agreement with the measurements. From Figure 13, the experimental data and CEM03 data have an inconsistency at energies 16 MeV. In addition, both the CEM03 data and experimental data results are decreasing at energies 25 MeV .

Table 4.13. Neutron Scattered Double Differential Cross Section (mb/MeV.sr) for p + $_5B^{10}$ Reaction

| $_5B^{10}$ (p, n); E_p= 30 MeV; θ= 2^0 , Total Double Differential Cross Section (mb/MeV.sr)		
E_n (MeV)	CEM03 – Code	Experimental; E_p= 30 MeV;θ= 2^0 (Clough et al. 1970)
1.000	1.895	…
2.000	2.466	…
3.000	1.861	…
4.000	1.215	…
5.000	0.879	…
6.000	0.768	…
7.000	0.663	...
8.000	0.731	…
9.000	0.725	…
10.000	0.651	…
11.000	0.704	…
12.000	0.786	…
13.000	0.891	…
14.000	0.978	…
15.000	1.197	…
15.035	…	1.006
15.106	…	0.882
15.570	…	0.951
16.000	1.363	…
16.036		0.98
17.000	1.515	…
17.035		1.022
17.639		0.871
18.000	1.637	…
18.044		0.706
19.000	1.817	…
19.574		0.818
20.000	1.882	…
20.141	…	1.950
20.250	…	2.792
20.449	…	2.820
21.000	2.097	…
21.125		0.213
22.000	2.156	…
22.383	…	2.808
22.673	…	1.995
23.264	…	0.009
23.999	…	0.005
24.000	2.325	…
24.265	…	0.003
25.388	…	0.343
25.566	…	1.074
25.898	…	1.130
000.26	1.464	…
26.525	…	0.193
27.993	…	0.139

Figure 4.13. Double differential cross section (mb/MeV.sr) of the Neutron generated as a result of bombardment of element $_5B^{10}$ with 30 MeV energetic protons and θ= 20 degree

4.3.2.3. Neutron Double Differential Cross Section for p + $_5B^{10}$ Reaction at E_p= 50 MeV; θ= 30^0

The $d^2σ/dE.dθ$ of emission (alpha, neutron and proton) particle for p + $_5B^{10}$ reactions are calculated by CEM03 code program. The calculate $d^2σ/dE.dθ$ of neutron emission for p + $_5B^{10}$ at 50 MeV incident energetic protonis shown in Figure 4.14 and Table 4.14. The shape of calculate results curve of $d^2σ/dE.dθ$ for neutron emission at this energy for four steps (Total, Cascade, Precompound and Evaporation) are different at angle 30^0 degree. As can be seen in Figure 4.14 at the beginning of the curve, total double differential cross section decreasing when neutron energy emission bring to 20 MeV. Neutron energy emission at value of 20 MeV is caused to decrease total double differential cross section as can be seen in Figure 4.14. After that value is not change although, where as neutron energy emission almost bring to 36 MeV, then it is descend once more. From the line graph, cascade double differential cross section is increasing slowly together with increasing neutron energy emission. On the other hand, evaporation is descend dramatically when neutron energies are increasing.

However, the precompound in this case not shown in this line graph because, all results are zero, the incident proton energy is bigger than target element, has small mass number. In addition, number of elastic interactions is 1755733, number of inelastic interactions is 1000000, reaction cross section is 342.84 mb, elastic cross section is 601.94 mb.

Table 4.14. Neutron Scattered Double Differential Cross Section (mb/MeV.sr) for p + $_5B^{10}$ Reaction

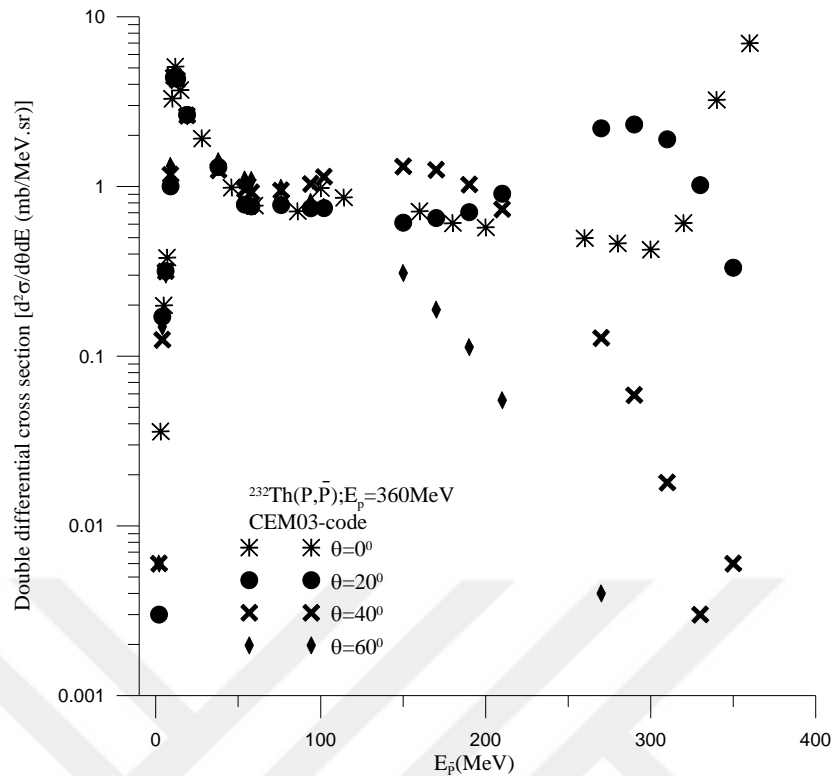| ^{10}B(p, n); E_p=50 MeV; θ= 30^0 CEM03 – Code			
E_n(MeV)	Total	Cascade	Total Evaporation
	Double differential cross section (mb/MeV.Sr)	Double differential cross section (mb/MeV.Sr)	Double differential cross section (mb/MeV.Sr)
1	2.045	000.0	2.045
2	2.886	0.402	2.484
3	2.271	0.411	1.859
4	1.602	0.398	1.204
5	1.241	0.381	0.860
6	0.999	0.384	0.614
7	0.856	0.397	0.458
8	0.790	0.427	0.363
9	0.703	0.430	0.273
10	0.684	0.418	0.266
11	0.721	0.485	0.236
12	0.684	0.481	0.202
13	0.674	0.487	0.187
14	0.693	0.518	0.174
15	0.684	0.527	0.156
16	0.766	0.595	0.170
17	0.740	0.608	0.132
18	0.783	0.665	0.117
19	0.768	0.658	0.110
20	0.790	0.686	0.103
21	0.795	0.707	0.087
22	0.815	0.733	0.082
24	0.849	0.788	0.061
26	0.895	0.848	0.047
28	0.871	0.836	0.034
30	0.886	0.869	0.017
32	0.943	0.932	0.0115
34	0.934	0.920	0.013
36	0.857	0.847	0.010
38	0.728	0.720	0.007
40	0.540	0.538	0.001
42	0.438	0.438	0.000
44	0.322	0.316	0.005

Figure 4.14. Double differential cross section (mb/MeV.sr) of the Neutron generated as a result of bombardment of element $_5B^{10}$ with 50 MeV energetic protons and $\theta= 30^0$ degree

4.3.2.4. Neutron Double Differential Cross Section for p + $_5B^{10}$ Reaction at $E_p= 50$ MeV; $\theta= 30^0$, Compare between CEM03 and Experimental Data

The comparison of calculate double differential cross section of neutron emission with experimental data at the incident proton energy 50 MeV with angle 30^0 degree are showing in Figure 4.15 and Table 4.15. For $^{10}B(p, xn)$ reaction the pre-equilibrium calculations (cascade- exciton CEM03 and hybrid models) are in agreement with the measurements.

From Figure 4.15 also the experimental data and CEM03 have an inconsistency at energies 36 MeV. In addition, both the experimental data and CEM03 data results are decreasing in energy 40 MeV.

Table 4.15. Neutron Scattered Double Differential Cross Section (mb/MeV.sr) for p + $_5B^{10}$ Reaction

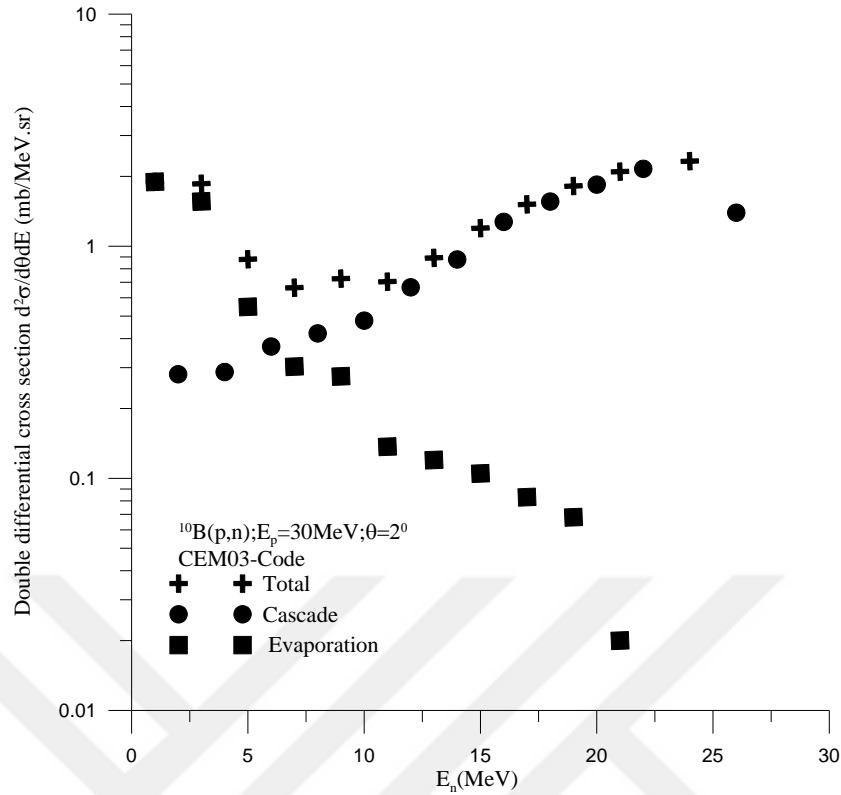| $_5B^{10}$ (p, n); E_p= 50 MeV; θ= 30^0, Total Double Differential Cross Section (mb/MeV.sr)		
E_n (MeV)	CEM03 – Code	Experimental E_p= 50 MeV; θ= 30^0 (Clough et al. 1970)
1.000	2.045	…
2.000	2.886	…
3.000	2.271	…
4.000	1.602	…
5.000	1.241	…
6.000	0.999	…
10.000	0.684	…
11.000	0.721	…
12.000	0.684	…
15.000	0.684	…
16.000	0.766	…
22.000	0.815	…
24.000	0.849	…
26.000	0.895	…
30.000	0.886	…
30.784	…	0.633
31.248	…	0.710
31.649	…	0.703
32.000	0.943	...
32.048	…	0.738
32.383	…	0.661
32.519	…	0.571
33.518	…	0.606
34.000	0.934	…
34.119	…	0.565
34.452	…	0.579
34.785	…	0.593
36.000	0.857	…
36.657	…	0.378
37.000	…	…
37.190	…	0.378
37.654	…	0.475
38.000	0.728	…
38.051	…	0.607
38.588	…	0.455
39.525	…	0.309
40.000	0.540	…
40.122	…	0.434
41.332	…	0.018
42.000	0.438	…
43.000	…	…
43.063	…	0.123
44.000	0.322	…
44.932	…	0.0193
45.533	…	0.0126

Figure 4.15. Double differential cross section (mb/MeV.sr) of the Neutron generated as a result of bombardment of element $_5B^{10}$ with 50 MeV energetic protons and $\theta= 30^0$ degree

4.3.2.5. Neutron Double Differential Cross Section for p+ $_5B^{10}$ Reaction at E_p= 186 MeV; θ= 0^0

CEM03 code program is also used to determination the double differential cross sections ($d^2\sigma/dE.d\theta$) of emission (alpha, neutron and proton) particle for p + $_5B^{10}$ reactions.

Figure 4.16 and Table 4.16 are showing the results of double differential cross section ($d^2\sigma/dE.d\theta$) of neutron emission for p + $_5B^{10}$ at 186 MeV incident energetic proton. Different shapes are recording at angle 0^0 degree of double differential cross section $d^2\sigma/dE.d\theta$ for neutron emission at this energy for four steps (Total, Cascade, Precompound and Evaporation).

It shows that at the beginning of the curve, total and cascade double differential cross section are decreasing a littile more when neutron energy emission is increasing. On the other hand, evaporation is decreasing gradually with increasing neutron energies. However, the results of precompound in this case are not showing in the line graph because,

all results are zero. The incident proton energy is bigger than target element, has small mass number. In addition, number of elastic interactions and number of inelastic interactions are about (2991607 and 1000000), respectively. Furthermore, (189.34 and 566.43 mb) are recorded as reaction cross section and elastic cross section, respectively.

Table 4.16. Neutron Scattered Double Differential Cross Section (mb/MeV.sr) for p + $_5$B^{10} Reaction

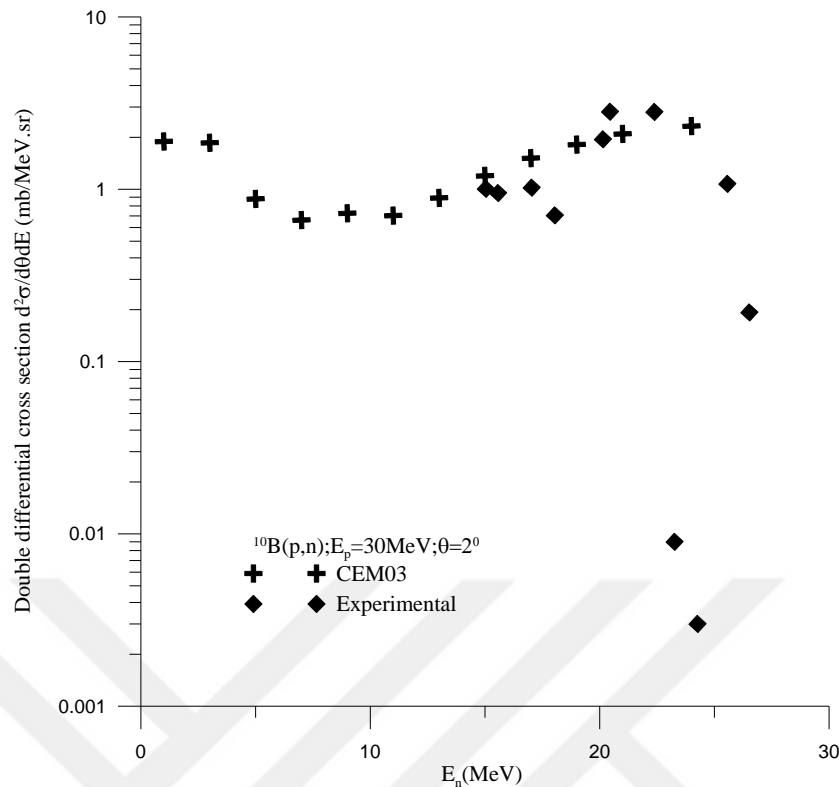| ^{10}B(p, n); E_p=186 MeV; θ= 0^0 CEM03 - Code			
E_n(MeV)	Total	Cascade	Evaporation
	Double differential cross section (mb/MeV.sr)	Double differential cross section (mb/MeV.sr)	Double differential cross section (mb/MeV.sr)
1	1.777	000.0	1.777
2	2.093	0.244	1.848
3	1.367	0.218	1.148
4	0.922	0.212	0.710
5	0.662	0.211	0.451
6	0.539	0.208	0.331
7	0.442	0.177	0.264
8	0.389	0.181	0.207
11	0.299	0.164	0.134
12	0.255	0.141	0.113
15	0.225	0.157	0.068
16	0.221	0.137	0.083
17	0.221	0.144	0.076
20	0.186	0.134	0.052
21	0.181	0.129	0.052
22	0.151	0.108	0.042
34	0.124	0.104	0.019
36	0.118	0.102	0.016
38	0.120	0.106	0.014
40	0.112	0.101	0.011
42	0.095	0.086	0.009
44	0.102	0.094	0.008
46	0.108	0.101	0.006
48	0.098	0.092	0.005
58	0.092	0.089	0.002
60	0.094	0.092	0.001
62	0.081	0.079	0.002
64	0.081	0.080	
66	0.083	0.082	
76	0.077	0.077	
78	0.075	0.074	
80	0.078	0.078	
84	0.072	0.072	
88	0.068	0.068	
90	0.082	0.082	

Figure 4.16. Double differential cross section (mb/MeV.sr) of the Neutron generated as a result of bombardment of element $_5B^{10}$ with 186 MeV energetic protons and $\theta = 0^0$ degree

4.3.2.6. Neutron Double Differential Cross Section for p + $_5B^{10}$ Reaction at E_p= 186 MeV; $\theta = 0^0$, Compare between CEM03 and Experimental Data

The comparison of calculate double differential cross section of neutron emission with experimental data at the incident proton energy 186 MeV with angle 0^0 degree are showing in Figure 4.17 and Table 4.17. For $^{10}B(p, xn)$ reaction the pre-equilibrium calculations (cascade- exciton CEM03 and hybrid models) are in good agreement with the measurements. From Figure 4.17, the CEM03 and experimental data have about inconsistency at energies 20 MeV.

Additionally, in the result for both the experimental and CEM03 are decreasing at energies 10 MeV.

Table 4.17. Neutron Scattered Double Differential Cross Section (mb/MeV.sr) for p + $_5B^{10}$ Reaction

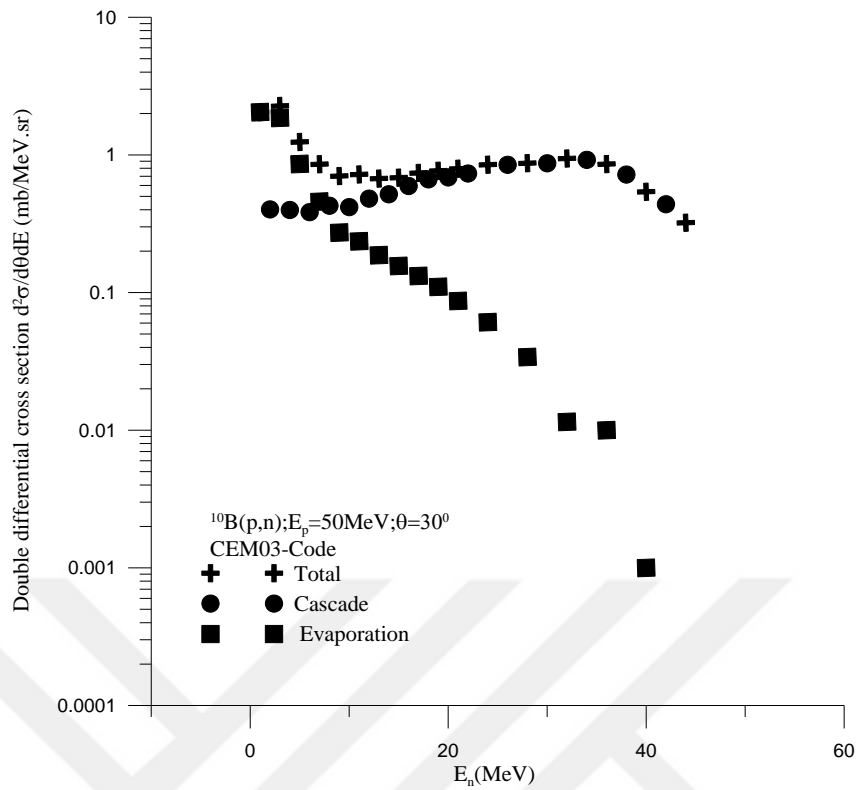| $_5B^{10}$ (p, n) reaction; E_p= 186 MeV; θ= 0^0, Total Double Differential Cross Section (mb/MeV.sr)		
E_n (MeV)	CEM03 – Code	Experimental E_p= 186 MeV; θ= 0^0 (Wang et al. 1994)
0.1	1.777	…
2.0	2.093	…
3.0	1.367	…
4.0	0.922	…
5.0	0.662	…
6.0	0.802	…
7.0	0.442	…
8.0	0.389	…
9.5	…	2.457
10.0	0.306	6.971
10.5	…	5.232
11.0	0.299	2.228
12.0	0.255	0.903
12.5	…	0.827
13.0	0.248	1.278
13.5	…	1.644
14.0	0.252	1.339
150	0.225	1.302
20.0	0.186	0.720
25.0	...	0.657
31.0	…	0.524
36.0	0.118	0.467
40.0	.0112	0.474
50.0	0.088	0.369
60.0	.0094	0.302
76.0	0.077	0.273
80.0	.0078	0.256
81.0	…	0.253
82.0	.0078	0.266
83.0	…	0.275
84.0	.0072	0.260
85.0	…	0.267
86.0	.0078	0.241
87.0	…	0.224
88.0	.0068	0.260
89.0	…	0.251
90.0	…	0.263
91.0	…	0.251
92,0	…	0.227
93.0	…	0.127
93.5	…	0.034

Figure 4.17. Double differential cross section (mb/MeV.sr) of the Neutron generated as a result of bombardment of element $_5B^{10}$ with 186 MeV energetic protons and $\theta= 0^0$ degree

4.3.2.7. Neutron Double Differential Cross Section for $p + _5B^{10}$ Reaction at $E_p= 186$ MeV; $\theta= 20^0$

The double differential cross sections ($d^2\sigma/dE.d\theta$) of emission (alpha, neutron and proton) particle for $p + _5B^{10}$ reactions are calculated by CEM03 code program. The calculate double differential cross section ($d^2\sigma/dE.d\theta$) of neutron emission for $p + _5B^{10}$ at 186 MeV incident energetic proton illustrative in Figure 4.18 and Table 4.18. The shape of calculate results curve of double differential cross section $d^2\sigma/dE.d\theta$ for neutron emission at this energy for four steps (Total, Cascade, Precompound and Evaporation) are different at angle 20^0 degree. It shows that at the beginning of the curve until up to 30 MeV, total and cascade double differential cross section decreasing a littile more when neutron energy emission is increasing. After that amount, they are almost steady as the neutron emission energy increases. On the other hand, evaporation is a gradual decreasing when neutron energies are increasing. However, the precompound in this case is not showing in the line graph since all results are zero. The incident proton energy is bigger than target element, it has small mass number.

In addition, number of elastic interactions is 2991607, number of inelastic interactions is 1000000, reaction cross section is 189.34 mb, elastic cross section is 566.43 mb.

Table 4.18. Neutron Scattered Double Differential Cross Section (mb/MeV.sr) for $p + {}_5B^{10}$ Reaction

E_n(MeV)	Total	Cascade	Evaporation
	Double differential cross section (mb/MeV.sr)	Double differential cross section (mb/MeV.sr)	Double differential cross section (mb/MeV.sr)
1	1.775	000.0	1.775
2	2.059	0.257	1.801
3	1.334	0.241	1.092
4	0.892	0.225	0.666
5	0.675	0.215	0.460
6	0.560	0.220	0.340
7	0.449	0.190	0.259
8	0.381	0.185	0.196
9	0.356	0.183	0.1732
12	0.270	0.151	0.1186
13	0.262	0.151	0.111
14	0.246	0.152	0.093
18	0.191	0.136	0.054
19	0.194	0.138	0.055
20	0.190	0.142	0.047
26	0.158	0.124	0.033
28	0.143	0.117	0.026
30	0.148	0.121	0.027
32	0.137	0.119	0.018
34	0.122	0.107	0.015
40	0.114	0.103	0.010
42	0.110	0.102	0.007
50	0.115	0.110	0.004
52	0.101	0.099	0.002
54	0.100	0.097	0.003
56	0.099	0.097	0.002
66	0.101	0.099	0.001
68	0.097	0.096	
70	0.112	0.110	
72	0.107	0.106	
74	0.102	0.102	
76	0.103	0.103	
78	0.111	0.110	
80	0.110	0.110	
82	0.115	0.115	
84	0.112	0.112	
86	0.112	0.112	
88	0.120	0.120	
90	0.133	0.133	

Table header: ^{10}B(p, n); E_p=186 MeV; θ= 20^0 CEM03 - Code
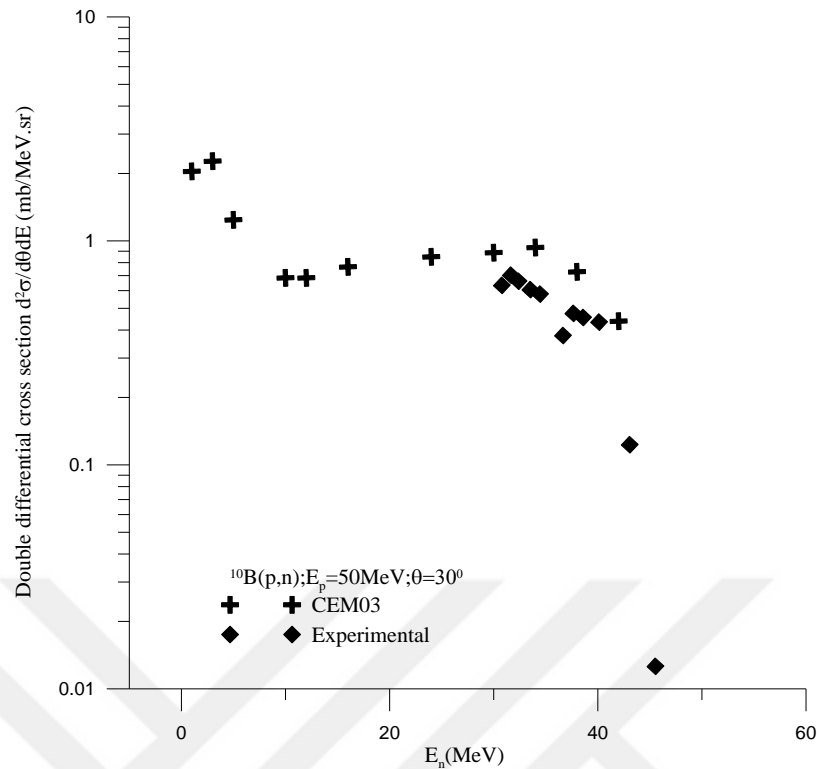
Figure 4.18. Double differential cross section (mb/MeV.sr) of the Neutron generated as a result of bombardment of element $_5B^{10}$ with 186 MeV energetic protons and $\theta = 20^0$ degree

4.3.2.8. Neutron Double Differential Cross Section for p + $_5B^{10}$ Reaction at E_p= 186 MeV; θ= 20^0, Compare between CEM03 and Experimental Data

The comparison of calculate double differential cross section of neutron emission with experimental data at the incident proton energy 186 MeV with angle 20^0 degree are demonstrated in Figure 4.19 and Table 4.19. For $^{10}B(p, xn)$ reaction the pre-equilibrium calculations (cascade- exciton CEM03 and hybrid models) are in good agreement with the measurements.

From Figure 4.19, the experimental and CEM03 data have about an inconsistency at energies 20 MeV. In addition, both the CEM03 and experimental data results are decreasing at energies 88 MeV.

Table 4.19. Neutron Scattered Double Differential Cross Section (mb/MeV.sr) for p + $_5B^{10}$ Reaction

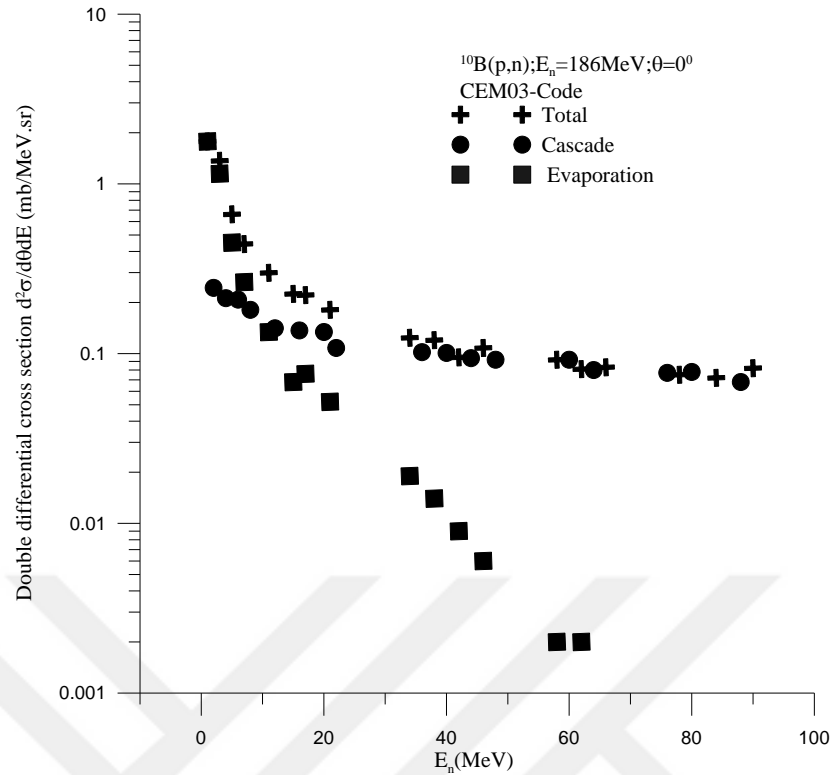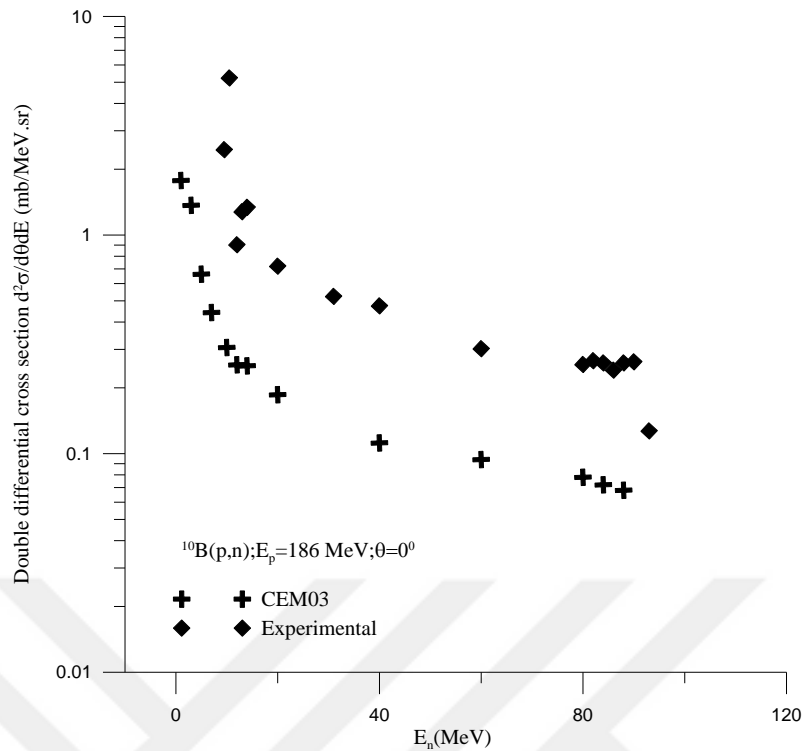| $_5B^{10}$ (p, n); E_p= 186 MeV; θ= 20^0, Total Double Differential Cross Section (mb/MeV.sr)		
E_n (MeV)	CEM03 – Code	Experimental E_p= 186 MeV; θ= 20^0 (Wang et al. 1994)
1.0	1.775	…
2.0	2.059	…
3.0	1.334	…
4.0	0.892	…
8.0	0.381	0.075
9.0	0.356	0.012
9.5	...	0.006
10.0	0.304	0.081
15.0	0.237	0.108
20.0	0.190	0.166
25.0	…	0.322
30.0	0.137	0.455
35.0	…	0.521
40.0	.0114	0.660
48.5	…	0.737
45.0	...	0.696
50.0	0.115	0.682
55.0	...	0.622
60.0	0.099	0.591
65.0	...	0.527
68.0	...	0.97
70.0	0.112	0.440
75.0	…	0.411
80.0	0.110	0.364
85.0	…	0.316
85.5	…	0.327
86.0	0.112	0.316
86.5	…	0.317
87.0	…	0.32
87.5	…	0.304
88.0	0.120	0.290
88.5	…	0.296
89.0	…	0.293
89.5	…	0.292
90.0	0.133	0.292
90.5	…	0.282
91.0	…	0.272
91.5	…	0.253
92.0	0.124	0.201
92.5	…	0.135
93.0	…	0.040

Figure 4.19. Double differential cross section (mb/MeV.sr) of the Neutron generated as a result of bombardment of element $_5B^{10}$ with 186 MeV energetic protons and $\theta= 20^0$ degree

4.3.2.9. Neutron Double Differential Cross Section for $p + {_5B}^{10}$ Reaction at $E_p= 186$ MeV; $\theta= 44^0$

The double differential cross sections ($d^2\sigma/dE.d\theta$) of emission (alpha, neutron and proton) particle for $p + {_5B}^{10}$ reactions are calculated by CEM03 code program. Figure 4.20 and Table 4.20, are showing the results of double differential cross section ($d^2\sigma/dE.d\theta$) of neutron emission for $p + {_5B}^{10}$ at 186 MeV incident energetic proton. Different results are found of double differential cross section $d^2\sigma/dE.d\theta$ for neutron emission at this energy for four steps (Total, Cascade, Precompound and Evaporation) at angle 44^0 degree.

It is shows that total and cascade double differential cross section are decreasing with increasing the neutron energy emission at the beginning of the curve until up to 40 MeV, after that amount, they are almost steady as the neutron emission energy increases. On the other hand, evaporation is a gradual decreasing when neutron energies are increasing. However, in the results of the line graph any point is not recorde for the precompound, the incident proton energy is bigger than target element, has small mass number.

Besides that, number of elastic interactions and number of inelastic interactions are about (2991607 and 1000000), respectively. Also, reaction cross section and elastic cross section are recorded by (189.34 and 566.43 mb), respectively.

Table 4.20. Neutron Scattered Double Differential Cross Section (mb/MeV.sr) for $p + {}_5B^{10}$ Reaction

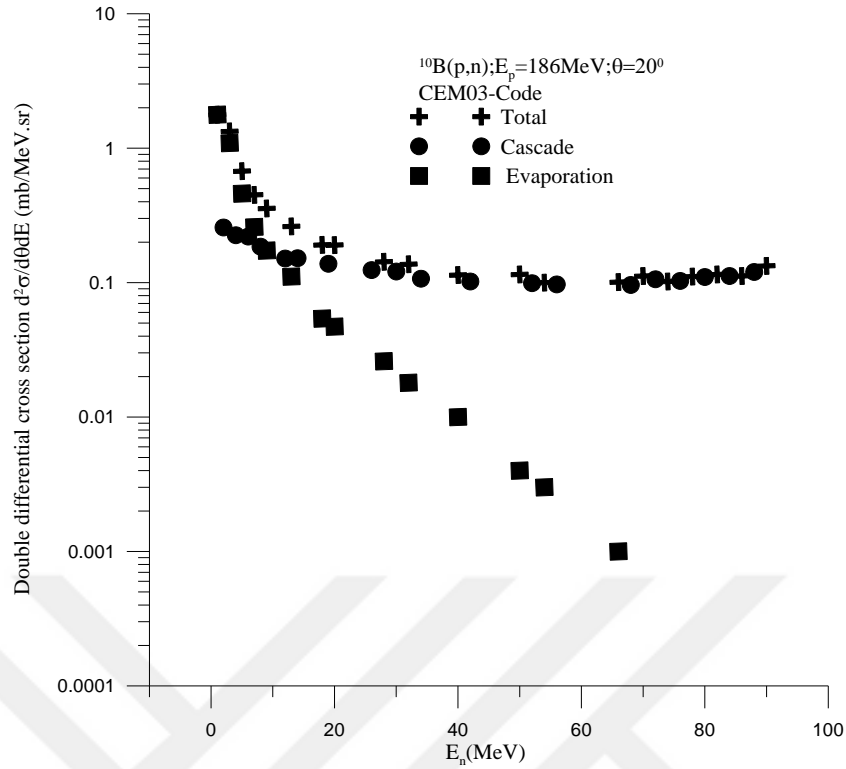| $E_n(MeV)$	${}^{10}B(p, n)$; E_p=186 MeV; θ= 44^0 CEM03 - Code		
	Total	Cascade	Evaporation
	Double differential cross section (mb/MeV.sr)	Double differential cross section (mb/MeV.sr)	Double differential cross section (mb/MeV.sr)
1	1.772	000.0	1.772
2	2.008	0.265	1.742
3	1.353	0.277	1.076
4	0.862	0.242	0.619
5	0.652	0.244	0.408
10	0.343	0.200	0.142
13	0.268	0.173	0.095
14	0.266	0.18	0.086
15	0.25	0.167	0.082
16	0.239	0.167	0.071
18	0.197	0.143	0.053
20	0.211	0.162	0.049
21	0.209	0.169	0.040
24	0.196	0.162	0.034
30	0.160	0.139	0.021
40	0.146	0.138	0.008
42	0.155	0.146	0.009
48	0.146	0.139	0.006
50	0.141	0.134	0.006
52	0.138	0.136	0.002
54	0.146	0.143	0.002
64	0.154	0.152	0.001
66	0.150	0.149	0.001
68	0.159	0.158	0.001
76	0.168	0.168	
90	0.169	0.169	
92	0.152	0.152	
94	0.164	0.164	
96	0.151	0.151	
98	0.158	0.158	
100	0.151	0.151	
106	0.144	0.144	
108	0.143	0.143	
110	0.146	0.146	
112	0.142	0.142	
118	0.118	0.118	
120	0.107	0.107	

Figure 4.20. Double differential cross section (mb/MeV.sr) of the Neutron generated as a result of bombardment of element $_5B^{10}$ with 186 MeV energetic protons and $\theta= 44^0$ degree

4.3.2.10. Neutron Double Differential Cross Section for $p + {}_5B^{10}$ Reaction at $E_p= 186$ MeV; $\theta= 44^0$, Compare between CEM03 and Experimental Data

The comparison of calculate double differential cross section of neutron emission with experimental data at the incident proton energy 186 MeV with angle 44^0 degree are showing in Figure and Table 4.21. For $^{10}B(p, xn)$ reaction the pre-equilibrium calculations (cascade- exciton CEM03 and hybrid models) are in good agreement with the measurements. From Figure 4.21, the experimental and CEM03 data have an inconsistency at energies 90 MeV.

In addition, CEM03 data at the begening of the cerve are decreasing with increasing energies. However, experimental data is increasing.

Table 4.21. Neutron Scattered Double Differential Cross Section (mb/MeV.sr) for p + $_5B^{10}$ Reaction

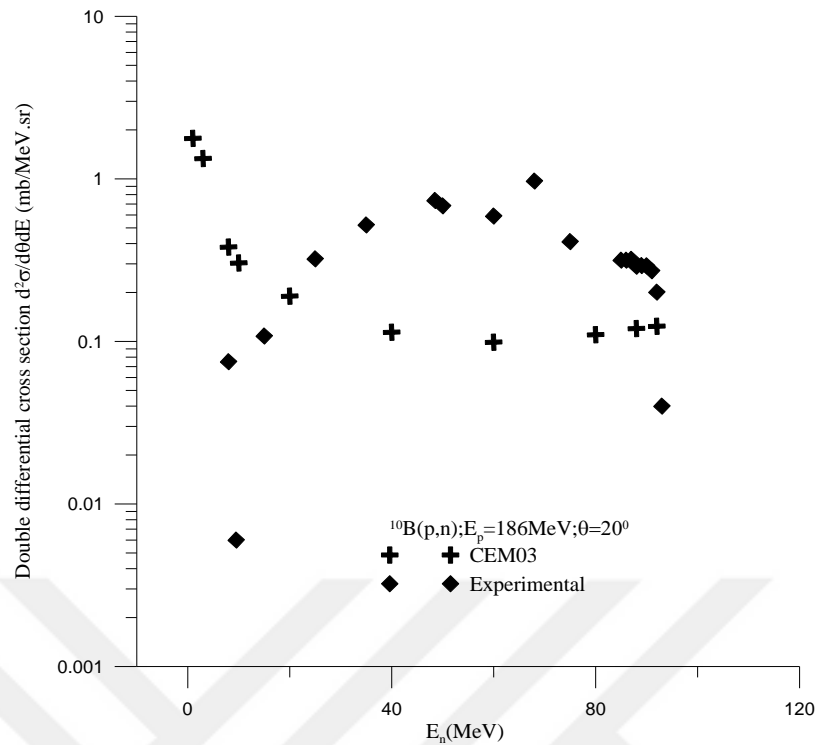| $_5B^{10}$ (p, n); E_p= 186 MeV; θ= 44^0, Total Double differential cross section (mb/MeV.sr)		
E_n (MeV)	CEM03 – Code	Experimental E_p= 186 MeV;θ= 44.4^0, (Wang et al. 1994)
1	1.772	…
2	2.008	…
3	1.353	…
4	0.862	…
5	0.652	…
6	0.510	…
7	0.449	...
8	0.384	...
9	0.347	...
10	0.343	...
11	0.308	...
12	0.302	...
13	0.268	...
14	0.266	...
15	0.250	...
16	0.239	0.003
17	...	0.003
18	0.197	0.001
20	0.211	0.007
25	...	0.011
30	0.160	0.017
35	...	0.032
40	0.146	0.040
45	...	0.052
50	0.141	0.062
55	...	0.077
60	0.149	0.087
65	...	0.100
70	0.152	0.111
75	...	0.122
80	0.150	0.129
85	...	0.139
90	0.169	0.145
95	...	0.149
100	0.151	0.149
105	...	0.142
107	...	0.151
110	0.146	0.136
115	...	0.137
120	0.107	...

Figure 4.21. Double differential cross section (mb/MeV.sr) of the Neutron generated as a result of bombardment of element $_5B^{10}$ with 186 MeV energetic protons and $\theta= 44^0$ degree

4.3.2.11. Neutron Double Differential Cross Section for $p + _5B^{10}$ Reaction at $E_p= 186$ MeV; $\theta= 49^0$

CEM03 code program is applied for calculation the double differential cross sections $(d^2\sigma/dE.d\theta)$ of emission (alpha, neutron and proton) particle for $p + _5B^{10}$ reactions. The calculate double differential cross section $(d^2\sigma/dE.d\theta)$ of neutron emission for $p + _5B^{10}$ at 186 MeV incident energetic proton are showing in Figure 4.22 and Table 4.22. The shape of calculate results curve of double differential cross section $d^2\sigma/dE.d\theta$ for neutron emission at this energy for four steps (Total, Cascade, Precompound and Evaporation) are different at angle 49^0 degree. It shows that at the beginning of the curve, total and cascade double differential cross section are decreasing when neutron energy emission is increasing. After that, they are almost steady as the neutron emission energy increases. On the other hand, evaporation is a gradual decreasing when neutron energies are increasing. However, the precompound in this case is not showing in the line graph because, all results are zero, the incident proton energy is bigger than target element, has small mass number. In addition, at energy 186 MeV with angles (0^0, 20^0, 44^0 and 49^0) degree almost

comparable to the amount especially at angles 44^0 and 49^0 because the values of those angles are tiny. Number of elastic interactions is 2991607, number of inelastic interactions is 1000000, reaction cross section is 189.34 mb, elastic cross section is 566.43 mb.

Table 4.22. Neutron Scattered Double Differential Cross Section (mb/MeV.sr) for p + $_5$B^{10} Reaction

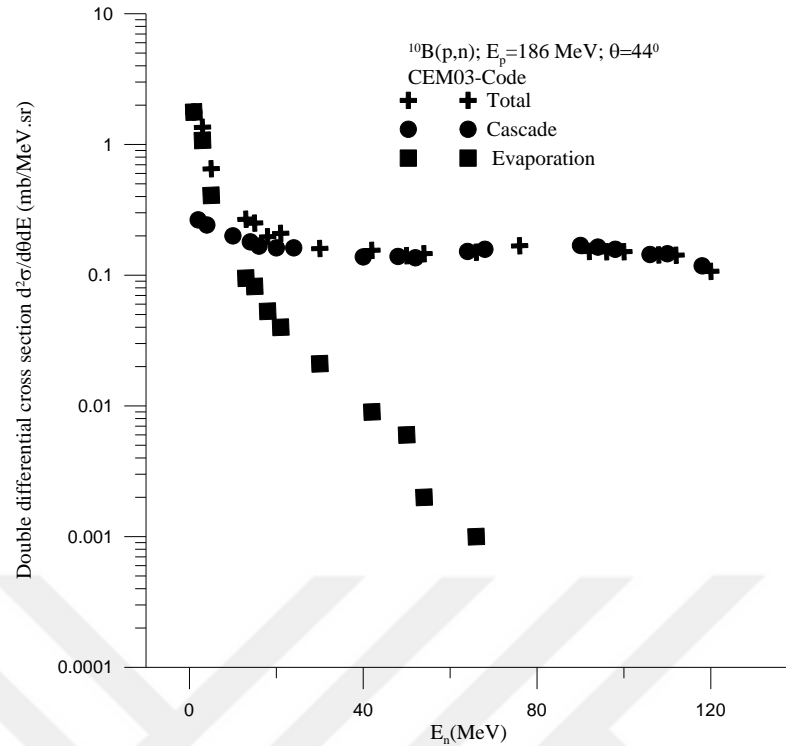| ^{10}B(p, n); E$_p$=186 MeV; θ= 49^0 CEM03 - Code			
E$_n$(MeV)	Total	Cascade	Evaporation
	Double differential cross section (mb/MeV.sr)	Double differential cross section (mb/MeV.sr)	Double differential cross section (mb/MeV.sr)
1	1.707	000.0	1.707
2	2.001	0.287	1.714
3	1.251	0.270	0.980
4	0.842	0.266	0.576
5	0.628	0.253	0.374
6	0.506	0.231	0.274
7	0.434	0.223	0.211
8	0.410	0.233	0.176
9	0.370	0.227	0.143
10	0.348	0.222	0.126
13	0.294	0.202	0.091
14	0.276	0.197	0.079
17	0.254	0.190	0.063
18	0.263	0.204	0.058
19	0.239	0.189	0.050
20	0.238	0.193	0.045
21	0.229	0.186	0.042
22	0.221	0.184	0.036
24	0.211	0.179	0.031
26	0.207	0.182	0.025
28	0.201	0.178	0.022
30	0.197	0.178	0.019
32	0.190	0.176	0.014
34	0.184	0.171	0.013
36	0.175	0.163	0.011
38	0.175	0.166	0.008
40	0.169	0.162	0.007
42	0.171	0.165	0.006
44	0.164	0.159	0.005
46	0.154	0.150	0.003
48	0.149	0.145	0.003
50	0.149	0.146	0.003
52	0.145	0.143	0.002
54	0.144	0.142	0.002
60	0.126	0.125	0.001
64	0.127	0.126	
68	0.109	0.108	
70	0.107	0.107	
84	0.078	0.078	
88	0.065	0.065	

Figure 4.22. Double differential cross section (mb/MeV.sr) of the Neutron generated as a result of bombardment of element $_5B^{10}$ with 186 MeV energetic protons and $\theta = 49^0$ degree

4.3.2.12. Neutron Double Differential Cross Section for p + $_5B^{10}$ Reaction at E_p= 186 MeV; θ= 49^0, Compare between CEM03 and Experimental Data

Figure 4.23 and Table 4.23, are showing the comparison of calculate double differential cross section of neutron emission with experimental data at the incident proton energy 186 MeV with angle 49^0 degree. For ^{10}B(p, xn) reaction the pre-equilibrium calculations (cascade- exciton CEM03 and hybrid models) are in good agreement with the measurements. The experimental and CEM03 data have an inconsistency at energies 70 MeV.

In addition, CEM03 data at the beginning of the cerve are decreasing with increasing energies. However, experimental data is increasing.

Table 4.23. Neutron Scattered Double Differential Cross Section (mb/MeV.sr) for p + $_5B^{10}$ Reaction

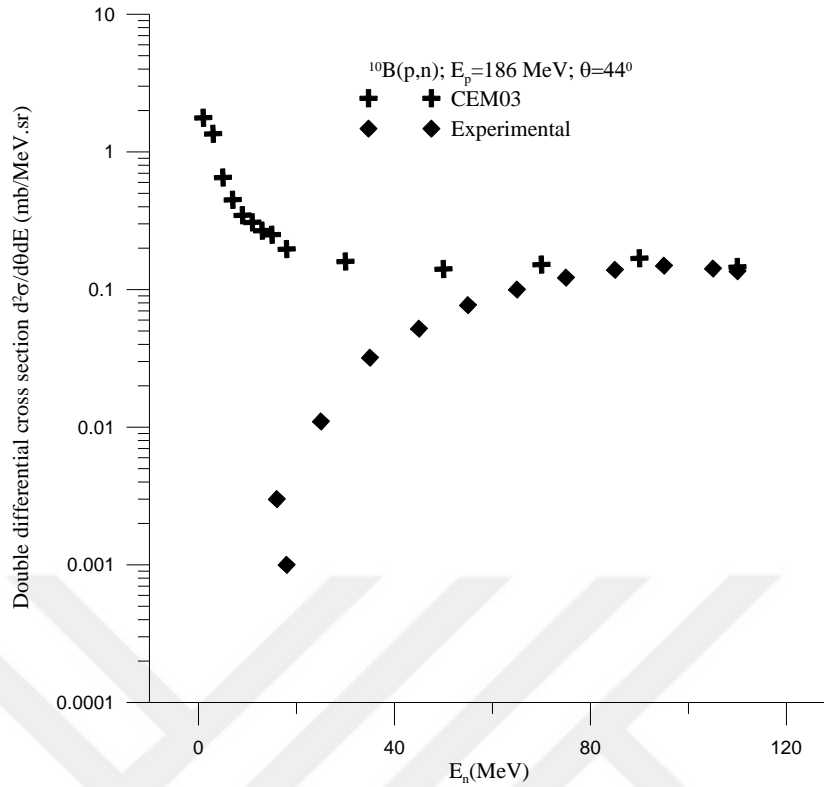| $_5B^{10}$ (p, n); E_p= 186 MeV; θ= 49[0], Total Double Differential Cross Section (mb/MeV.sr)		
E_n (MeV)	CEM03 – Code	Experimental E_p= 186 MeV; θ= 49[0], (Wang et al. 1994)
1	1.707	…
2	2.001	…
3	1.251	…
4	0.842	…
5	0.628	…
6	0.506	…
7	0.434	…
8	0.410	…
9	0.370	…
10	0.348	…
11	0.331	…
12	0.313	…
13	0.294	…
14	0.276	…
15	0.267	…
16	0.260	…
17	0.254	…
18	0.263	0.001
25	…	0.003
30	0.197	0.006
35		0.014
40	0.169	0.020
45	…	0.028
50	0.149	0.034
55	…	0.043
60	0.126	0.054
65	…	0.065
70	0.107	0.075
75	…	0.088
80	0.081	0.100
85	…	0.106
90	0.064	0.114
95	…	0.120
100	…	0.119
105	…	0.122
109	…	0.128
110	…	0.124
115	…	0.118
116	…	0.102
117	…	0.043

Figure 4.23. Double differential cross section (mb/MeV.sr) of the Neutron generated as a result of bombardment of element $_5B^{10}$ with 186 MeV energetic protons and θ= 49^0 degree

4.3.2.13. Alpha Double Differential Cross Section for p + $_5B^{10}$ Reaction at E_p= 660 MeV; θ= 90^0

The double differential cross sections ($d^2σ/dE.dθ$) of emission (alpha, neutron and proton) particle for p + $_5B^{10}$ reactions are calculated by CEM03 code program. The calculate double differential cross section $d^2σ/dE.dθ$ of alpha emission for p + $_5B^{10}$ at 660 MeV incident energetic proton illustrative in Figure 4.24 and Table 4.24. The form of calculate results curve of double differential cross section ($d^2σ/dE.dθ$) for alpha emission at this energy for four steps (Total , Cascade , Precompound and Evaporation) are different at angle 90^0 degree. From the line graph, total and evaporation double differential cross section gradually decreasing when alpha energy emission is increasing. Although, cascade double differential cross section is increasing and decreasing alternately slowly together with increasing alpha energy emission. On the other hand, the precompound in this case is not showing in this graph since, all results are zero, the incident proton energy is bigger than target element, has small mass number.

In addition, number of elastic interactions is by 2311831, number of inelastic interactions is 1000000, reaction cross section is 215.50 mb, elastic cross section is about 498.21 mb.

Table 4.24. Alpha Scattered Double Differential Cross Section (mb/MeV.sr) for p + $_5B^{10}$ reaction, E_P=660 MeV energy with θ= 90^0 degree Calculation have been made by CEM03 code program

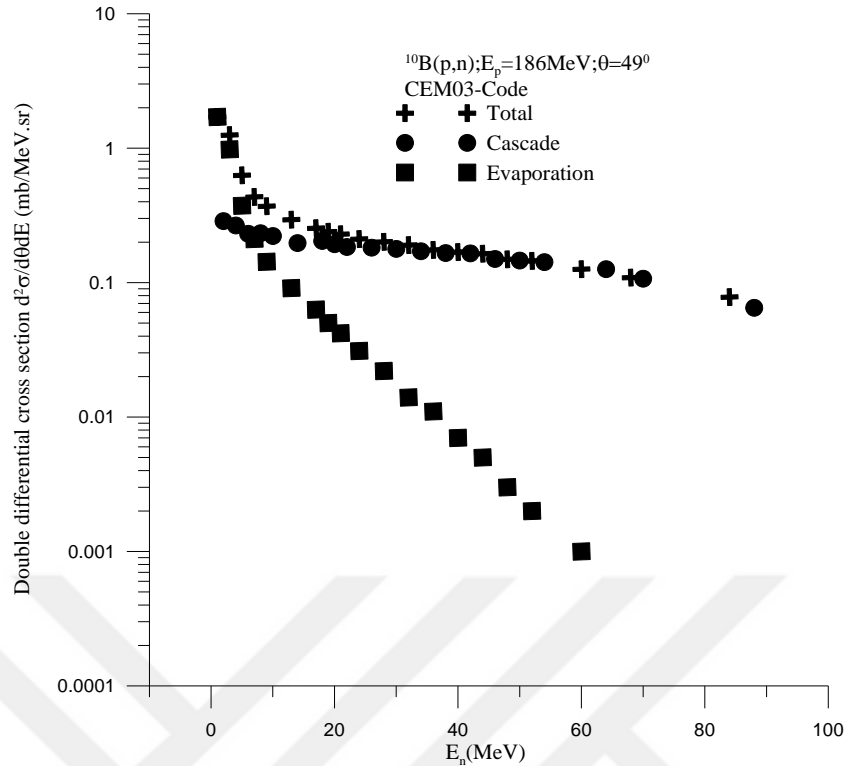| ^{10}B(p, α); E_p=660 MeV; θ= 90^0 CEM03 - Code			
	Total	Cascade	Evaporation
$E_α$(MeV)	Double differen-tial cross section (mb/MeV.Sr)	Double differen-tial cross section (mb/MeV.Sr)	Double differential cross section (mb/MeV.Sr)
1	0.678	…	0.677
2	1.034	0.001	1.033
3	1.087	0.003	1.08
4	0.915	0.002	0.913
5	0.767	0.003	0.764
6	0.642	0.001	0.640
7	0.550	…	0.55
8	0.475	0.001	0.474
9	0.375	0.001	0.374
10	0.321	0.001	0.320
11	0.275	0.001	0.274
12	0.223	0.003	0.220
13	0.201	0.001	0.199
14	0.167	0.001	0.165
15	0.138	0.001	0.137
16	0.133	0.001	0.131
17	0.108	0.001	0.107
18	0.090	…	0.089
19	0.073	…	0.072
20	0.053	0.001	0.051
21	0.046	…	0.045
22	0.033	…	0.033
24	0.036	…	0.035
26	0.026	…	0.025
28	0.016	…	0.016
30	0.012	…	0.012
32	0.012	…	0.012
34	0.010	…	0.012
36	0.005	…	0.005
38	0.008	…	0.007
40	0.005	…	0.005
42	0.002	…	0.001
44	0.002	…	0.002
46	0.002	…	0.002
58	0.001	…	0.001

Figure 4.24. Double differential cross section (mb/MeV.sr) of the Alpha generated as a result of bombardment of element $_5B^{10}$ with 660 MeV energetic protons and $\theta= 90^0$ degree

4.3.2.14. Alpha Double Differential Cross Section for p + $_5B^{10}$ Reaction at $E_p= 660$ MeV; $\theta= 90^0$, Compare between CEM03 and Experimental Data

The comparison of calculate double differential cross section of alpha emission with experimental data at the incident proton energy 660 MeV with angle 90^0 degree are showing in Figure 4.25 and Table 4.25.

For $^{10}B(p, x\alpha)$ reaction the pre-equilibrium calculations (cascade- exciton CEM03 and hybrid models) are in good agreement with the measurements. The CEM03 and experimental data have an inconsistency at energies 10 MeV. Additionally, both the experimental and CEM03 data results are decreasing.

Table 4.25. Alpha Scattered Double Differential Cross Section (mb/MeV.sr) for p + $_5$B^{10} Reaction

$_5$B^{10} (p, α); E$_p$= 660 MeV; θ= 90^0, Total Double Differential Cross Section (mb/MeV.sr)		
E$_α$ (MeV)	CEM03 – Code	Experimental E$_p$= 660 MeV;θ= 90.0^0, (Bogatin et al. 1976)
1.00	0.678	…
2.00	1.034	…
3.00	1.087	…
4.00	0.915	…
5.00	0.767	…
6.00	0.642	…
7.00	0.550	...
7.54	...	0.554
8.00	475.0	...
9.00	0.375	...
9.02	...	0.434
10.00	0.321	...
10.27	...	0.39
10.60	...	0.361
11.00	0.275	
11.15	...	0.314
12.00	0.223	…
12.78	...	0.288
13.00	0.201	...
14.00	0.167	...
14.1	...	0.214
14.65	...	0.202
15.00	0.138	...
15.52	...	0.186
16.00	0.133	...
16.83	...	0.150
17.00	0.108	...
17.38	...	0.143
17.93	...	0.127
18.00	0.090	...
18.47	...	0.12
19.00	0.073	...
19.02	...	0.110
20.00	0.053	...
21.00	0.046	...
22.00	0.033	…
22.09	...	0.065
22.62	...	0.078
23.22	...	0.071
24.00	0.036	...
26.00	0.026	...
28.00	0.016	...
33.22	...	0.021
40.00	0.005	...
46.00	0.002	...
58.00	0.001	...

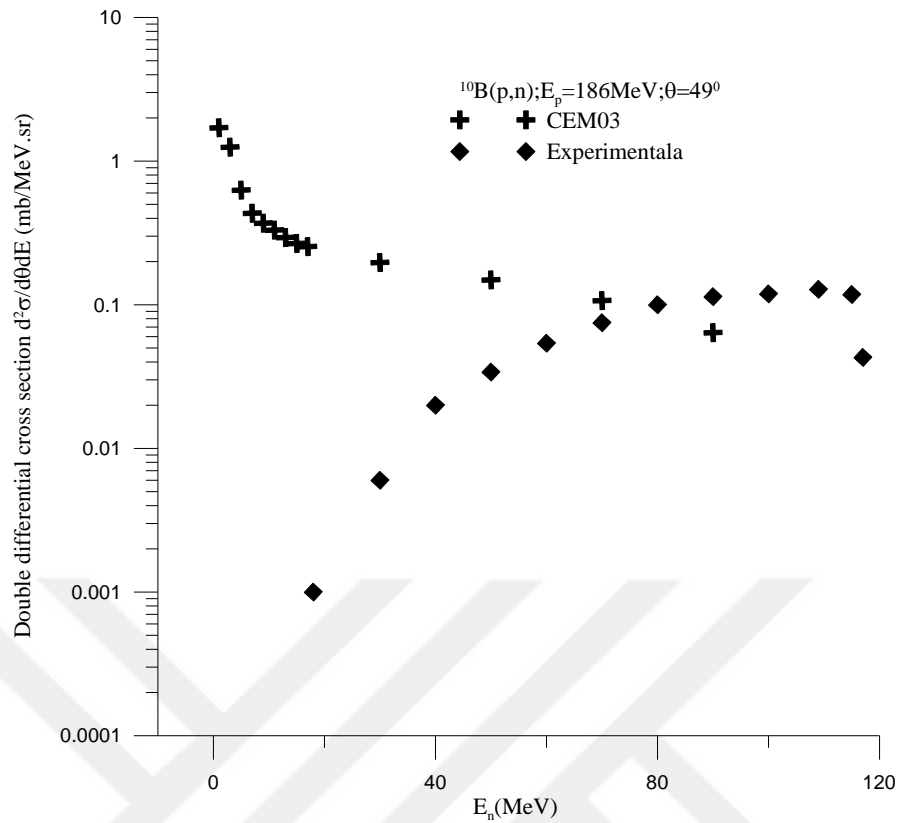Figure 4.25. Double differential cross section (mb/MeV.sr) of the alpha generated as a result of bombardment of element $_5B^{10}$ with 660 MeV energetic protons and θ= 90^0 degree

4.3.2.15. Alpha Double Differential Cross Section for p + $_5B^{10}$ Reaction at E_p=186 MeV; θ= (0^0, 20^0, 40^0, 60^0)

CEM03 code program is used to calculation of the double differential cross sections ($d^2\sigma/dE.d\theta$) of emission (alpha, neutron and proton) particle for p + $_5B^{10}$ reactions. The calculate outcome of the double differential cross sections ($d^2\sigma/dE.d\theta$) of alpha particle emission for p + $_5B^{10}$ reaction at the proton incident energy 186 MeV are showing in Figure 4.26 and (Table 4.26).

The calculate results are at angles 0^0, 20^0, 40^0 and 60^0 that results for total double differential cross section are various for different angles. At the beginning of the curves, total double differential cross section for different angles are decreasing gradually together with increasing alpha energy emission. The form of calculate results curve are similar to each others. However, when alpha energy emission is increasing the total double differential cross section is separate, since they are various at angles.

On the other hand, total double differential cross section for (0^0) degree is different to others because at the end of energy emission is increasing when alpha energy emission is increasing. In addition, number of elastic interactions is 2980182, number of inelastic interactions is 1000000, reaction cross section is 189.98 mb and elastic cross section is 566.18 mb.

Table 4.26. Alpha Scattered Double Differential Cross Section (mb/MeV.sr) for p + $_5B^{10}$ reaction, E_P=186 MeV energy with θ= (0^0, 20^0, 40^0, 60^0) degree Calculation have been made by CEM03 code program

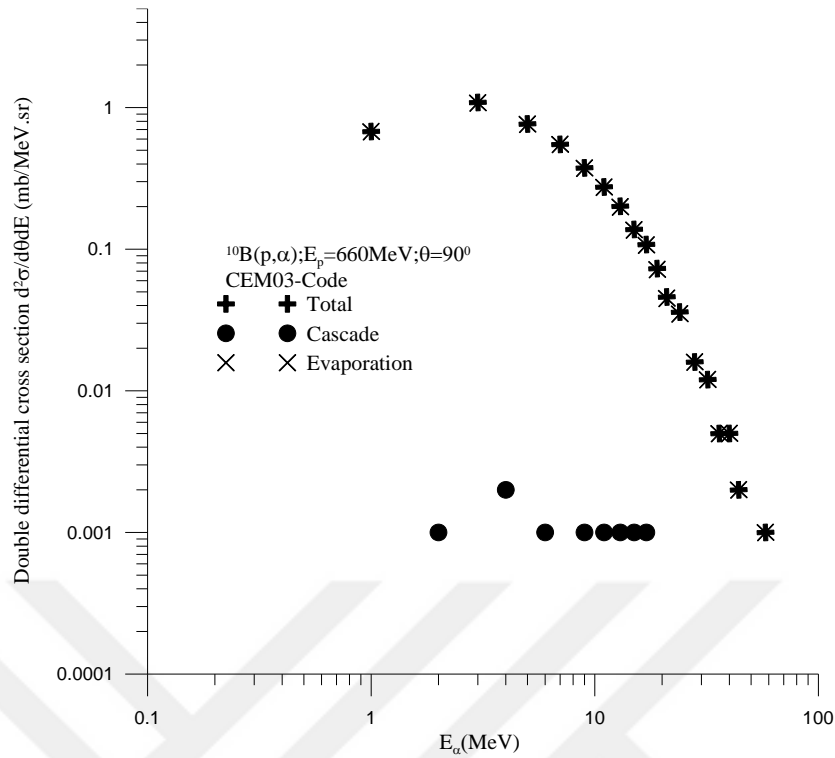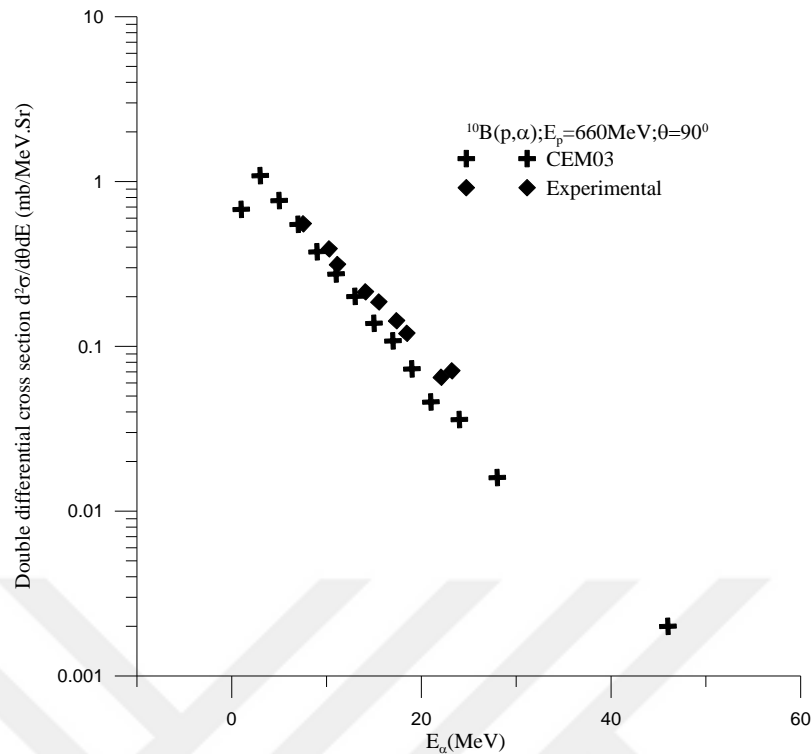| E_α(MeV)	^{10}B(p, α); E_p=186 MeV; θ= (0^0, 20^0, 40^0, 60^0) respectively			
	Total Double Differential Cross Section (mb/MeV.sr) CEM03 – Code			
	Angle θ= 0^0	Angle θ= 20^0	Angle θ= 40^0	Angle θ= 60^0
1	0.762	0.787	0.755	0.765
2	1.473	1.405	1.389	1.337
3	1.582	1.513	1.438	1.328
4	1.403	1.364	1.296	1.258
5	1.168	1.169	1.143	1.06
6	1.021	1.07	1.014	0.905
7	0.951	0.929	0.845	0.757
8	0.750	0.811	0.760	0.652
9	0.696	0.671	0.632	0.526
10	0.551	0.552	0.537	0.445
11	0.487	0.477	0.437	0.354
12	0.445	0.403	0.364	0.306
13	0.372	0.359	0.315	0.258
14	0.302	0.294	0.268	0.224
15	0.250	0.235	0.213	0.175
16	0.195	0.208	0.192	0.145
17	0.179	0.183	0.162	0.130
18	0.147	0.164	0.13	0.110
19	0.115	0.142	0.110	0.080
20	0.151	0.124	0.094	0.076
21	0.161	0.099	0.080	0.068
22	0.085	0.091	0.079	0.050
24	0.072	0.079	0.059	0.046
26	0.058	0.048	0.048	0.033
28	0.057	0.044	0.039	0.024
30	0.033	0.032	0.029	0.018
32	0.028	0.027	0.020	0.013
34	0.031	0.018	0.017	0.010
36	0.021	0.018	0.013	0.008
38	0.010	0.013	0.008	0.006
40	0.011	0.012	0.007	0.004
42	0.008	0.009	0.006	0.003
44	0.007	0.006	0.005	0.003
46	0.006	0.006	0.004	0.002
48	0.004	0.004	0.003	0.001
50	0.001	0.004	0.001	0.001
52	0.003	0.003	0.001	0.001

Figure 4.26. Double differential cross section (mb/MeV.sr) of the alpha generated as a result of bombardment of element $_5B^{10}$ with 186 MeV energetic protons and θ= (0^0, 20^0, 40^0, 60^0) degree respectively

4.3.2.16. Neutron Double Differential Cross Section for p + $_5B^{10}$ Reaction at E_p=186 MeV; θ= (0^0, 20^0, 40^0, 60^0)

The double differential cross sections ($d^2σ/dE.dθ$) of emission (alpha, neutron and proton) particle for p + $_5B^{10}$ reactions are calculated by CEM03 code program. The calculate product of the double differential cross sections ($d^2σ/dE.dθ$) of neutron particle emission for p + $_5B^{10}$ reaction are showing in Figure and Table 4.27, at the proton incident energy 186 MeV. Different results are recording for total double differential cross section at angles 0^0, 20^0, 40^0 and 60^0 . At the beginning of the curves, total double differential cross section for different angles are decreasing sharply when is neutron energy emission increasing. The form of calculate results curve are similar to each other, they are decreasing while amount energy bring to above 40 MeV except 40^0 and 60^0 degree, after that accounts of total double differential cross section are various. From the graph, total double differential cross section on 40 MeV is not change until the quantity almost bring to 160 MeV for 0^0 degree, but after this value which is increasing.

However, total double differential cross section for 20^0 degree is increasing until amount nearly bring to top of 160 MeV, after that which is decreasing with increasing neutron energy emission. In addition, number of elastic interactions is 2980182, number of inelastic interactions is 1000000, reaction cross section is 189.98 mb and elastic cross section is 566.18 mb.

Table 4.27. Neutron Scattered Double Differential Cross Section (mb/MeV.sr) for p + $_5$B^{10} Reaction

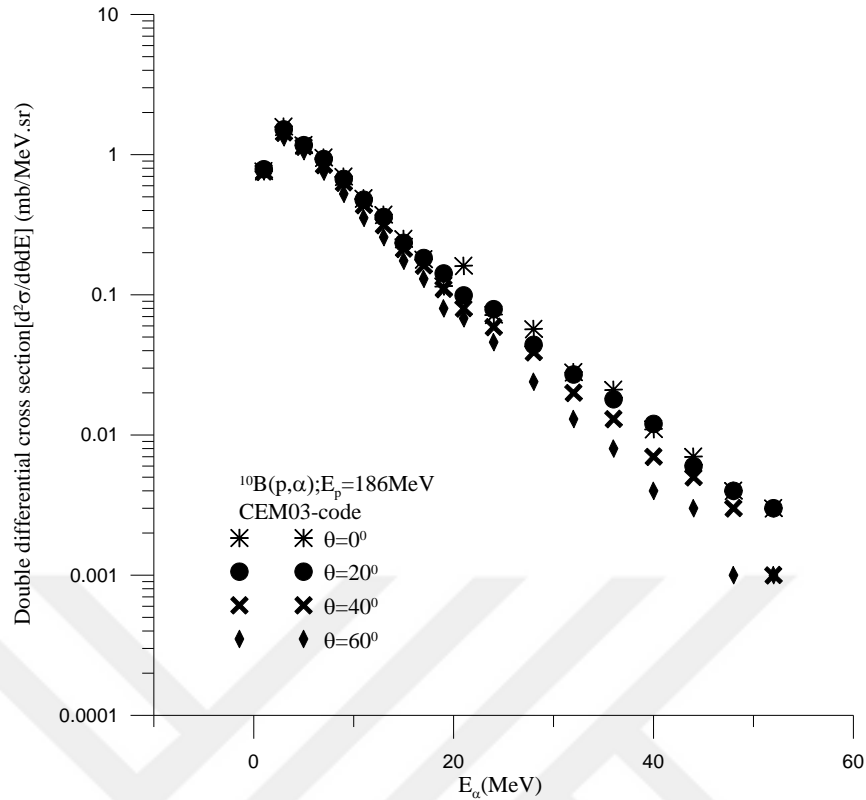| E_n(MeV)	^{10}B(p, n) reaction; E_p=186 MeV; θ= (0^0, 20^0, 40^0, 60^0) respectively			
	Total Double Differential Cross Section (mb/MeV.sr) CEM03 - Code			
	Angle $\theta= 0^0$	Angle $\theta= 20^0$	Angle $\theta= 40^0$	Angle $\theta= 60^0$
1	1.664	1.787	1.734	1.659
2	2.104	2.028	2.025	1.955
3	1.395	1.391	1.324	1.19
4	0.941	0.876	0.884	0.791
5	0.750	0.706	0.639	0.616
6	0.537	0.506	0.518	0.501
7	0.483	0.442	0.453	0.439
9	0.392	0.339	0.380	0.374
10	0.280	0.309	0.333	0.340
15	0.250	0.223	0.250	0.271
16	0.224	0.207	0.245	0.264
17	0.179	0.214	0.251	0.257
18	0.193	0.201	0.239	0.246
20	0.195	0.176	0.220	0.240
24	0.174	0.171	0.195	0.210
34	0.126	0.128	0.172	0.168
36	0.111	0.125	0.167	0.161
38	0.104	0.11	0.161	0.157
40	0.132	0.099	0.156	0.155
42	0.120	0.108	0.158	0.137
50	0.089	0.097	0.154	0.117
56	0.094	0.090	0.160	0.095
58	0.083	0.085	0.160	0.090
60	0.072	0.098	0.146	0.085
70	0.084	0.084	0.155	0.064
80	0.092	0.092	0.160	0.039
90	0.070	0.094	0.149	0.026
100	0.084	0.117	0.129	0.015
110	0.074	0.158	0.108	0.008
120	0.078	0.217	0.081	0.005
130	0.081	0.258	0.064	0.003
140	0.067	0.335	0.040	0.001
150	0.069	0.386	0.023	0.000
160	0.073	0.395	0.010	0.000
170	0.329	0.306	0.003	0.000
180	1.21	0.118	0.000	0.000
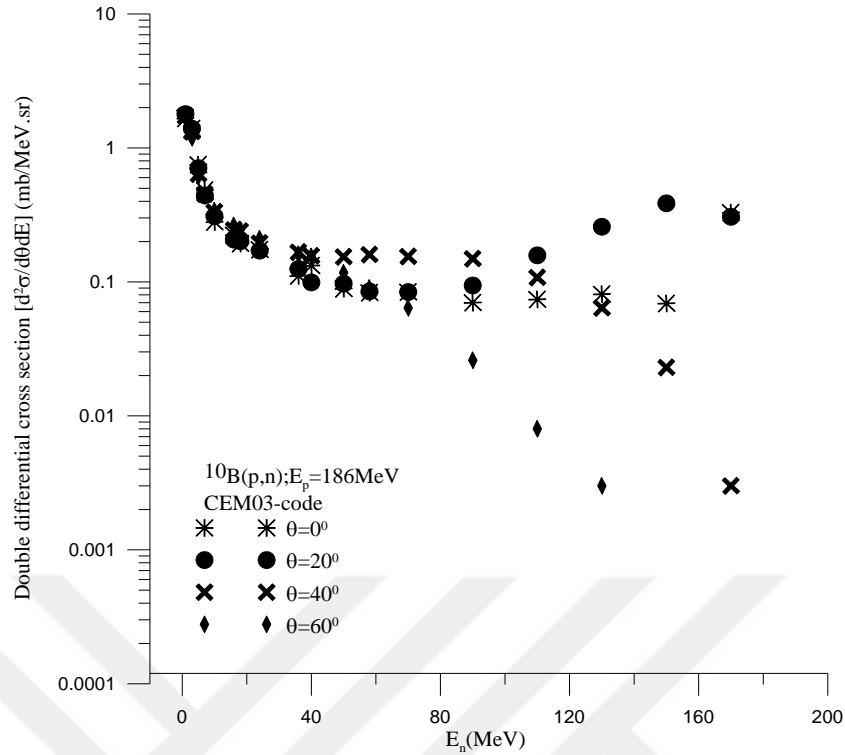
Figure 4.27. Double differential cross section (mb/MeV.sr) of the neutron generated as a result of bombardment of element $_5B^{10}$ with 186 MeV energetic protons and θ= (0^0 , 20^0 , 40^0 , 60^0) degree respectively

4.3.2.17. Proton Double Differential Cross Section for p + $_5B^{10}$ Reaction at E_p=186 MeV; θ= (0^0, 20^0, 40^0, 60^0)

CEM03 code program is used to calculation of the double differential cross sections ($d^2\sigma/dE.d\theta$) of emission (alpha, neutron and proton) particle for p + $_5B^{10}$ reactions.

The calculate consequences of the double differential cross sections ($d^2\sigma/dE.d\theta$) of proton particle emission for p + $_5B^{10}$ reaction at the proton incident energy 186 MeV are showing in Figure 4.28 and Table 4.28. The calculate results at angles 0^0, 20^0, 40^0 and 60^0 for total double differential cross section are various for different angles. At the beginning of the curves, total double differential cross section for different angles are increasing sharply when proton energy emission is increasing. The peaks of the curves at high proton emission energy are participating of the immediate reaction mechanism. The form of calculate results curve are similar to each others. Total double differential cross section are decreasing when amount of energy bring to 40 MeV, after that accounts of total double differential cross section are various.

From the graph, total double differential cross section on 40 MeV is increasing until the quantity almost bring to 90 MeV for 40^0 degree, but after this value it is decreasing. However, subsequent to the peak, total differential cross section for 60^0 degree is decreasing with increasing proton energy emission.

On the other hand, for 20^0 degree behind the highest point of total double differential cross section is decreasing when is proton energy emission increasing until amount nearly bring to 72 MeV, after that which is increasing dramatically while proton energy emission bring to 160 MeV. Then, it is decreasing once more. As well as, for 0^0 degree total double differential is not change until bring to 160 MeV, after that value is increasing sharply when proton energy emission is increasing. In addition, number of elastic interactions is 2980182, number of inelastic interactions is 1000000, reaction cross section is 189.98 mb and elastic cross section is 566.18 mb.

Table 4.28. Proton Scattered Double Differential Cross Section (mb/MeV.sr) for $p + {}_5B^{10}$ Reaction

${}^{10}B(p, \acute{p})$; E_p=186 MeV; θ= (0^0, 20^0, 40^0, 60^0) respectively			
$E_{\acute{p}}$(MeV)	Total Double Differential Cross Section (mb/MeV.sr) CEM03 – Code		
	Angle θ= 0^0	Angle θ= 20^0	Angle θ= 40^0	Angle θ= 60^0
1	0.125	0.135	0.131	0.135
2	0.551	0.511	0.532	0.524
3	1.061	1.036	1.060	1.072
4	0.971	0.962	1.000	0.990
5	0.865	0.882	0.930	0.953
6	0.782	0.823	0.866	0.892
9	0.660	0.683	0.725	0.76
12	0.551	0.559	0.638	0.643
13	0.485	0.522	0.577	0.619
14	0.527	0.498	0.553	0.591
16	0.394	0.425	0.518	0.559
17	0.410	0.417	0.494	0.533
18	0.457	0.403	0.470	0.513
19	0.370	0.358	0.450	0.484
40	0.206	0.210	0.391	0.347
42	0.185	0.199	0.418	0.345
44	0.191	0.203	0.417	0.321
46	0.217	0.188	0.427	0.311
48	0.188	0.203	0.423	0.307
50	0.177	0.189	0.437	0.288
52	0.178	0.192	0.447	0.273
54	0.204	0.194	0.447	0.262
60	0.173	0.185	0.480	0.226
62	0.153	0.188	0.495	0.205

Continue Table 4.28

| 64	0.190	0.194	0.507	0.198
72	0.150	0.197	0.539	0.150
74	0.184	0.205	0.540	0.139
76	0.173	0.205	0.563	0.129
78	0.162	0.220	0.561	0.116
84	0.134	0.250	0.555	0.095
86	0.139	0.261	0.541	0.090
90	0.149	0.271	0.550	0.072
92	0.152	0.295	0.553	0.067
94	0.137	0.313	0.527	0.060
100	0.126	0.361	0.486	0.044
112	0.162	0.529	0.381	0.019
114	0.132	0.596	0.367	0.015
120	0.112	0.704	0.296	0.010
130	0.137	0.866	0.240	0.007
140	0.117	1.118	0.156	0.003
150	0.116	1.302	0.084	
160	0.167	1.261	0.038	
170	0.69	0.923	0.011	
180	2.545	0.461	0.001	
190	1.812	0.047		
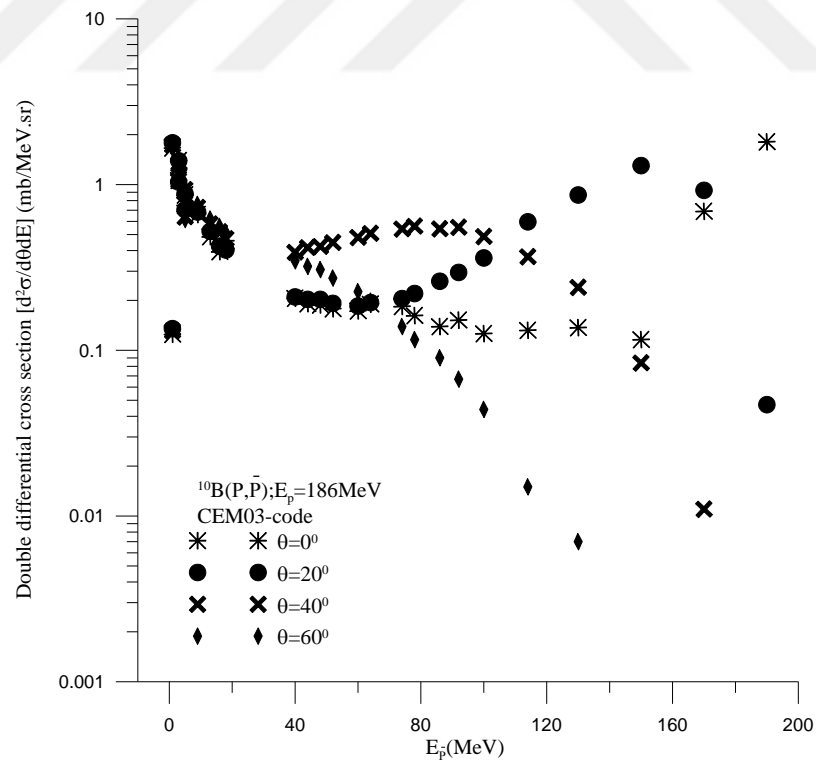
Figure 4.28. Double differential cross section (mb/MeV.sr) of the proton generated as a result of bombardment of element $_5B^{10}$ with 186 MeV energetic protons and θ= (0^0, 20^0, 40^0, 60^0) degree respectively

5. CONCLUSION

In this study, nuclear theory models are applied to calculate $d^2\sigma/dE.d\theta$ for (p, xα), (p, xn) and (p, xṕ) reactions on ^{232}Th and ^{10}B target nuclei which have been measured for (20 to 660) MeV incident proton energy ranges by using CEM03.1 codes. The results are compared with the published experimental data.

In this research, $d^2\sigma/dE.d\theta$ are calculated on a several targets at different energies. Also, the incident proton energies are used randomly, for instance 20 MeV, 500 MeV and 186 MeV for Thorium and Boron elements, because the expereimental data bank in internet website Nuclear Energy Agency (NEA) has this incident energy ranges.

The computational results on $d^2\sigma/dE.d\theta$ for reactions process are given in Tables and Figures (1 to 28), the theoretical model computations apply for reactions are in good agreement with the experimental data. Generally the theoretical models including intra-nuclear cascade (INC) model, pre-equilibrium and equilibrium reaction theories prepared the good attributive of the Figures and importance of the $d^2\sigma/dE.d\theta$ of alpha particle, neutron and proton emissions. Therfore, we used proton energy induced in nuclear reaction for $d^2\sigma/dE.d\theta$ data which are very essential for more than a few practical applications. In this research, especially calculation results has several errors because the program do not reproduce the output or consequence at occasionally, CEM03.1 program that has a specially method.

In the CEM03.1 program code results for p + $_{90}$Th^{232} interaction and particles (α, n, p) are calculated, respectively. As a result in this code for p + $_{90}$Th^{232} at E$_p$=(20, 360, 500, 500) MeV at angles θ= (60.25^0, 20^0, 40^0, 70^0) in that order, in this reactions alpha (α) emitted has been made for four steps (Total, Cascade, Precompound, Evaporation). For all results in Figures (4.1, 4.2, 4.3, 4.4) at the beginning of the curves indicates double differential cross section $d^2\sigma/dE.d\theta$ for four steps   are increasing when alpha energy emitt

ed then each one changed. However, at E_p=20 MeV cascade double differential cross section $d^2\sigma/dE.d\theta$ not shown at angle 60.25^0 because all results are zero, the incident proton energy is smaller than target element, it has a large mass number.

On the other hand, as a result in CEM03.1 code for $p + {}_{90}Th^{232}$ at E_p=360 MeV in this reaction (α, n, p) produced has been made for compared total double differential cross section $d^2\sigma/dE.d\theta$ at angles θ= (0^0, 20^0, 40^0, 60^0) respectively.

In the alpha energy emitted, as can be seen in Figure 4.9 when total double differential cross section $d^2\sigma/dE.d\theta$ at the beginning of the curve for all angles at 360 MeV are increasing with increases alpha energy emitted then they are decreasing.

However, for neutron energy emitted in Figure 4.10 total double differential cross section in the same incident energy and angles are decreasing sharply with increases neutron energy emitted. In the last case for this reaction in the same incident energy but in emitted proton energy shows in Figure 4.11 at the beginning of the curve total cross section are increasing sharply but when the curve bring to the peack then total cross section $d^2\sigma/dE.d\theta$ decreasing.

Likewise, for $p + {}_5B^{10}$ reaction make for several energy ranges and various angles, in these reactions neutron energy emitted for all interactions with out at E_p=660 MeV, in this reaction alpha energy emitted and produced has been made for four steps (Total, Cascade, Precompound, Evaporation) at angle θ= 90^0. As can be seen in Figure 4.24 total and evaporation are equivalent but cascade cross section increasing and decreasing alternately.

Otherwise, for $p + {}_5B^{10}$ reaction at all energy range with all various angles precompound did not show, because all results are zero and the incident proton energy is largest than target element, it has a small mass number. As a result in CEM03.1 code for $p + {}_5B^{10}$ at E_p=186 MeV in this reaction (α, n, p) produced has been made for compared total double differential cross section $d^2\sigma/dE.d\theta$ at angles θ= (0^0, 20^0, 40^0, 60^0) respectively.

In the alpha energy emitted, as can be seen in Figure 4.26 when total double differential cross section $d^2\sigma/dE.d\theta$ at the beginning of the curve for all angles at 186 MeV are increasing with increases alpha energy emitted until bring to the highest then they are decreasing sharply.

While, for neutron and proton energy emitted are similar but in proton energy emitted at beigning of the curve total double differential cross section $d^2\sigma/dE.d\theta$ increases with increases proton energy emitted. Overall, all results of CEM03.1are compared to experimental values and they are in good agreement with the measurements at all energy ranges except for E_p=360 MeV with angle θ= 22^0 . This is because the program is not duplication the output or consequence at occasionally, CEM03.1 code has a special method.

REFERENCES

Abdelbagi AM (2017) The investigation of the neutron total cross section & measurement of the nuclear radius with comparison of Ramsauer model. International Journal of Pure and Applied Physics 13(3): 495-504

Adair RK (1954) Nuclear potential well depth. Physical Review 94(3): 737

Angelone M, Atzeni S & Rollet S (2002) Conceptual study of a compact accelerator-driven neutron source for radioisotope production, boron neutron capture therapy and fast neutron therapy. Nuclear Instruments and Methods in Physics Research Section A: Accelerators, Spectrometers, Detectors and Associated Equipment 487(3): 585-594

Armbruster P & Benlliure J (2001) Basic Nuclear Data at High and Intermediate Energy for Accelerator-Driven Systems. NUPECC–Nuclear Science: Impact, Applications, Interactions [http://www. nupecc. org/iai2001/report/A6. pdf]

Armstrong TW, and Chandler KC (1977) HETC Monte-Carlo Nucleon-Meson Transport Code, Report CCC-178, ORNL

Barashenkov VS and Toneev VD (1972) Interaction of High Energy Particle and Nuclei with Atomic Nuclei, Atomizdat, Moscow

Barros GP, Pereire C, Veloso MAF, Costa AL, Reis PAL (2010) Neutron production evaluation from a ADS target utilizing the MCNPX 2.6.0 code.Brazilian Journal of Physics 40(4): 414-418

Basdevant JL, Rich J, and Spiro M (2005) Fundamentals in nuclear physics: From nuclear structure to cosmology. Springer Science & Business Media

Bauer GS (2001) Physics and technology of spallation neutron sources. Nuclear Instruments and Methods in Physics Research Section A: Accelerators, Spectrometers, Detectors and Associated Equipment 463(3): 505-543

Bertini HW (1963) Low-energy intranuclear cascade calculation. Physical Review 131(4): 1801

Brobeck et al. (1947) Phys. Rev. 71: 449-450

Bethe HA (1937) Rev. Mod. Phys. 9, 69 (1937) Rev. Mod. Phys 9: 69

Bogatin VI, Litvin VF, Lozhkin OV, Perfilov NA & Yakovlev YP (1976) Isotopic effects in high-energy nuclear reactions and isospin correlations of fragmentation cross sections. Nuclear Physics A 260(3): 446-460

Bauer GS (1996) 2nd Int. Conf. on Accelerator Driven Transmutation Technologies, Kalmar, Sweden, June 3-7: 159

Barashenkov VS and Toneev VD (1972) Interaction of High Energy Particle and Nuclei with atomic Nuclei, Atomizdat, Moscow.

Blann M and Vonach HK (1983) phys. Rev. C2, 8147

Bauer GS, IAEA and Vienna (1995) TECDOC-836, p97

Bohr N (1936) Neutron capture and nuclear constitution

Boudard A, Cugnon J, Leray S & Volant C (2002) Intranuclear cascade model for a comprehensive description of spallation reaction data. Physical Review C 66(4): 044615

Bowman CD, Arthur ED, Lisowski PW, Lawrence GP, Jensen RJ, Anderson JL & Engel LN (1992) Nuclear energy generation and waste transmutation using an accelerator-driven intense thermal neutron source. Nuclear Instruments and Methods in Physics Research Section A: Accelerators, Spectrometers, Detectors and Associated Equipment 320(1-2): 336-367

Brobeck WM, Lawrence EO, MacKenzie KR, McMillan EM, Serber R, Sewell DC & Thornton RL (1947) Initial performance of the 184-inch cyclotron of the University of California. Physical Review 71(7): 449

Bowman et al. (1992) Nucl. Instr. and Meth. A 320-336

Carminati F, Roche C, Rubio JA, Rubbia C, Revol JPC & Klapisch R (1993) An energy amplifier for cleaner and inexhaustible nuclear energy production driven by a particle beam accelerator (No. CERN-AT-93-47-ET). P00019698

Carsughi F, Derz H, Ferguson P, Pott G, Sommer W & Ullmaier H (1999) Investigations on Inconel 718 irradiated with 800 MeV protons. Journal of nuclear materials 264(1-2): 78-88

Clough AS, Batty CJ, Bonner BE & Williams LE (1970) A microscopic analysis of the (p, n) reaction on 1p-shell nuclei. Nuclear Physics A 143(2): 385-403

Cockcroft JD, Walton ETS (1932) Experimental with High Velocity Positive Ions - (I) Further Developments in the Method of Obtaining High Velocity Positive Ions, Proceeding of the Royal Society A 136: 619-630

Cottingham WN and Greenwood DA (2001) An introduction to nuclear physics. Cambridge University Press

Cugnon J (1993) Cascade models and particle production: A comparison. In Particle Production in Highly Excited Matter(pp. 271-293). Springer, Boston, MA

Cunningham BB, Hopkins HH, Lindner M, Miller DR, Oconnor PR, Perlman I & Thompson RC (1947, January) Transmutations with High-Energy Deuterons in the 184-Inch Cyclotron. In Physical Review (Vol. 72, No. 8, pp. 739-740). One Physics Ellipse, College Pk, Md 20740-3844 Usa: American Physical Soc

David JC, Filges D, Gallmeier F, Khandaker M & Konobeyev A (2011) Benchmark of spallation models. Prog Nucl Sci Technol 2: 942-947

Demirkol I (2006) Analysis of Isotopic Yields of Primary Residues in 1 A GeV 208Pb+p Reactions. Chinese Journal of Physics 44(6): 418-431

Dulera IV, Basak A, Kelkar PP and Sinha RK (2005) Compact high temperature reactor (CHTR), Contributed paper, CDROM Proceedings of the Sixteenth Annual Conference of Indian Nuclear Society (INSAC- 2005) edited by S Ganesan et al, Nov. 15–18, 2005, Mumbai

Demirkol İ & Tel E (2011) Multiplicity of particles per primary reaction at 1500 MeV for the nuclei used on the accelerator-driven systems. Annals of Nuclear Energy 38(5): 1078-1083

Drosg M & Hoop B (2016) Estimation of Double-Differential Angle-Dependent Neutron Production Cross Sections from Tritons on 197Au at Energies from 5.97 to 19.14 MeV. Nuclear Science and Engineering 182(4): 563-570

Ernst JW, Friedland and Stockhorstz H, Physik (1987) A328, 333

Enqvist T, Wlazło W, Armbruster P, Benlliure J, Bernas M, Boudard A & Pravikoff M (2001) Isotopic yields and kinetic energies of primary residues in 1 A GeV 208Pb+ p reactions. Nuclear Physics A 686(1-4): 481-524

Ershaidat NM (2006) Longitudinal Space Charge Impedance of Non-Resistive Cylindrical Pipe in the Presence of a Uniform Background of Charged Particles. ABHATH AL-YARMOUK, 237

Fernández-Menchero L & Otranto S (2014) Fully and double differential cross sections for the single ionization of H2O by bare ion impact. Journal of Physics B: Atomic, Molecular and Optical Physics 47(3): 035205

Fesbach H (1992) Theoretical nuclear physics: nuclear reactions

Furusaka M, Mizumoto M, Nomura T, Kuno Y, Nagamine K, Niimura N & Watanabe N (1999) The joint project for high intensity proton accelerators (No. JHF-99-3)

Gadioli E and Hodgson PE (1992) Pre-equilibrium nuclear reactions (No.15). Oxford University Press, USA

Ganesan S (2007) Nuclear data requirements for accelerator driven sub-critical systems-A roadmap in the Indian context. Pramana 68(2): 257-268

Geissel H, Armbruster P, Behr KH, Brünle A, Burkard K, Chen M & Langenbeck B (1992) The GSI projectile fragment separator (FRS): a versatile magnetic system for relativistic heavy ions. Nuclear Instruments and Methods in Physics Research Section B: Beam Interactions with Materials and Atoms 70(1-4): 286-297

Getahun G (2011) Pre-Equilibrium Evaporation Of Neutrons From Some + 93nb Systems At Cyclotron Energies

Gibson DK & Reid ID (1986) Double differential cross sections for electron ejection from helium by fast protons. Journal of Physics B: Atomic and Molecular Physics 19(20): 3265

Ganesan S (2004) New reactor concepts and new nuclear data needed to develop them, Invited talk, International Conference on Nuclear Data ND, Santa Fe, USA, American Institute of Physics (AIP) Conference Proceedings CP769, May 2005, pp. 1411–1416

Ganesan S (2005) Nuclear data needed to develop new nuclear systems, role of n TOF facilities to measure resonance cross-sections and nuclear data needs of thorium fuel cycle, Invited talk, Nuclear Physics & Astrophysics at CERN (NuPAC), Oct. 10–12, 2005, CERN, Geneva, Switzerland

Gudima KK, Mashnik SG and Toneev VD (1983) Nucl. Phys. A401 329

Gudima KK, Ososkov GA and Toneev VD (1975) Sov. J. Nucl. Phys. 21-138

Gudima KK, Mashnik SG & Toneev VD (1983) Cascade-exciton model of nuclear reactions. Nuclear Physics A 401(2): 329-361

Guertin A, Auduc S, Riviere G, Eudes P, Haddad F, Lebrun C & Louvel M (2005) Proton induced reactions on naturalU at 62.9 MeV. arXiv preprint nucl-ex/0512022

Handbook DF (1993) Nuclear physics and reactor theory. Washington DC: Department of Energy

Hauser W and Feshbach H (1952) The inelastic scattering of neutrons. Physical review 87(2): 366

Harp GD & Miller JM (1971) Precompound decay from a time-dependent point of view. Physical Review C 3(5): 1847

Harp GD, Miller JM & Berne BJ (1968) Attainment of statistical equilibrium in excited nuclei. Physical Review 165(4): 1166

Harvey BG (1959) Spallation, chapter 3 in Progress in Nuclear Physics, Editor O. R. Frisch, Pergamon Press, volume 7: 90-120

Heilbron JL, Seidel RW, Wheaton BR, Lawrence and his Laboratory: A Historian's View of the Lawrence Years (1996) Web Publication [http://www.lbl.gov/Science-Articles/ResearchReview/Magazine/1981/]

Hossain MK, Taher MA & Das MK (2015) Understanding Accelerator Driven System (ADS) Based Green Nuclear Energy: A Review. World Journal of Nuclear Science and Technology 5(04): 287

Ishibashi K, Takada H, Nakamoto T, Shigyo N, Maehata K, Matsufuji N & Nakamura T (1997) Measurement of neutron-production double-differential cross sections for nuclear spallation reaction induced by 0.8, 1.5 and 3.0 GeV protons. Journal of nuclear science and technology 34(6): 529-537

Iwamoto H, Koba Y, Imamura M, Fukui Y, Fukuda Y, Kiyohara K & Kalinnikov V (2009) Measurement of Light Charged Particle Production Double-Differential Cross Section for 360-and 500-MeV Proton Induced Reactions (No. JAEA-CONF--2009-004)

Junghans A, Neutron beams for nuclear data measurements"Helmholtz-Zentrum Dresden-Rossendorf" Postfach 510119, 01314 Dresden, Germany (2014) email: A.Junghans@hzdr.de

Kadi Y & Revol JP (2001, September) Design of an accelerator-driven system for the destruction of nuclear waste. In Lectures given at the Workshop on Hybrid Nuclear Systems for Energy Production, Utilisation of Actinides & Transmutation of Long-Lived Radioactive Waste Trieste (pp. 3-7)

Kerveno M, Haddad F, Eudes P, Kirchner T, Lebrun C, Slypen I & Louvel M (2002) Hydrogen isotope double differential production cross sections induced by 62.7 MeV netrons on a lead target. Physical Review C 66(1): 014601

Kirkby P & Link WT (1966) Faraday-cup measurement of proton total reaction cross sections at 100 MeV. Canadian Journal of Physics 44(8): 1847-1862

Koning A, Hilaire S & Goriely S (2013) TALYS-1.6 A Nuclear Reaction Program. User Manual (NRG, The Netherlands), First Edition: December 23: 2013

Kox S, Gamp A, Perrin C, Arvieux J, Bertholet R, Bruandet JF & Longequeue N (1987) Trends of total reaction cross sections for heavy ion collisions in the intermediate energy range. Physical Review C 35(5): 1678

Krása A (2008) Neutron Emission in Spallation Reactions of 0.7–2.0 GeV Protons on Thick, Lead Target Surrounded by Uranium Blanket (Doctoral dissertation, Dissertation Thesis, FJFI–ČVUT, Prague)

Krása A (2010) Spallation reaction physics. Czech Republic: Czech Technical University Lecture

Kadi Y (2001) Nuclear data methods for ADS design, ICTP Workshop, [http://www.iaea.org/inis/aws/fnss/auxiliary/abdussalam] 2005.html

Kabach C (1995) Phys. G: Nucl. Part. Phys 21(1995): 1449

Lane AM and Lynn JE (1959) Analysis of experimental data on nucleon capture reactions. Nuclear Physics 11: 646-669

Lane AM and Thomas RG (1958) R-matrix theory of nuclear reactions. Reviews of Modern Physics 30(2): 257

Lee JF (1963) Statistical thermodynamics. Addison-Wesley Pub. Co

Masarik J, Kim KJ & Reedy RC (2007) Numerical simulations of in situ production of terrestrial cosmogenic nuclides. Nuclear Instruments and Methods in Physics Research Section B: Beam Interactions with Materials and Atoms 259(1): 642-645

Mashnik SG and Toneev VD (1974) Joint Institute for Nuclear Research Communication P4-8417

Mashnin SG (2005) Monte-Carlo Code System to Calculate Nuclear Reactions in the Framework of the Improved Cascade-Exciton Model

Mason TE, Abernathy D, Ankner J, Ekkebus A, Granroth G & Miller S (2005, June) The Spallation Neutron Source: A powerful tool for materials research. In AIP Conference Proceedings (Vol. 773, No. 1, pp. 21-25). AIP

Meot F, Tahar MH and Tsoupas N (2015) High Power from Fixed-filed Rings in the Accelerator-driven Sub –critical Reactor Application. Physics procedia 66: 129-139

Michel R, Bodemann R, Busemann H, Daunke R, Gloris M, Lange HJ & Neumann S (1997) Cross sections for the production of residual nuclides by low-and medium-energy protons from the target elements C, N, O, Mg, Al, Si, Ca, Ti, V, Mn, Fe, Co, Ni, Cu, Sr, Y, Zr, Nb, Ba and Au. Nuclear Instruments and Methods in Physics Research Section B: Beam Interactions with Materials and Atoms 129(2): 153-193

Michel R, Peiffer F & Stück R (1985) Measurement and hybrid model analysis of integral excitation functions for proton-induced reactions on vanadium, manganese and cobalt up to 200 MeV. Nuclear Physics A 441(4): 617-639

Milazzo-Colli L, Braga-Marcazzan GM & Milazzo M (1975) Further measurements of the probability of α cluster pre-formation by means of (p, α) reactions in heavy elements. Il Nuovo Cimento A (1965-1970), 30(4): 632-652

Mukaiyama T (2003) OMEGA Programme in Japan and ADS Development at JAERI. Review of national accelerator driven system programmes for partitioning and transmutation, 153

NEA Nuclear Science Committee (2002) Accelerator-driven Systems (ADS) and Fast Reactor (FR) in Advanced Nuclear Cycles, A Comparative Study. Nuclear Energy Agency Organization for Economic and Co-operation Development, ISBN 92-64

Nifenecker et al. (1999) Hybrid Nuclear Reactors, Progress in Particle and Nuclear Physics 43, 683-827 [http://lpsc.in2p3.fr/gpr/PPNPport/node1.html]

Nifenecker H, Meplan O & David S (2003) Accelerator driven subcritical reactors. CRC Press

Nigussie B (2012) Complete And Incomplete Fusion Studies

Niita K, Sato T, Iwase H, Nose H, Nakashima H & Sihver L (2006) PHITS-a particle and heavy ion transport code system. Radiation measurements 41(9): 1080-1090

Nuclear Reactions Some Basics I. Reaction Cross Sections [https://facultystaff. richmond.edu/~ggilfoyl/research/nuclear Cross Sections. pd]

OECD Nuclear Energy Agency (2002) Accelereator-driven Systems (ADS) and Fast Reactors (FR) in Advanced Nuclear Fuel Cycles: A Comparative Study. OECD

Patrick CE (2017) Measurement of the antineutrino double-differential charged-current quasi-elastic scattering cross section at MINERVA. Springer

Pienkowski L, Bohlen HG, Cugnon J, Fuchs H, Galin J, Gatty B & Jahnke U (1994) Hot nuclei in reactions induced by 475 MeV, 2 GeV 1H and 2 GeV 3He. Physics Letters B 336(2): 147-151

Rhodes CJ (2013) Current Commentary: Thorium-based nuclear power. Science progress, 96(2), 200 [http://www.world-nuclear.org/info/Current-and-Future-Generation/Accelerator-driven-Nuclear-energy/]

Röder J, Ehrhardt H, Bray, Fursa DV & McCarthy IE (1996) Absolute triple differential cross section for electron-impact ionization of helium at 40 eV. Journal of Physics B: Atomic, Molecular and Optical Physics 29(10): 2103

Rose (1991) RF: BNL-NCS-17541

Rossi B (1933) Über die Eigenschaften der durchdringenden Korpuskularstrahlung im Meeresniveau. Zeitschrift für Physik 82(3-4): 151-178

Rubbia et al. (2001) A European Roadmap for Developing Accelerator Driven Systems (ADS) for Nuclear Waste Incineration, ENEA. ISBN 88-8286-008-6 [inrwww.fzk.de/ads-roadmap.html]

Rubbia C, Aleixandre J & Andriamonje S (2001) A european roadmap for developing accelerator driven systems (ADS) for nuclear waste incineration. ENEA Report, 88

Rubbia C, Roche C, Rubio JA, Carminati F, Kadi Y, Mandrillon P & Gelès C (1995) Conceptual design of a fast neutron operated high power energy amplifier (No. CERN-AT-95-44-ET)

Rutherford E (1919) Collision of alpha particles with light atoms. III. Nitrogen and oxygen atoms, Philosophical Magazine 37: 571-580

Rubbia et al. (1995) Preprint CERN/AT/95-44(ET)

Sarpün IH, Yalim H, Aydin A & Kaplan A (2014) Calculation of double–differential cross sections for proton impact alpha emission at 62 MeV. Journal of Nuclear Sciences 1(1): 001-005

Sinha RK and Kakodkar A (2006) Nucl. Engg. Design 236-683

Serber R (1947) Nuclear reactions at high energies. Physical Review 72(11): 1114

Saha D and RK Sinha (2005) Indian advanced nuclear reactors, Invited talk, CDROM Proceedings of Sixteenth Annual Conference of Indian Nuclear Society (INSAC-2005) edited by S Ganesan et al, Nov. 15–18, 2005, Mumbai

Serber R (1948) Beam Dynamics In The Linear Accelerator. In Physical Review (Vol. 73, No. 5, pp. 535-535) One Physics Ellipse, College PK, MD 20740-3844 USA: American Physical Soc

Shetty NV (2013) Study of particle transport in a high power spallation target for an accelerator-driven transmutation system (Doctoral dissertation, Hochschulbibliothek der Rheinisch-Westfälischen Technischen Hochschule Aachen)

Sümmerer K & Blank B (2000) Modified empirical parametrization of fragmentation cross sections. Physical Review C 61(3): 034607

Takizuka T, Proceedings of the Int. Conf. on Accelerator-Driven Transmutation Technologies and Applications, Las Vegas, NV, USA, 64 (August 1994)

Taieb J, Schmidt KH, Tassan-Got L, Armbruster P, Benlliure J, Bernas M & Legrain R (2003) Evaporation residues produced in the spallation reaction 238U+ p at 1 AGeV. Nuclear Physics A 724(3-4): 413-430

Tashenov S, Bäck T, Barday R, Cederwall B, Enders J, Khaplanov A & Surzhykov A (2011) Measurement of the correlation between electron spin and photon linear polarization in atomic-field bremsstrahlung. Physical review letters 107(17): 173201

Titarenko YE, Shvedov OV, Igumnov MM, Mashnik SG, Karpikhin EI, Kazaritsky VD & Prael RE (1998) Experimental and computer simulation study of the radionuclides produced in thin 209Bi targets by 130 MeV and 1.5 GeV proton-induced reactions. Nuclear Instruments and Methods in Physics Research Section A: Accelerators, Spectrometers, Detectors and Associated Equipment 414(1): 73-99

Tolstov KD (1989) Aspects of accelerator-breeding (No. JINR--18-89-778). Joint Inst. for Nuclear Research

Vasil'kov RG, Gol'Danskii VI, Pimenov BA, Pokotilovskii YN & Chistyakov LV (1978) Neutron multiplication in uranium bombarded with 300–660-MeV protons. Soviet Atomic Energy 44(4): 377-383

Vértes A, Nagy S, Klencsár Z, Lovas RG & Rösch F (Eds) (2010) Handbook of Nuclear Chemistry: Vol. 1: Basics of Nuclear Science; Vol. 2: Elements and Isotopes: Formation, Transformation, Distribution; Vol. 3: Chemical Applications of Nuclear Reactions and Radiation; Vol. 4: Radiochemistry and Radiopharmaceutical Chemistry in Life Sciences; Vol. 5: Instrumentation, Separation Techniques, Environmental Issues; Vol. 6: Nuclear Energy Production and Safety Issues. Springer Science & Business Media

Voronko VA, Kostin VY, Levchuk LG, Migalenya VY, Nagaichenko VI, Sidorenko VV & Tolstov KD (1991) Energy spectra of neutrons generated by relativistic nuclei in extended lead target. Soviet Atomic Energy 71(6): 1028-1030

Wachter JA, Miranda PA, Morales JR, Cancino SA & Correa R (2015) Measurements of 67 Ga production cross section induced by protons on nat Zn in the low energy range from 1.678 to 2.444 MeV. Nuclear Instruments and Methods in Physics Research Section B: Beam Interactions with Materials and Atoms 344: 59-62

Wagenaar DJ (1995) The Bragg Curve. Retrieved from [http://www.med.harvard. edu /jpnm/physics/nmltd/radprin/sect7/7.1/7_1.3.html]

Wang L, Yang X, Rapaport J, Goodman CD, Foster CC, Wang Y & Luther B (1994) (p, n) quasifree excitations in p-shell nuclei at 186 MeV. Physical Review C 50(5): 2438

Weisskopf VF & Ewing DH (1940) Erratum: On the Yield of Nuclear Reactions with Heavy Elements (Phys. Rev. 57, 472 ((1940)). Physical Review 57(10): 935

World Nuclear Association (2014) Accelerator-driven nuclear energy. Information Library, http://www. worldnuclear. org/info/Current-and-Future-Generation/Accelerator-driven-Nuclear-Energy

Yariv Y & Fraenkel Z (1981) Intranuclear cascade calculation of high energy heavy ion collisions: Effect of interactions between cascade particles. Physical Review C 24(2): 488

Zeman J (2003) Reactor Physics I, CVUT (in Czech)

Ziegler JF (1988) The stopping and range of ions in solids. In Ion Implantation Science and Technology (Second Edition)(pp. 3-61)

CURRICULUM VITAE

Fulname: Majd Hamad SMAIL

Gender: Male

Martial: Married

Date of birth: 11.7.1981

Birth place: Erbeel

Nationality: IRAQ

Address : www.majed.hamad@ymail.com

Telephon No. : 009647504705378 _ 009647507221270

I was born in 1981. Iwas graduated from the University of Salahaddin faculty of Education department of physics production in 2004. I enrolled at the postgraduate programme in Bingol University Institute of Science Department of physics in 2016, and finished my research in 2018.